# Naval Research Reviews

Office of Naval Research
Three/1998
Vol L

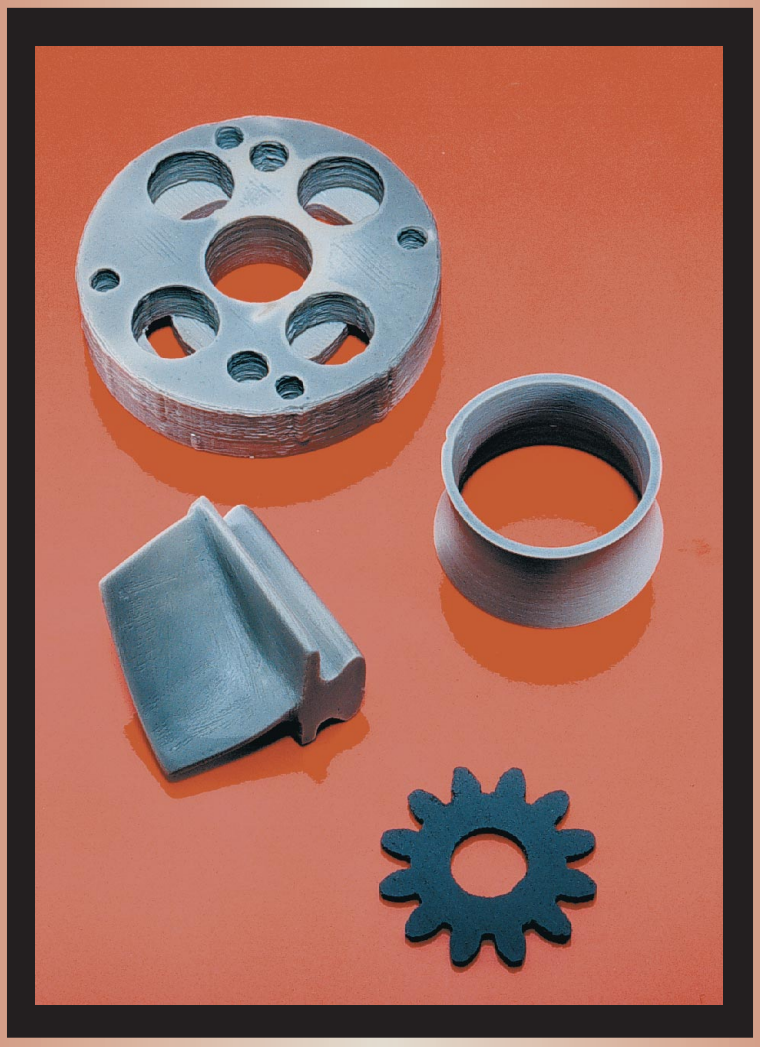

## Advances in Manufacturing: Building Parts by Layers

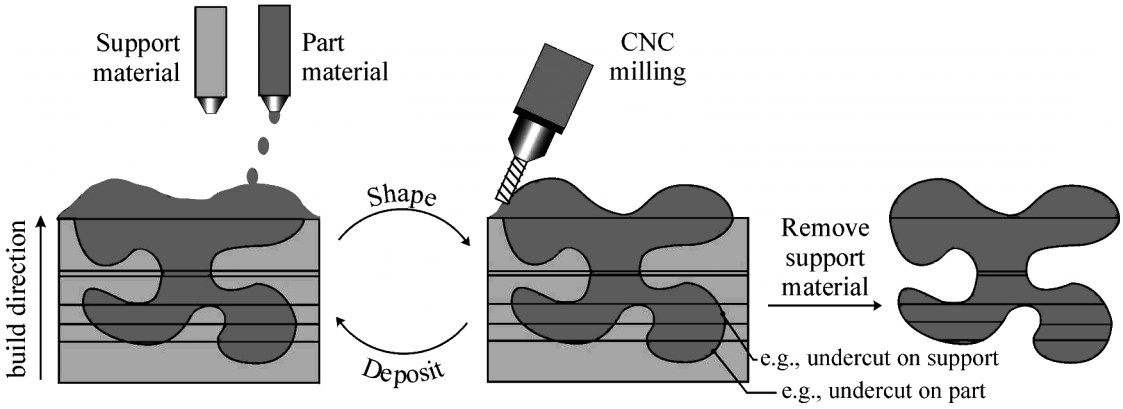


Shape Deposition Manufacturing (SDM) is one of several layered manufacturing (LM) methods highlighted in this issue. It is a process that incrementally builds up complex parts by systematically combining material additive processes with material removal processes. The advantages of each type of process are thus combined such that novel structures can be fabricated with SDM that could not be practically fabricated with either material additive or material removal processes alone.

# Naval Research Reviews

**Office of Naval Research**
**Three/1998**
**Vol L**


## Articles



## Departments





**About the cover**
This figure shows four parts produced at Rutgers University by one particular method of layered manufacturing known as Fused Deposition. From top to bottom the parts are: (1) a fluidic control device, (2) a turbine blade, (3) a nozzle shape for a rocket engine, and (4) a thin gear. (1) – (3) are made of silicon nitride, while (4) is made of stainless steel.


*Naval Research Reviews* publishes articles about research conducted by the laboratories and contractors of the Office of Naval Research and describes important naval experimental activities. Manuscripts submitted for publication, correspondence concerning prospective articles, and changes of address, should be directed to Code 00PA, Office Naval Research, Arlington, VA 22217-5660. Requests for subscriptions should be directed to the Superintendent of Documents, U.S. Government Printing Office, Washington, DC 20403. *Naval Research Reviews* is published from appropriated funds by authority of the Office of Naval Research in accordance with Navy Publications and Printing Regulations. NAVSOP-35.

# Foreword

*Dr. George Spanos, Guest Editor, Materials Science and Technology Division, Naval Research Laboratory*

*Dr. Steve Fishman, Guest Editor, Materials Science and Technology Division, Office of Naval Research*

*Dr. Ralph Wachter, Guest Editor, Manufacturing Technology Division, Office of Naval Research*

A challenge in manufacturing is to invent new processes for the rapid production of complex functional and structural components. One very promising class of manufacturing processes, descriptively called Layered Manufacturing (LM), has been made possible through recent advances in several fields of science and technology including materials science, mechanical engineering, and information technology. LM offers unique capabilities, important for agile manufacturing and logistics, to create rapidly on-demand manufactured components of complex design.

The essential characteristic of a LM process is its successive building up of a part layer-by-layer by precise computer-controlled deposition of materials. This process is roughly analogous to stacking masonry bricks to form different brick wall designs. Since LM is a material additive process, it differs from traditional manufacturing approaches of machining, which involve removal of material. LM processes also differ from traditional laminate composite manufacturing where, for instance, layers of composite tape are shaped and bonded together.

The Office of Naval Research in cooperation with the Defense Advanced Research Projects Agency and the National Science Foundation has been advancing the science and technology for LM. Through joint efforts, the range of materials has been expanded considerably from, e.g., plastics, to metals and ceramics, and towards functionally graded materials. Methods for selective precise deposition of materials in LM are now quite varied and include, e.g., high intensity light sources, hot extrusion, and metal droplet deposition; a few hybrid approaches are even combining LM with machining and cutting. These processes have motivated new materials science research into solidification, bonding between layers, and evolution of microstructure and residual stress in LM components.

This issue of Naval Research Reviews provides an overview of the science, technology and applications of LM. Our first article, by Mr. Patrick Bergan of the Naval Undersea Warfare Center, highlights Naval applications of LM and, in particular, their use of selective laser sintering technology from DTM Corporation, a spin-off company from the University of Texas at Austin. The article describes where LM technology can significantly affect affordability.

Professors Emanuel Sachs and Michael Cima at the Massachusetts Institute of Technology (MIT) developed a method for forming parts from metal powders by an ink-jet like process, which they aptly named "3D Printing." The article discusses advantages of the process for making parts with highly complex external and internal geometries such as internal cooling channels for injection mold tooling. Their research has been licensed by MIT to the company, Soligen Technologies, Inc.

Professor Fritz Prinz at Stanford University and Dr. Lee Weiss at Carnegie Mellon University describe a novel approach for making complex metal, ceramic and plastic parts. Known as Shape Deposition Manufacturing, it involves combining techniques of material deposition with material removal, e.g., using 5-axis machining for precisely shaping individual layers to a specified tolerance during the layering process. They discuss several applications relevant to the Department of Defense (DoD) including a composite steel/copper injection molding tool, a miniature turbine wheel assembly, and a rugged casing with embedded wiring for a wearable computer for underwater use.

A multidisciplinary research team at Rutgers University, lead by Professor Steven Danforth of the Ceramic and Materials Engineering Department, present a LM method known as Fused Deposition of Ceramics (FDC) in which hot extruded ceramic-loaded organic filaments are used to deposit the layers. Their paper surveys FDC for structural ceramics, bio-ceramics, and piezo-electric transducers.

Dr. G. Allen Brady and Professor John Halloran at the University of Michigan describe a technique for producing ceramic parts, based on conventional stereolithography, which uses a laser to scan an outline of a shape on a layer of photosensitive polymer. They developed new ultraviolet-curable polymers with a suspension of ceramic powder to produce ceramic parts. The authors show examples of fully dense ceramic parts with excellent microstructures.

Dr. Susanna Ventura and her collaborators in the Electrochemical and Polymer Technology Center at SRI International have developed an innovative technique for producing ceramic parts using digital, pixelated visible light projected on a photocurable ceramic dispersion. Their process, known as "Direct Photoshaping," uses digital micromirror technology, developed by Texas Instruments, Inc., to expose and cure specific regions of each layer all at once to rapidly build up a part with embedded ceramic powder. The polymer can subsequently be burned off and the resulting "green" ceramic object sintered to final density. A silicon nitride turbine vane for a gas turbine engine has been produced by this method.

Professor Harris Marcus of the Institute of Materials Science at the University of Connecticut and his colleagues describe a very different LM process that uses lasers to decompose locally reactant gases in a controlled manner. Their process is known as selective area laser deposition. The authors show how to build ceramic parts and how to join separate ceramic pieces together with this process.

Professor Debasish Dutta and his colleagues at the University of Michigan are investigating digital representations of parts with graded materials and microstructures, for

LM computer aided design. A distinct advantage of LM is the conceptualization of a part as a stack of layers, which actually simplifies computation, design, and manufacturing processes.

The articles in this issue of the Naval Research Reviews provide insight into tomorrow's manufacturing capabilities. These capabilities have important implications for production and productivity. LM will advance affordable manufacturing technologies without the need for conventional or specialized tooling and without the need for part fixturing. LM will replace some traditional manufacturing processes but not all. LM will complement some conventional high-volume manufacturing processes by enabling the rapid production of machine tooling, e.g., from durable, erosion-resistant, high temperature materials.

The capability of LM to produce nearly arbitrary shapes lends itself to rapid, flexible, customized production.[1] LM technology is often capable of producing more kinds of parts with less lead time, setup time, production time, assembly, and effort than, e.g., by comparable machining. Moreover, as greater precision is achieved with LM, part size and not geometric complexity will be the dominant factor in part cost and time whereas in comparable conventional machining both part size and complexity are significant factors. And with lower costs of small-lots and reduced production time, customization of commodity parts on-demand with LM will become an alternative to traditional mass production of standard machined parts and stockpiles of inventories.

Layered Manufacturing also has important implications for repair and replacement of parts for which engineering designs are no longer available or where designs never existed. The capability to reverse engineer, e.g., using x-ray tomography or coordinate measurement machines, can provide geometric information necessary for replicating a part with LM. Moreover, complex part designs stored on a computer can be electronically transferred to sites such as shipyards and potentially directly on-board ships or submarines, where LM would be used. With these capabilities, LM will be well suited for engineering service bureaus engaged in online/Internet commerce.

Industry is adopting today's commercial LM technologies but mostly for use in early product design models and for nonfunctional prototyping of parts. This will change as commercial LM technologies improve, are certified, and can manufacture complex parts with more materials and better dimensional accuracy than with the plastics that are widely and commercially available today. Traditional machine shops with their hazards and noise may be replaced by LM technologies in quiet environments with less exposure to hazardous materials and less waste. LM will move rapid prototyping to rapid manufacturing.

We expect future LM research to achieve part features down to micron scales with specified microstructural and materials properties. This capability will enable fabrication of complex components in one operation with minimal postprocessing and assembly. And someday, we anticipate LM will find its way into the office as your desktop "3D" fax machine.

[1]For these reasons, LM is also referred to as "solid freeform fabrication (SFF)" for its ability to produce complex parts and as "rapid prototyping" because often LM can produce a part more quickly than other means.

# Profiles in Science

## Joseph J. Beaman

Dr. Joseph J. Beaman is the Andersen Consulting Endowed Professor in Manufacturing Systems Engineering at the University of Texas, Austin, where he has been on the faculty since 1979. His particular interest in manufacturing is Solid Freeform Fabrication, which is also known as desktop manufacturing. It is a technology that produces freeform solid objects directly from a computer model of the object without part-specific tooling or human intervention. Professor Beaman has been a principal investigator of the Office of Naval Research.

One of his successful desktop manufacturing approaches is selective laser sintering, where components are built by material addition rather than by material removal. In selective laser sintering, a directed laser beam is used to consolidate individual powder particles in selected regions. Compared to manual manufacturing methods, selective laser sintering is inherently fast. In addition, this process has the potential to produce accurate, structurally sound three-dimensional renditions of objects designed in a computer and to make such objects available to the user in minutes or hours. The benefits of this new process include greatly reduced prototyping cost and design time, and the capacity to achieve, in one operation, shapes that would otherwise require multiple operations or in some cases shapes impossible to manufacture with standard techniques

Professor Beaman is also a founder of DTM Corporation, which specializes in selective laser sintering. This technology is a freeform fabrication technology developed in Beaman's laboratory at the University of Texas at Austin and is the first private commercial venture with the University of Texas' Center for Development, Technology and Transfer.

# Potential Navy Applications for Selective Laser Sintering (SLS) Technology

*Patrick Bergan, Naval Undersea Warfare Center - Division Keyport, Keyport, WA*

## Abstract

Maintaining Navy weapons systems and support equipment is a continuous process, requiring periodic repair and replacement of parts. Procurement of spare parts is becoming increasingly difficult as fewer of the traditional defense suppliers exist. This problem is especially prevalent in the procurement of low quantity, high value, complex metal parts which are traditionally machined, forged or cast. These types of parts have long supplier lead times and high unit costs because of the need to produce complex tooling, forming dies, casting molds and perform Numerical Control (NC) programming. To help maintain equipment and improve lifecycle support in Navy ship and shore facilities, new technologies are needed to reduce the cost and lead-time associated with producing high value metal parts. Selective Laser Sintering (SLS) is a cutting edge, rapid manufacturing technology intended to address this problem. SLS uses a high power laser to fuse metal powder in a layer-by-layer buildup process to produce a part on demand. Potential applications include production of metal spare parts, fabrication of metal molds for plastic parts and creation of complex tooling. SLS technology is still in its infancy, but initial results have been promising and the process clearly has a large number of potential Navy applications.

## Introduction

The mission of the Naval Undersea Warfare Center (NUWC)-Keyport is to test and maintain weapons for a variety of undersea warfare programs. As a part of this function, NUWC depots must repair or replace components from weapons systems damaged by corrosion, wear and other problems. Due to the complexity of the parts and difficulties in finding sources of manufacture, procurement of new replacement parts is often a time consuming and costly process.

To help meet this challenge, NUWC-Keyport is constantly looking at new technologies and processes to improve

the repair and fabrication of weapons components. One innovative technology that has potential for helping with this problem is the Selective Laser Sintering (SLS) process. SLS is a new manufacturing technology which uses rapid prototyping techniques, in combination with conventional Hot Isostatic Pressing (HIP), to produce actual metal parts, not just plastic prototypes. The goal of the SLS project is to develop a rapid manufacturing process for creating high value, metal parts - traditionally produced by conventional casting, forging or machining processes.

The SLS project team contacted NUWC in 1997 to look at the possibility of applying the SLS process to weapons components and more conventional shipboard parts. Initial metallurgical results produced in the first phase of the project showed that the basic SLS process had good potential. These results, in combination with the inherently rapid build-up process, showed that SLS technology holds promise as a method to rapidly produce replacement parts.

# SLS Background

SLS uses a revolutionary process, patented by the University of Texas, for solidifying layers of metal powder into an actual part using a high power laser. The SLS technique builds the part layer by layer in a process similar to that used by Stereolithography equipment. A layer of powdered metal is deposited on a work surface. A high power laser fuses the powder in the proper shape for each "slice" of the part. Successive layers are produced in this manner until the part is complete.

Normally if a metal powder is completely melted, the surface tension of the liquid metal causes the material to "pool" together, destroying the geometry of the cross-section. The SLS process uses an innovative technique for preventing this from happening. This problem is avoided by using a laser to totally fuse only a thin outside layer of each slice. The interior of each slice is only partially fused- allowing the cross section to maintain the proper geometry.

After SLS processing, the part is not yet complete. At this point, the part consists of a porous interior encapsulated by an impermeable shell (Figure 1). This shell acts as a self-contained "can" for the follow-on Hot Isostatic Pressing (HIP) operation. Using a conventional HIP process, the porous portion of the part is compressed to full density using hot pressurized gas. The impermeable shell acts as a mold or forming die for the HIP operation.

Unlike conventional Stereolithography, which produces a prototype facsimile of a part, the end product of SLS is an actual metal part. Not all part features can be produced in this manner. Features such as tight tolerance holes, threads and fine surface finishes may require subsequent machining. However, the SLS process would be beneficial for producing parts with complex contours, normally requiring castings, forgings or complex machining.

**Figure 1**
*Image of "Canned" SLS Part.*

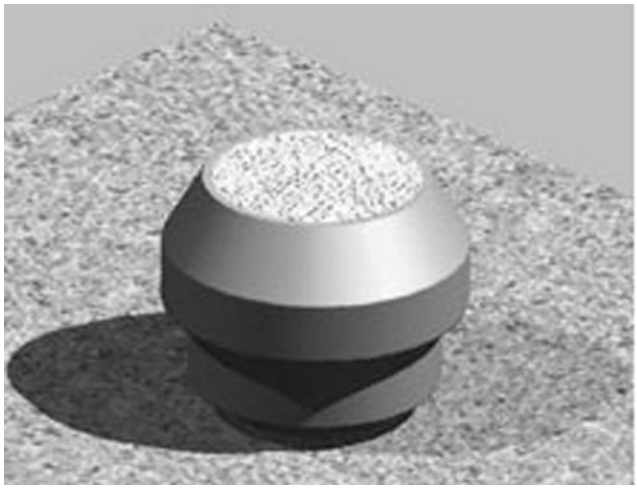

# Potential Navy Applications of SLS

The SLS process is appealing to the Navy because of the potential to quickly produce replacement parts. During regular maintenance on torpedoes and other weapons, NUWC depots constantly use replacement parts from component inventories. As parts are consumed, spare parts inventories need to be constantly restocked. Often, these parts are weapons components with unusual shapes and features to meet tight packaging and functional requirements. Additionally, these parts often use exotic materials to minimize corrosion and meet high structural or temperature requirements.

With these types of requirements, replacement parts are often difficult to procure. Sources of supply and manufacture are becoming increasingly difficult to locate. Parts often require complex tooling, forming dies or casting molds for conventional manufacturing processes, adding significant cost and production lead-times to the part acquisition. This problem is compounded when emergency replacements are required for out of stock spare parts. In this situation, procurement of parts in small quantities often results in very high unit cost and unsatisfactory lead times. With smaller weapons inventories, this problem becomes more prevalent as smaller lot sizes of parts are procured.

Repair and replenishment problems are not limited to just weapons components, but also occur in ancillary support equipment and more common shipboard components. Many of these systems can contain high value metal parts requiring periodic repair or replacement. In many cases, spare parts inventories may not exist because of the unique nature of the part or an infrequent need for replacements. When fully developed, rapid manufacturing techniques, like SLS,

could significantly help reduce equipment downtime by producing parts needed for unexpected repair work.

SLS could also be applied to the creation of tooling to support conventional manufacturing processes. Molds needed to produce complex rubber or plastic components can be expensive and time consuming to produce. Undersea weapons and support equipment utilize a considerable number of custom, unique cable connectors and other plastic parts. Similarly, shipboard equipment can contain a number of different types of plastic or rubber parts, which may not be on hand for emergency replacement. If the part is out of stock and the original manufacturer is not available, molds may need to be produced for emergency replacements. In these situations, the need to produce molds can make for extremely high unit costs and long replacement lead times.

Tooling is usually a significant cost for parts produced conventionally by Computer Numerical Control (CNC) machining. By their nature, parts produced using CNC equipment typically can contain complex features and geometry. Similarly, the "workholding" tooling and fixtures needed to support the part during machining can be complex. For one time replacement of parts or small lot sizes, the expense and time needed to produce support tooling often extends the replacement part cost and schedule. Applying a rapid manufacturing process like SLS to the creation of CNC tooling could benefit another problem area in producing replacement parts.

**Figure 2**
*MK 46 Rotary Valve.*

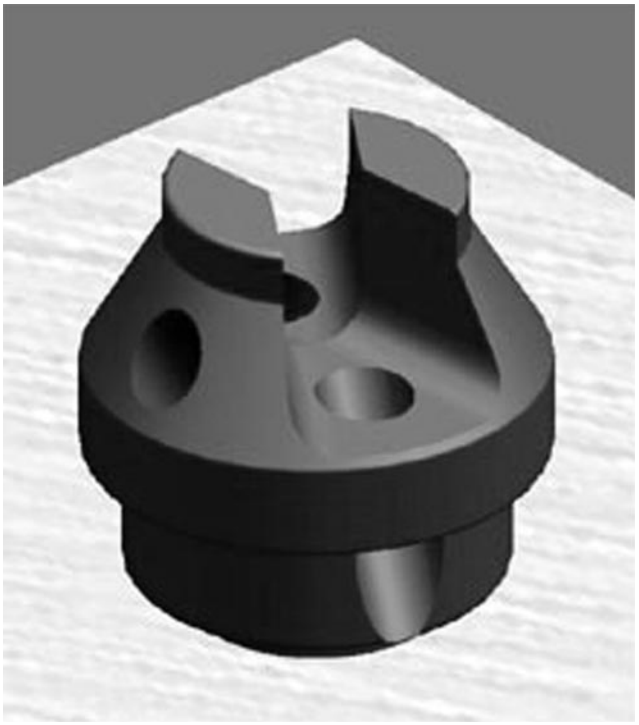

# Typical Part Applications

SLS would provide the greatest benefit in producing high value parts with complex features or difficult tooling requirements. In the undersea warfare arena, there are many examples of this type of part. Components within a torpedo must meet many difficult requirements. Parts must endure high stresses due to pressure at depth and a corrosive environment from seawater and torpedo fuel. Many parts must withstand very high temperatures during test runs. To meet all functional requirements and fit in a very physically confining package, many of the parts have unusual geometries. As a result of this, conventional machining or casting of these parts typically requires a considerable investment in tooling, setup time and machine time.

An example of this type of part is the Rotary Valve utilized in the Lightweight (MK 46) Torpedo (shown in Figure 2). During a torpedo run, this part functions as a timing valve to direct torpedo fuel in the proper sequence to the torpedo cylinder barrel. The part must withstand high temperatures, high fuel pressures and function in a corrosive environment. The Rotary Valve is currently fabricated out of Molybdenum in a powder metallurgy process. Critical areas on the valve are then subsequently machined to tolerance.

Conventionally, this part would require an expensive forming die to be produced. With the free-form fabrication abilities in SLS, the raw shape of the part could be produced without tooling with some minor subsequent machining operations. The time spent in sintering, subsequent HIP processing and follow on machining could possibly be accomplished in days rather than weeks.

A similar example of a high value, complex shaped part is the Radius Boot (shown in Figure 3). This part is used on submarines to pay out wire attached to Towed Array equipment. The Radius Boot must withstand a corrosive sea water environment and exhibit excellent wear resistance.

Currently, this part is fabricated out of Titanium in a CNC machining process using custom-built cutting tools. This is another example of a part which would be difficult to produce quickly in an emergency replacement scenario. In this case, it would clearly be a benefit if a rapid manufacturing process, like SLS, could produce this type of part without the need for custom cutting tools or workholding fixtures.

SLS technology would not only be beneficial in directly producing parts. Another potential use of SLS would be in the production of general tooling for CNC machining or molds for plastic parts. Undersea weapons programs use many types of custom plastic parts produced by plastic injection molding. As is the case with other torpedo parts, these parts typically have unusual geometries and tight tolerances.

The ADCAP A-Cable (shown in Figure 4) is just one example of a part used with the peripheral equipment of the

**Figure 3**
*Radius Boot (Section View).*

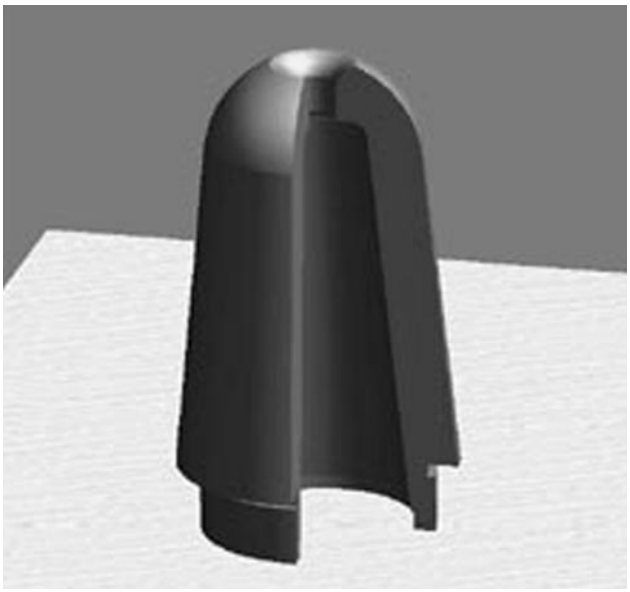

torpedo. The connector end of the A-cable is plastic injection molded around a "bed" of connector pins and other electrical components. The molds to produce this part are expensive because the geometry of the connector body is complex and the tooling must hold the internal connector components precisely during the molding process.

The A-Cable mold was machined conventionally requiring a great deal of cost and a long lead-time. If this part could be produced in an SLS process, considerable time and expense could be avoided. This would be especially beneficial in instances where replacement parts which do not have any tooling available must be made.

**Figure 4**
*A-Cable Connector Mold.*

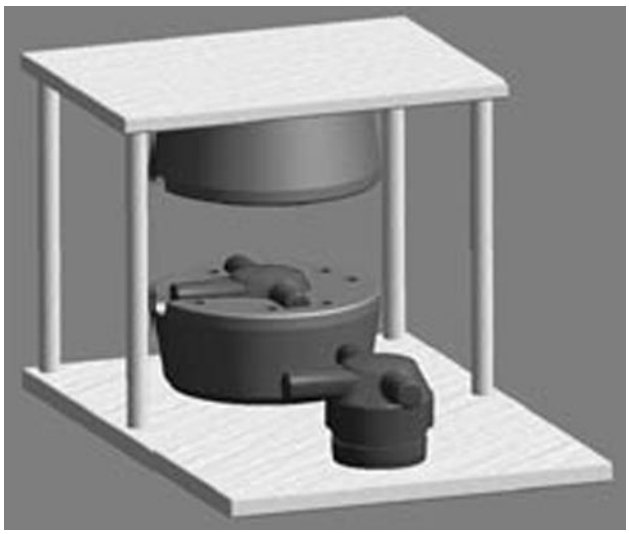

# Closing

The Rotary Valve, Radius Boot and A-Cable connector are typical examples of parts needing periodic replacement or repair. Within all the systems on board ships, submarines and on shore stations, there are certainly numerous quantities of high value, complex parts contained in Navy equipment. In an era of declining defense budgets and fleet reductions, maintaining weapons systems, support equipment and stocking spare parts inventories will be more challenging in the future. Provisioning of replacement parts becomes more of a problem as fewer of the traditional commercial sources exist to produce replacement parts. New technologies and processes are needed to enable high value parts to be produced on demand.

The ability to make actual parts or tooling from a variety of materials in days, rather than weeks or months, makes SLS a potentially valuable tool. While the SLS technology is still in its infancy, this type of rapid manufacturing technology clearly has potential to address some maintainability problems for the Navy.

Currently, the SLS project is in the midst of Phase I. The goal of Phase I is to demonstrate and test the metallurgical qualities of the process and refine the basic technology. Initial testing performed on Titanium, Inconel 625 and Mild Steel/Nickel alloys have had promising results. Development work is proceeding on refining surface finishes and improving dimensional control.

Phase II of the project, scheduled to begin in Fiscal Year 1999, will involve the production of a higher power laser sintering station to use in an actual test-bed setting. In this phase of the project, NUWC-Keyport will function as the DOD test-bed for the project. The SLS process will be used to develop process parameters and techniques that can be applied to production of actual components for Navy use.

# Biography

Patrick Bergan is a Mechanical Engineer specializing in the fields of manufacturing technology and mechanical design at the Naval Undersea Warfare Center – Division Keyport. Mr. Bergan initially functioned as the Lead Engineer in the Robotics and Technology Group which successfully implemented several robotic systems and Computer Integrated Manufacturing (CIM) initiatives. Mr. Bergan is currently the Lead Manufacturing Technologist in the Industrial Technology and Operations Department at NUWC-Keyport. In this position, Mr. Bergan is involved in a number of advanced manufacturing technology projects including Selective Laser Sintering, Laser Cladding for Torpedo Repair and a number of mechanical design/manufacturability analysis projects.

# Fabricating Metal Tooling and Metal Parts by 3D Printing

*Emanuel Sachs, Samuel Allen, Michael Cima, Xiaorong Xu, Javier Baños, James Serdy, David Brancazio, and Honglin Guo, Massachusetts Institute of Technology, Cambridge, MA*

## Abstract

Three Dimensional Printing is being used to create metal parts directly by repetitively spreading a layer of metal powder and then selectively joining the powder in that layer by ink-jet printing of a binder material. The printed green part is then removed from the powderbed and furnace post-processed to yield a fully dense metal part which can be used as a tool for subsequent forming operations or can serve as an end-use metal part. This paper focuses on the application to injection molding tooling.

The *in situ* fabrication of cooling channels within an injection mold which are conformal to the molding surface has been shown to result in 15% shorter cycle time while yielding parts with 10% less distortion as compared to a conventional production tool. A "Conformal Cooling Criterion" has been developed to facilitate the design of such cooling channels. Printed textures on the interior of cooling channels have been further shown to be capable of an 8-fold increase in heat transfer coefficients as compared to smooth channels.

With the present materials system, dimensional variability is introduced during the furnace processing and data taken on a set of 20 tools shows that the current tolerance is approximately ±.25%. Surface finish improvements due to improved drop placement accuracy have been demonstrated, allowing for hand finishing of tools. Materials systems are under development with the goals of hardness higher than the current system (30 HRC) and lower shrinkage (better dimensional control).

## Introduction

### Three Dimensional Printing

Three Dimensional Printing (3DP) is a process for the rapid fabrication of three dimensional parts directly from

**Figure 1**
*A schematic diagram of the 3D Printing process.*

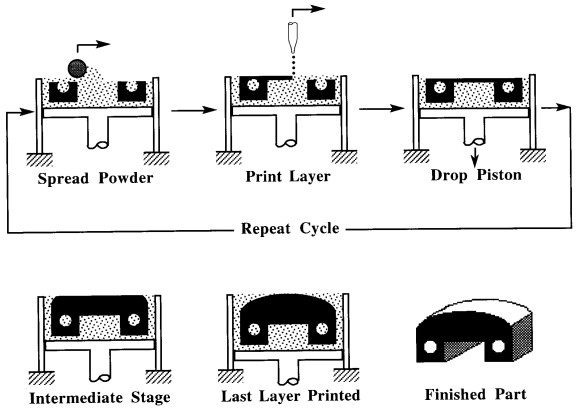


computer models [1,2]. A solid object is created by printing a sequence of two-dimensional layers. The creation of each layer involves the spreading of a thin layer of powdered material followed by the selective joining of powder in the layer by ink-jet printing of a binder material. The powder bed is lowered at the completion of each layer by lowering the bottom of the rectangular cylinder which contains the bed. Figure 1 depicts the steps involved in creating a part. Unbound powder temporarily supports unconnected portions of the component, allowing overhangs, undercuts and internal volumes to be created. The unbound powder is removed upon process completion, leaving the finished part.

3D Printing offers three key features which define its competitive advantages:

• *Geometric Flexibility.* Any geometry can be created with a minimum feature size of 100 microns. The resolution of edge location is approximately 10 microns. Overhangs and undercuts can be created because the powder acts as a support medium for the part under construction.

• *Material Flexibility.* A part can be constructed out of any material which can be obtained as a powder, including ceramics, metals and polymers. The composition of a part may be controlled on a local basis by printing different materials through different nozzles, resulting in the ability to control composition on a 100 micron length scale.

• *Production Rate.* Ink-jet technology may be scaled up using multiple nozzle technology.

3D Printing is being exploited for a wide range of applications including many applications that are being commercialized. Soligen Incorporated of Northridge, CA, provides metal castings made using 3D Printed ceramic molds and cores [3, 4]. Z Corp. of Somerville, MA, provides 3D Printing machines for the office modeling application used to produce models to verify geometry. Therics, Incorporated of Princeton, NJ, is developing various medical applications based on 3D Printing technology. Specific Surfaces of Franklin, MA, is using 3D Printing to create ceramic filters for hot gas filtration. ExtrudeHone Corporation of Irwin, PA, provides machines and services for the fabrication of metal tooling and metal parts by 3D Printing [5]. Several other application areas are under development including fine resolution metal parts and ceramic parts for electronic and structural applications. Military applications under development include: i) ceramic cores for lost-wax casting, ii) dies for injection of ceramic cores, iii) tools for resin transfer molding, iv) die casting tools with conformal cooling, and v) structural ceramic parts for high performance engines.

## Tooling by 3D Printing

This paper focuses on the application of 3D Printing to the fabrication of tooling and specifically to the fabrication of tooling for injection molding. Direct printing of tooling involves the following steps (see Figure 2):

1. Print a polymeric binder into stainless or tool-steel powder. This step defines a green part within the powder bed.

2. Remove the loose powder, thereby revealing the green part (60% dense).

3. Burn out the polymeric binder in a furnace and lightly sinter the part.

4. Infiltrate the part with a copper alloy in a second furnace operation, typically performed at 1100°C. At this point, the part is fully dense.

5. Finish the tooling to achieve desired surface finish and dimensions as required.

**Figure 2**
*Process sequence for creating tooling directly by 3D Printing.*

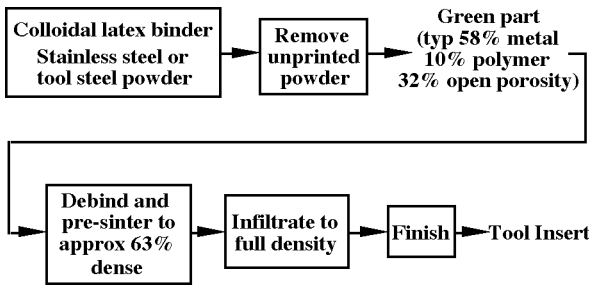


Figures 3a and 3b show the scalability of the process. Figure 3a shows an 8-jet printhead and Figure 3b shows the printed layer which is created by raster scanning the 8-jet printhead over the surface of the powder. Figure 3c shows a set of tooling inserts emerging from the powder bed. Figure 3d shows a tooling insert after sintering. Figure 3e shows the same core, together with its mating cavity after finish-

**Figures 3**

*a) An 8-jet multiple nozzle printhead. b) Printing a layer of binder with a raster-scanned 8-jet printhead. c) Printed tools emerging from the powder bed. d) A core after printing and sintering. e) A finished tool set and a glass filled nylon part injected in it. f) A set of tooling inserts printed for various industrial applications. All tools have been infiltrated and approximately half of the tools have been finished and used to inject parts. For scale, the tool in the lower left hand corner is 150 mm long.*

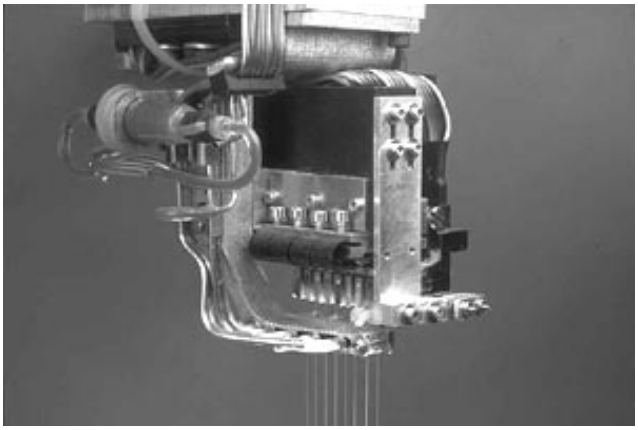

(a)

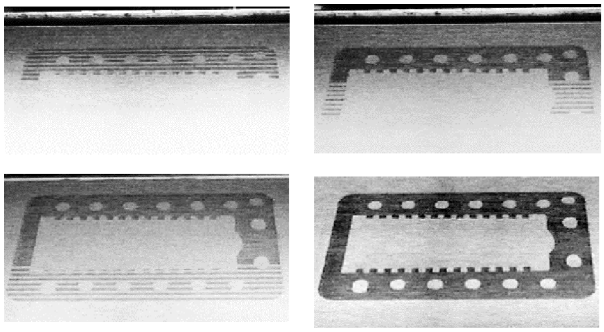

(b)

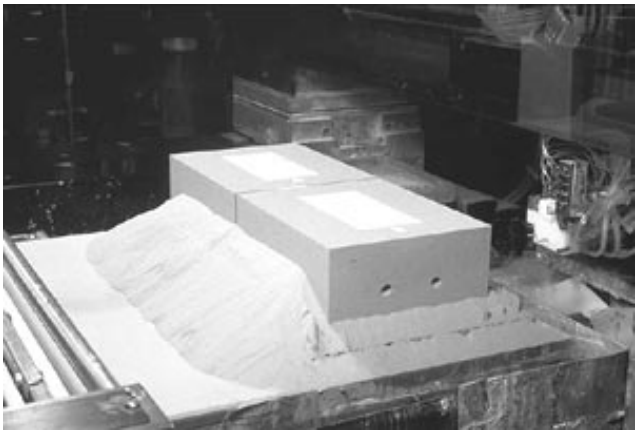

(c)

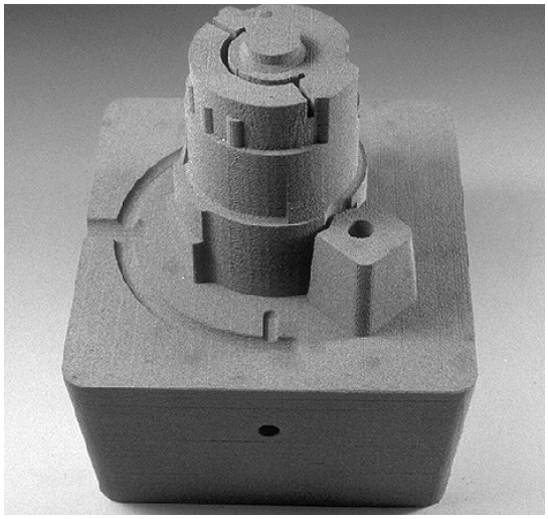

(d)

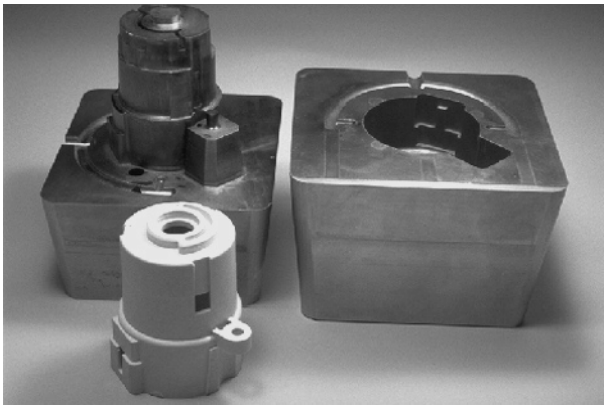

(e)

(f)

ing, together with a glass filled nylon part injected into this cavity.

Periodically, a set of tools is fabricated for our industrial sponsors to serve as a benchmark for our process. The project is currently engaged in the fabrication of the third such set of tools. The results presented in this paper are derived from the second set of tools made. Figure 3f shows a "family portrait" of 14 of 22 tooling inserts made in the second set of tooling. The tool inserts in the foreground have been finished and used to inject plastic parts in materials including glass filled nylon and polycarbonate. Each tool set was designed by a different company and is typically relevant to a different industrial sector. Each company chose to finish the tool set in a different manner ranging from hand polishing to EDM. The tools toward the back of the photo are in earlier stages of processing and some are in the as infiltrated condition. A number of the tool inserts in this photo have conformal cooling channels within them (see below). All the tools were printed with 420 stainless steel powder and a bronze (90 copper, 10 tin) infiltrant. The hardness of these tool inserts is in the range of 25-30 HRC.

# Conformal Cooling

## Performance of Conformal Cooling

Control of internal geometry is one of the key capabilities in tooling made by 3D Printing and this capability has been used to create cooling channels which are conformal to the molding cavity [6, 7]. Such cooling channels have been shown to improve the control of mold temperature, reduce the cycle time and improve the dimensional control of injected parts. Recent work by an industrial sponsor has extended this approach to a high volume commercial product. Figure 4 shows the outline of the mold cavity with a representation of the serpentine conformal cooling channel printed in place (details are absent at the request of the sponsor). This cavity was run in controlled tests against the cavity used in production with the results summarized in bullet form below.

**Figure 4**
*A cavity with a serpentine cooling channel.*

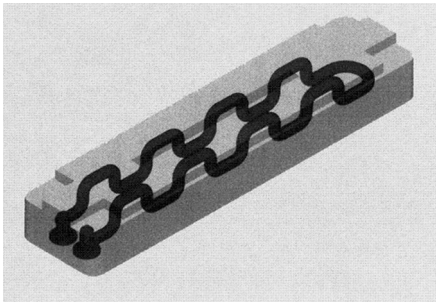

• **At one set of molding conditions, a 15% improvement in cycle time was obtained using the 3D Printed cavity with conformal cooling SIMULTANEOUS with a 9% reduction in part distortion.** It was further noted that the factor limiting even further reduction in cycle time in the cavity with conformal cooling was freezing of the sprue and not the cavity itself, thus offering the potential of further cycle time reduction with a runner system redesign.

• **At a second set of molding conditions, a 37% reduction in part distortion was obtained using the 3D Printed cavity with conformal cooling with the same cycle time as the production tool.**

## Design of Conformal Cooling

To take full advantage of the geometric flexibility of 3D Printing, the design of conformal cooling lines can be quite complex and effort has gone into the codification of this design process. This codification begins with a formal definition of what is meant by conformal cooling lines and follows with tools designed to address the trade-offs associated with the design of these cooling lines.

As the name implies, conformal cooling is used to signify cooling channels which conform to the surface of the molding cavity. However, in this paper, the term conformal cooling has a further significance which is related to the transient heat transfer within the mold. When a mold with conventional cooling channels is started up it takes some time (and many injection cycles) before the mold reaches a steady state operating temperature. With each injection cycle, a heat pulse propagates in from the plastic and eventually the steady sate is reached. However, if the cooling lines are placed very close to the surface, the steady state condition is reached very quickly. In fact, if the lines are close enough to the surface, the steady state is reached after one injection cycle. By our definition, cooling lines are conformal only if they are close enough to the surface to allow the tool to reach a steady state operating temperature within one injection cycle. In the case where the heat transfer between the cooling line surface and the fluid within it is high, a simplified expression for a "Conformal Cooling Criterion" can be obtained as follows:

$$\text{Tool Time Constant} = \frac{\rho c l^2}{K} < \text{Cycle Time}$$

This condition states that the time constant for thermal equilibration of the tool is related to three thermophysical properties of the mold (thermal conductivity, $K$, mass density, $\rho$, and specific heat, $c$) and to the square of the distance from the mold surface to the cooling lines ($l$). When this time constant is less than one injection cycle, steady state will be reached after one injection cycle.

In addition to satisfying the proximity condition embodied in the "Conformal Cooling Criterion", conformal cooling lines must be designed so that: i) the flow be suffi-

**Figure 5**
*a) Drawings of a complex cooling line design in a core. b) A 3D Printed core with conformal cooling lines (see Figure 6a).*

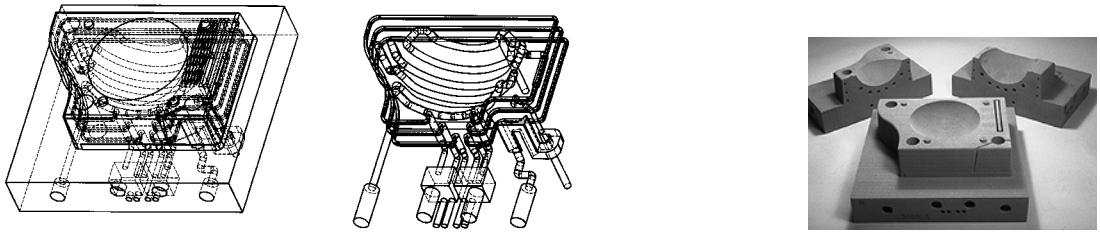

(a) (b)

cient given a maximum allowed pressure drop, ii) the temperature drop along the cooling line not exceed a certain value, say 2°C, iii) the surface temperature of the mold be sufficiently uniform between cooling lines, and iv) the mold have sufficient strength, and low enough deflection over the cooling channels. These conditions may be expressed in mathematical form and used to develop specific designs. Figures 5a and 5b show the result of the application of these methods to a complex injection molding core.

## Heat Transfer Augmentation

In order for cooling channels to be effective either in standard cooling geometries or in conformal cooling geometries, there must be effective heat transfer between the wall of the cooling channel and the fluid within it. Conventional wisdom has it that the flows within the cooling channels must be turbulent so as to provide the high heat transfer coefficients required. However, turbulent flows require high flow rates and significant pumping requirements. In order to reduce the pumping requirements, the use of heat transfer augmentation features was investigated. With guidance from the literature on heat transfer augmentation, 14 different surface textures were designed and printed. These textures are all based on ribs which are approximately 450 microns wide and stand 250 microns from the surface. The textures may be grouped into three categories: i) ribs perpendicular to the direction of the flow, ii) ribs at an angle with respect to the flow, iii) V-shaped ribs. Figure 6a shows a schematic of a block made by 3D printing with 4 channels printed within it, each of which has a different surface texture. Figures 6b - 6d show examples of each of the three classes of surface texture. Two controls were also fabricated and tested. In one case, the channel was fabricated by wire EDM so as to produce a smooth surface. In the other case, a channel with no surface texture features was tested in the as printed condition.

The steady state heat transfer performance of the two controls and the 14 surface textures was measured using water as the working fluid over a range of Reynolds numbers from 1,000 to 15,000. Figure 7 shows the measured heat transfer coefficients for the two control channels and the two surface textures with best performance as a function of Reynolds number. As may be seen, the as printed surface roughness itself provides some heat transfer augmentation as compared to the smooth channel. Most significant, however, is that 2 of the V-shaped geometries provide almost an order or magnitude increase in heat transfer coefficient over the performance of the smooth channel. This improvement is observed throughout the range of flow tested which encompasses both laminar and low turbulent regimes (the transition between these regimes is at approximately a Reynolds number of 3,000). The other 12 textures range in performance from not much better than the smooth channel to approximately half the performance observed in the best textured channel. Figure 8 presents data on the pressure drop versus Reynolds number for the same four channels as performance is depicted in Figure 7. As may be seen, there is little or no penalty in pumping requirement for the channels with surface texture.

From this work, it seems that 3D Printed tools could incorporate heat transfer augmentation features which would substantially reduce the pumping requirement by allowing for effective heat transfer even with laminar flow. Further, the scalability of 3D Printing opens up the possibility of utilizing the process to make heat exchangers in small and moderate quantity.

# Dimensional Control

The dimensional control of tooling made by 3D Printing is governed by the furnace processing steps and in particular by uncertainty in the shrinkage during the sintering operation. During the sintering operation there is some shrinkage of the part which is associated with the formation of a skeleton which can subsequently be infiltrated. The CAD file is "prestretched" by the amount of anticipated shrinkage. A green part is then printed and these green parts have been found to conform quite closely to the "prestretched" CAD dimensions. At the present time, the

**Figure 6**
*a) Schematic of a 3D Printed block with channels with surface textures. b) Perpendicular printed ribs on the interior of 5 mm x 5 mm channels for heat transfer augmentation. c) Angled printed ribs on the interior of 5 mm x 5 mm channels for heat transfer augmentation. d) V-shaped printed ribs on the interior of 5 mm x 5 mm channels for heat transfer augmentation.*

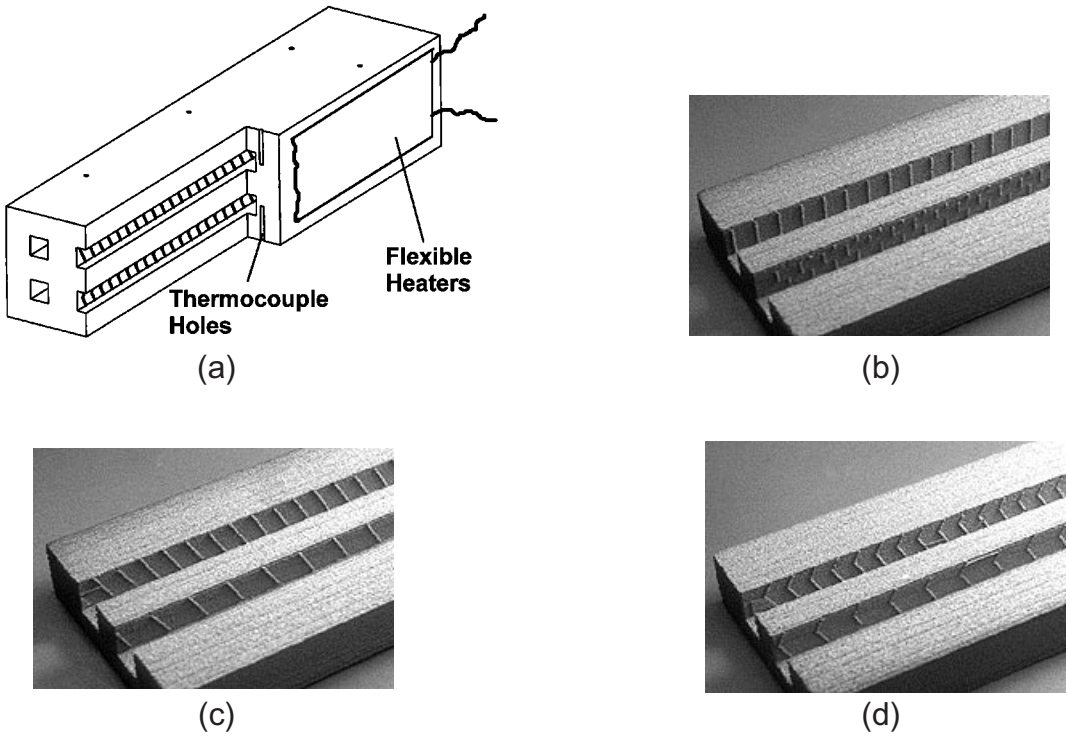


shrinkage during the sintering step is 1.8 ± .25 % (linear), which represents a nominal shrinkage of 1.8% and an uncertainty in shrinkage of .25%. While the nominal shrinkage can be anticipated by "prestretching" the CAD file, the uncertainty in shrinkage dictates a loss of dimensional control which scales with part dimension.

Based on previous observations, a specification range was created which contemplates a multiplicative error which is expected to scale with part size and an additive error which reflects uncertainty in the location of the edges of the part which is not expected to scale with part size. This specification range is illustrated as the trapezoidal shaded region in Figure 9 where the vertical axis is the error in linear dimension (deviation from desired dimension) of the infiltrated tool and the horizontal axis is the length of a particular dimension. The vertical intercepts represent the additive error while the slope of the top and bottom of the spec range represent the multiplicative error.

Figure 10 shows data taken on 18 tools in both the fast and slow axes within the print plane. As can be seen, 81 of the 107 data points lie within the anticipated spec range. Figure 11 shows analogous data for the vertical axis. In this case less data is available but the ratio of 15 out of 21 points (on 6 tools) within the specification range is roughly comparable to the in plane print data. While the results were not quite as good as expected, it does seem that we have come close to defining a proper specification range which anticipates the dimensional control of our tooling. Further, it can be noted that most of the data of Figures 10 and 11 has a positive bias, and so correction of this bias would further improve the results. Nonetheless, the dimensional control

**Figure 7**
*Heat transfer coefficient as a function of Reynolds Number for control and textured channels.*

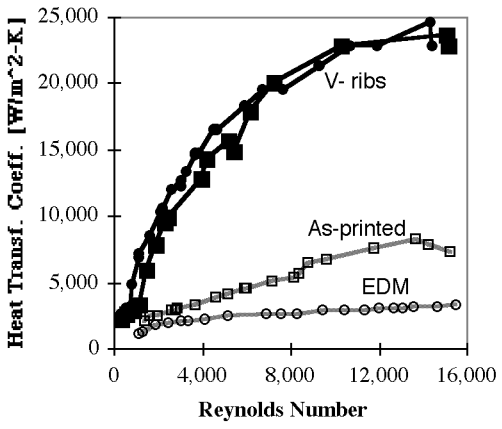

**Figure 8**
*Pressure drops as a function of Reynolds Number for control and textured channels.*

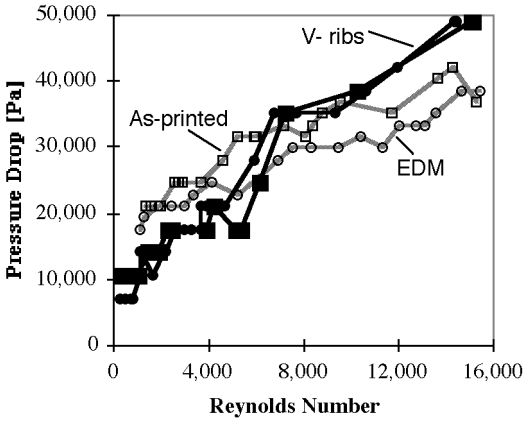


of our tooling is not sufficient for net shape tooling inserts (perhaps by a full order of magnitude). Thus, materials systems with substantially improved dimensional control are a major thrust for this project. The primary thrust is to develop systems which have less shrinkage, on the assumption that the uncertainty in shrinkage will scale with the magnitude of the shrinkage.

**Figure 9**
*Illustration of the specification range for 3D Printed tooling.*

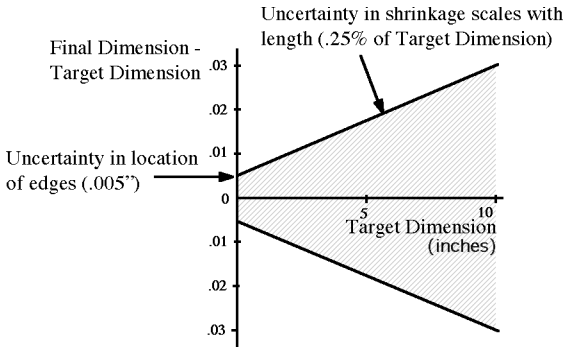


# Surface Finish

Figure 12b shows a detail area of the cavity geometry of Figure 12a created with two different printing approaches. The detail to the right illustrates a significant improvement in surface finish which has been achieved by control of the droplet landing position with 10 micron resolution in each of the two in-layer axes (contrast this with 10 micron x 150 micron resolution in the detail at the left). This achieve-

**Figure 10**
*Data on dimensional control of 3D Printed tooling within the print plane.*

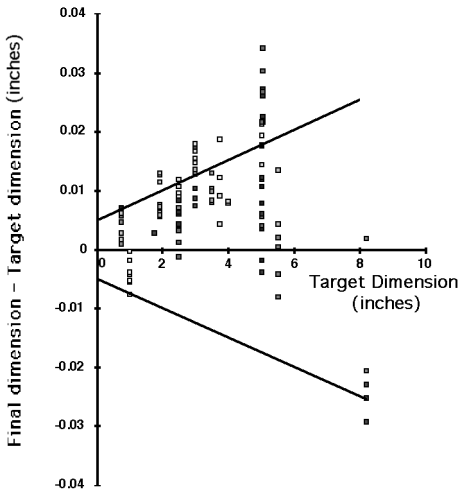


ment represents a combination of new printhead hardware, new software used to create the printing instructions from an .STL model and the integration of on-line measurement used to characterize and adapt to changes in the performance of the printhead [8].

**Figure 11**
*Data on dimensional control of 3D Printed tooling in the vertical axis.*

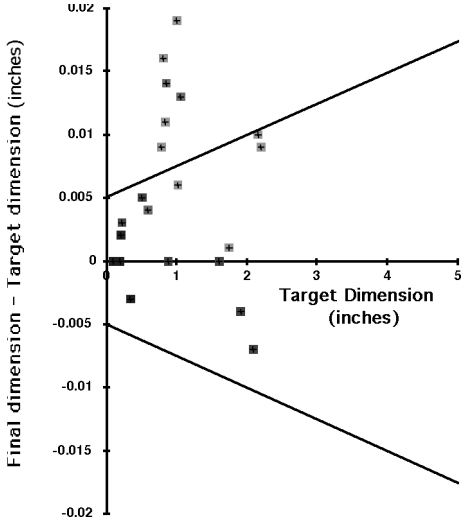


# Harder Tooling

As noted earlier, the current tooling materials system is 420 stainless powder, infiltrated with bronze, a system

**Figure 12**
*a) An infiltrated core and cavity set. b) A detailed view of the "k" in the tool of Figure 21 with low resolution (left) and high resolution (right).*

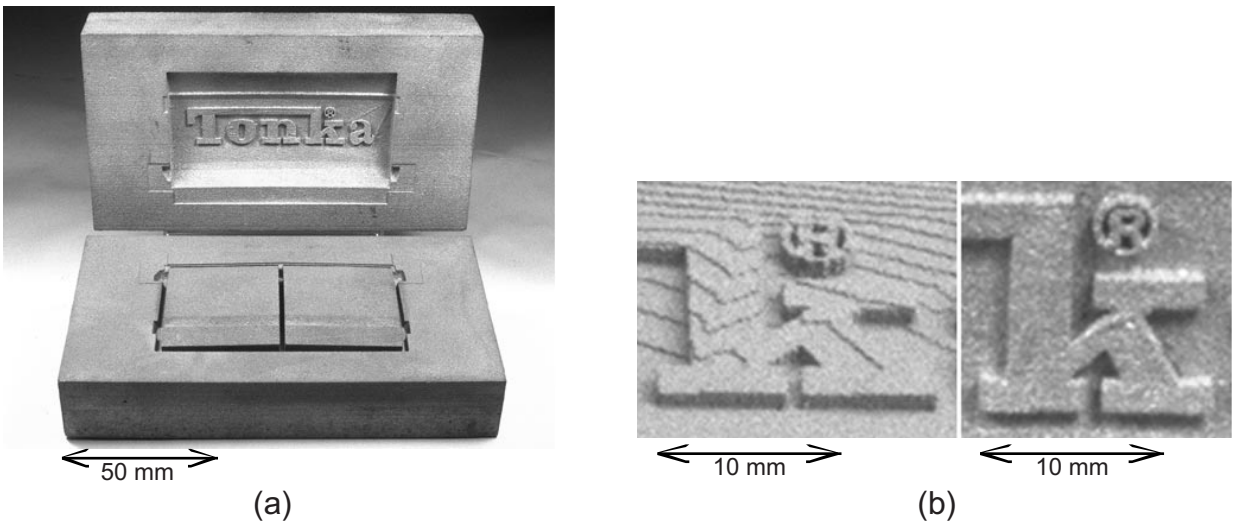


which produces a hardness of 25-30 on the Rockwell C scale. However, this hardness is actually the result of a composite system which has particles which are quite hard (HRC 50+) and infiltrant which is much softer (HRB scale).

A goal of the project is to develop materials systems with higher hardness and with greater uniformity of hardness between powder and infiltrant though the use of hardenable infiltrants. However, when the molten infiltrant contacts the powder, mutual solubility and fast inter-diffusion at the infiltration temperatures can lead to changes in the composition of both powder and infiltrant resulting in a loss of hardenability of both (as well as possible distortion). Thus, an important goal of the project is to understand the interaction of powder and infiltrant, design materials systems which minimize this interaction, and manage any remaining interaction. Toward this end, computer-aided alloy design has been used in the 3DP material system selection. The computer modeling can simulate the thermodynamic interaction of the multi-component 3DP system at any temperature. The simulation results show the mole fraction of each phase and the composition of each phase at equilibrium state. In addition, the simulation can also show the melting point of the infiltrant, the phase transformation temperature and the effect of an additive element on the thermodynamic equilibrium.Good agreement between the computer calculation and experimental result has been obtained for the interaction of the 420 stainless/bronze system. This tool is now being used to design alloy systems.

# Conclusions

Three Dimensional Printing is being applied to the fabrication of tooling directly from a computer model using metal powders. Stainless steel powder is spread and a polymeric binder is ink-jet printed to define a green part which is removed from the powder bed. The binder is burned out and the part lightly sintered. The porous preform is then infiltrated with a copper alloy to produce a fully dense part. This paper reports on results attained on a set of approximately 20 tooling inserts, ranging in size from 5 cm to 20 cm in length. The tools were fabricated using hardenable stainless steel powder with a resultant tooling hardness of 25-30 Rockwell C. Significant improvements in surface finish were obtained using improved printing technology with the result that tools could be finished by hand and used to inject parts. Dimensional control of tools conformed well to the expected result of being dominated by control of shrinkage and being predictable to within ± .25%.

Thermal management of the tool is a crucial component of injection molding, substantially determining the cycle time and part quality for a given part design. The ability of the technology to create internal geometry has been exploited in the form of cooling channels which are conformal to the molding cavity. Such channels have been shown to result in substantial improvements of production rate and part quality when compared to conventional tooling. Methodologies for the design of tools with complex conformal cooling lines have been developed. Especially important is the development of a "Conformal Cooling Criterion" which provides an upper limit to the spacing between the molding cavity and the cooling line. Order of magnitude improvements in heat transfer coefficients have been demonstrated through the use of printed-in-place surface textures on the channels. In the future, such heat transfer enhancement can result in substantially reduced pumping requirements.

Critical areas for the technology center around the de-

velopment of new materials systems. Work is under way on the development of low shrinkage systems in order to improve dimensional control and on the development of alloy systems with higher hardness. 3D Printing of tooling and metal parts is being commercialized by ExtrudeHone Corporation of Irwin, PA.

# Acknowledgments

Support for this work from the Technology Re-Investment Project, Cooperative Agreement (DMI - 9420964), members of the Three Dimensional Printing Industrial Consortium and the DARPA/ONR Solid Freeform Fabrication program under contract #N000149410832 is gratefully acknowledged.

# Biographies

Emanuel Sachs is Professor of Mechanical Engineering and specializes in the design of manufacturing processes. He is a co-inventor of the Three Dimensional Printing Process for the creation of 3D parts directly from a computer model by a layered building process. Prior to joining the faculty, Dr. Sachs spent seven years working in the field of photovoltaics (solar cells), including 2 years at Mobil-Tyco Solar Energy Corp, and 5 years at Arthur D. Little, Inc. Dr. Sachs is the author or co-author of more than 80 technical papers and is the inventor or co-inventor of more than 25 patents. Dr. Sachs was awarded the B.S., M.S. and Ph.D. degrees, all in Mechanical Engineering and all from MIT in 1975, 1976, and 1983, respectively. Dr. Sachs was a Hertz Fellow and earned the Hertz Foundation Doctoral Thesis Prize in 1983. Together with co-workers, Dr. Sachs was awarded an IR&D 100 award in 1994 for his work on 3D Printing.

Samuel M. Allen is Professor of Physical Metallurgy in the Department of Materials Science and Engineering at M.I.T. He was educated at Stevens Institute of Technology (B. Eng., 1970) and at M.I.T. (S.M., 1971; Ph.D., 1975). In 1976, Prof. Allen was Visiting Lecturer at the University of California, Berkeley. After several years as a Research Associate at M.I.T., he joined the M.I.T. Faculty in 1979. He worked for Nippon Steel Corporation in Kawasaki, Japan for the 1987-88 academic year, and was Visiting Professor at Hiroshima University in 1989. His research interests include phase transformations, solid/solid interfaces, structure/property relations in high-temperature alloys, three-dimensional printing of metal tools for plastic injection molding, and alloys for high-strain actuators. Prof. Allen is co-authoring with his colleague Ned Thomas an undergraduate textbook "The Structure of Materials," to be published by John Wiley & Sons in December, 1998.

Michael Cima is a Professor of Materials Science and Engineering at MIT. He earned a B.S. in chemistry in 1982 (phi beta kappa) and a Ph.D. in chemical engineering in 1986, both from the University of California at Berkeley. He received the Norton chair at MIT in 1988. Prof. Cima became Director of the Ceramics Processing Research Laboratory in 1989 and received a tenured appointment from MIT in 1992, and was promoted to full Professor in 1995. He was elected a Fellow of the American Ceramics Society in 1997 and has recently been awarded the Sumitomo Electric Industries Chair at MIT. His general research interests include: powder processing, ceramics processing, slurry and ink formulation, ceramic thin films, and ceramics manufacturing. He is author or coauthor of over one hundred scientific publications and six patents. Prof. Cima is also a coinventor and coprincipal investigator on MIT's 3D printing process and has recently applied this technology to drug delivery systems.

Xiaorong Xu received his B.S. degree in precision engineering from the University of Science and Technology of China in 1992 and M.S. degree in mechanical engineering from the State University of New York at Stony Brook in 1995. He is currently a Ph.D candidate at the Lab for Manufacturing and Productivity, Department of Mechanical Engineering, Massachusetts Institute of Technology. His research interests include precision instrumentation, polymer processing, process development and control, solid freeform fabrication, CAD and Internet application.

Javier V. Baños has a Bachelor of Science and a Master of Science degree in Mechanical Engineering, both from MIT. As a graduate student, he worked as a research assistant at MIT's Three Dimensional Printing Laboratory, where his work focused on the application of the 3D Printing technology for building heat transfer-enhancing cooling channels on metal surfaces. Mr. Banos was the recipient of a National Science Foundation Graduate Fellowship, and currently works as an analyst for Arthur D. Little, Inc.

James Serdy, Sponsored Research Technical Staff with the Laboratory for Manufacturing and Productivity, has been working with the 3DP project for the past 7 years. Prior professional experience includes production managment with Sintered Metals Corp. and R & D in solar photovoltaics with Arthur D. Little, Inc. and with Mobil/Tyco Laboratories.

David Brancazio received his B.S. and M.S. degrees from MIT in '89 and '91, respectively, and since then has held the position of Assistant Laboratory Director for the Three Dimensional Printing Laboratory. During this period he has designed and/or coordinated the design of major pieces of equipment including the main 3D Printing machine, developed and maintained this equipment, conducted research projects, coordinated lab and machine throughput, coordinated student activity and projects, and worked with sponsors and licensees.

Honglin Guo is currently a Yield Enhancement Engineer at Texas Instruments, working in the Semiconductor Group. In December of 1997, he completed a Ph.D. in metallurgy on post processing and materials selection for 3-D

Printing, under the direction of Samuel Allen and Emanuel Sachs at the 3DP Lab at M.I.T.

# REFERENCES


1. Sachs, E., Haggerty, J., Cima, M., Williams, P., "Three Dimensional Printing Techniques", US Patent # 5,204,055, April 20, 1993.
2. Sachs, E., Cima, M., Williams, P., Brancazio, D., and Cornie, J., "Three Dimensional Printing: Rapid Tooling and Prototypes Directly From a CAD Model", *Journal of Engineering for Industry*, Vol. 114, No. 4, November 1992, pp. 481-488.
3. Sachs, E., Cima, M., Bredt, J., Curodeau, A., "CAD-Casting: The Direct Fabrication of Ceramic Shells and Cores by Three Dimensional Printing", *Manufacturing Review*, Vol. 5, No 2, June 1992, pp. 118-126.
4. Sachs, E., Curodeau, A., Gossard, D., Jee, H., Cima, M., Caldarise, S., "Surface Texture by 3D Printing", *Proceedings of 1994 Solid Freeform Fabrication Symposium*, Austin, TX, August 8-10, 1994, pg. 56-64.
5. Michaels, S., Sachs, E., Cima, M., "Three Dimensional Printing of Metal and Cermet Parts", *Proceedings P/M²TEC '94 Conference - Advances in Powder Metallurgy and Particulate Materials*, May 8-11, 1994, Toronto, Canada.
6. Sachs et al., "Production of Injection Molding Tooling with Conformal Cooling Channels using The Three Dimensional Printing Process", *Solid Freeform Fabrication Symposium Proceedings*, August 7-9, 1995, pp. 448-467.
7. Sachs, E., Allen, S., Cima, M., Wylonis, E., and Guo, H., "Production of Injection Molding Tooling with Conformal Cooling Channels using The Three Dimensional Printing Process", to appear in *Polymer Engineering and Science*.
8. Sachs, E., Brancazio, D., Milner, J., Bredt, J., Serdy, J., Curodeau, A., "High Rate, High Quality 3D Printing through Machine Design, On-line Measurement, and Control", to appear in *International Journal of Machine Tools and Manufacturing.*

# Novel Applications and Implementations of Shape Deposition Manufacturing

*Fritz B. Prinz, Stanford University, Stanford, CA*
*Lee E. Weiss, Carnegie Mellon University, Pittsburgh, PA*

## Abstract

Shape Deposition Manufacturing (SDM) is a solid freeform fabrication (SFF) process that incrementally builds up complex parts by systematically combining material additive processes with material removal processes. The advantages of each type of process are thus combined such that novel structures can be fabricated with SDM that could not be practically fabricated with either material additive or material removal processes alone. Examples of such structures, which are relevant to Navy/DOD applications, are described in this paper including a waterproof wearable computer with embedded electronics, a composite steel/copper injection mold tool, and a miniature turbine wheel assembly. In addition, this article presents a novel implementation of a SDM system based upon the integration of deposition apparatus (i.e., material additive process) with an existing computer-numerically-controlled (CNC) milling machine (i.e., a material removal process). Such an implementation is a cost-effective way to create high-quality SFF machines.

## 1. Introduction

Most solid freeform fabrication (SFF) systems are based upon a material additive, layered manufacturing method. Computer-aided-design (CAD) models are first decomposed into thin cross-sectional layer representations, then physical parts are built up in custom automated fabrication machines, layer-by-layer, using material additive processes (1). Layers of sacrificial structures are simultaneously built up to fixture and support the growing shapes. While layered manufacturing facilitates rapid prototyping (e.g., quickly fabricating "models", as opposed to production parts) of arbitrarily complex shapes, the resulting surface finish and accuracy, which are critical factors for being able to fabricate functional parts, are compromised by the "stair-steps"

**Figure 1**
*Shape Deposition Manufacturing.*

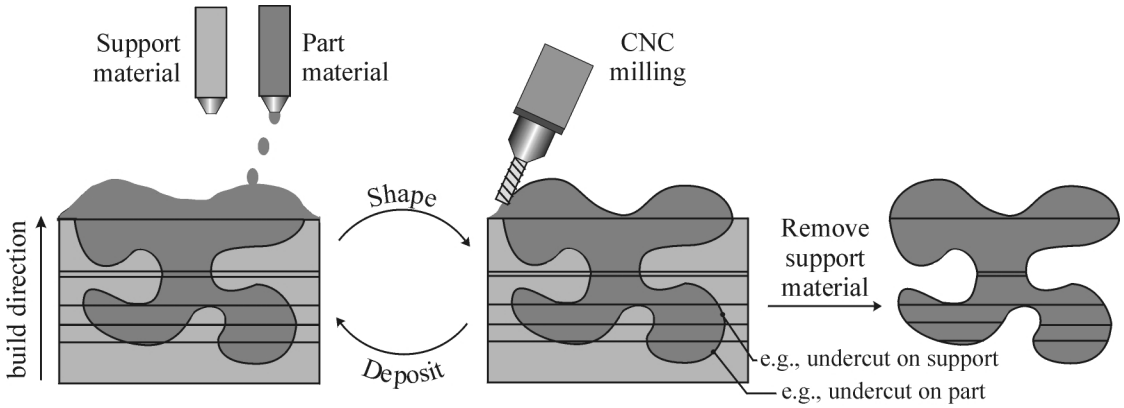


from layer-to-layer. High accuracy and quality surface finishes, required for such applications as custom tooling, precision assemblies, and structural ceramics, are best achieved with material removal processes such as 3- and 5-axis computer-numerically-controlled (CNC) milling and electrical discharge machining (EDM) machines.

Shape Deposition Manufacturing (SDM) is a SFF process for which the original goal was to combine the advantages of geometry decomposition and material addition with the advantages of material removal processes (Figure 1). The basic SDM fabrication methodology is to deposit individual segments of a part, and of support material structure, as near net shapes, then machine each to net-shape before depositing and shaping additional material (2). This method takes advantage of the basic SDM decomposition strategy which is to decompose shapes into segments or 'compacts', such that undercut features need not be machined, but are formed by depositing onto previously deposited and shaped segments. For example, undercut part features are formed by depositing onto shaped support material compacts, and vice-versa. In addition, the decomposition plan preserves the 3D-geometry information of the outer surface of each compact so that the desired shape of the CAD model can be accurately replicated when 5-axis machining is available. Each compact in each layer is deposited as a near-net shape using one of several available deposition processes that are described in subsequent sections. The thickness of each compact depends not only on the local part geometry, but also on

**Figure 2**
*Multi-material structures with embedded components. (a) Example of a heterogeneous structure. (b) Sequence for depositing and shaping; each compact is deposited, then shaped before proceeding to next compact.*

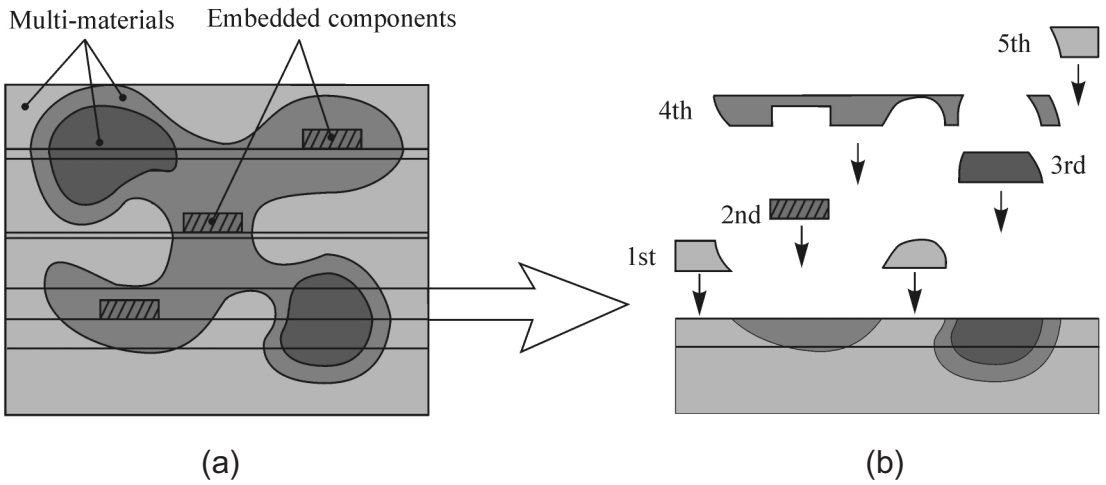

deposition process constraints. After the entire part is built up, the sacrificial support material is removed to reveal the final part.

In addition to the rapid prototyping of complex shapes, selective additive material processing enables the fabrication of multi-material structures and it also permits prefabricated components to be embedded within the growing shapes as depicted in Figure 2a. Another goal of SDM research is to investigate how the capability to fabricate such heterogeneous structures enables the manufacture of novel product designs (3). An example of the compact splitting strategy and sequence for depositing and shaping materials for a typical layer of a heterogeneous structure is depicted in Figure 2b. Note how depositing onto the machined surface of one compact forms the undercut surface of another compact on top of the first compact. Several examples of heterogeneous designs are described in subsequent sections including a waterproof wearable computer with embedded electronics, and a composite steel/copper injection molding tool. In addition to heterogeneous designs, novel assemblies of parts can also be directly built up with SDM by using sacrificial material to separate the individual parts. An example of a miniature metal turbine assembly is described in this paper.

Another key issue for our research is how to implement SDM in a cost-effective fashion. Until recently, SDM operations have been executed by building up the parts on pallets and transferring them to individual operating stations using a robotic palletizing system (4). Robotic manipulation was used in order to create a flexible system, for an R&D environment, which could be easily modified in order to investigate alternative deposition, shaping or other intermediate processing operations. Such a system, however, is too expensive and large for general dissemination of this technology. The next section describes a novel, cost effective and compact implementation of SDM.

# 2. Integrated CNC Shaping and Deposition Machine

Commercialized SFF systems are customized machines, and high performance SFF apparatus can be relatively expensive. As an alternative to customization, or to robotic automation, we are exploring implementing SDM by simply adding deposition apparatus directly to existing CNC milling machines such as are typically found in machine shops throughout the world. In addition to shaping operations, the CNC milling machine provides the precision

**Figure 3**
*Integrated CNC shaping/deposition machine for SDM. (a) Fadal VMC-15 CNC milling machine with integral extruder. (b) ACR extruder.*

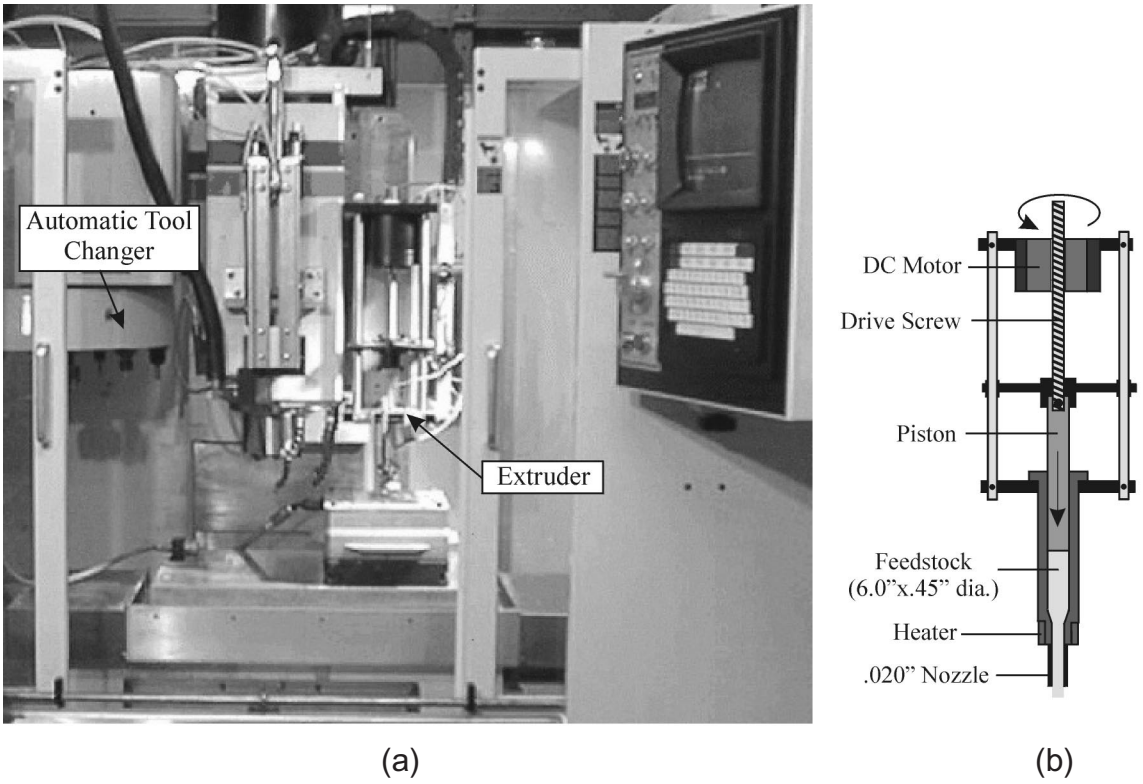

motion control required for deposition. When not being used for SDM, such an integrated CNC deposition and shaping machine can still be used as a conventional milling machine.

For one example, the integrated CNC deposition/shaping machine shown in Figure 3a is being used to investigate the fabrication of 'green' ceramic parts using an extrusion deposition process (5). Green materials, which are deposited by the extruder, are composed of ceramic powders densely bound in polymeric binders. After the green part is built up and removed from the machine, the binder is burned out in a furnace. Then, the part is sintered to fuse the powder to form the final ceramic part. The CNC machine is based upon a commercially available Fadal VMC-15 3-axis mill with an automatic tool changer carousel[1]. An Advanced Ceramics Research extruder[2] is mounted on a pneumatically actuated slide that is attached to the Z-axis spindle housing of the CNC machine. The slide is retracted when the extruder is not in use (e.g., during machining operations) and lowers the extruder into the workspace during deposition operations. The extruder is used to deposit both support and part materials; currently, we manually switch extrusion tubes/nozzles preloaded with the different materials. Being able to quickly build complex ceramic parts is important for many military applications such as components for high-performance miniature turbine engines for drone aircraft.

An example of a 'green' ceramic part built on the integrated SDM machine is shown in Figure 4. The part material is silicon nitride, and the support material is ACR 200, a proprietary non-ionic, water-soluble, machinable thermoplastic. While this particular shape could have been cut directly from a block of 'green' ceramic stock, such conventional machining would require re-orienting, re-fixturing, and registering the part after the top-side has been cut in order to cut the bottom-side. Another advantage of SDM over conventional machining is that first depositing shapes in near-net, before machining, reduces the waste of costly materials.

We have also explored the use of an integrated SDM machine that incorporated conventional welding to directly deposit steel and copper parts (6). We are currently creating an SDM machine for fabricating wax molds for molding gel-cast or thermoset materials (5).

# 3. Multi-Material (Heterogeneous) Structures

We believe that one of the most important roles for SFF in the future will be to help manufacture heterogeneous product designs. Several of these novel products that have been built with SDM are described below. While conventional manufacturing methods could have been used to fabricate these products, these methods would have required additional time-consuming operations, including the need for custom fixturing and tooling, complex assembly operations, and high-strength material joining processes.

## 3.1. Steel/Copper Tooling

Injection molding is the process of forming plastic parts by first flowing heated plastic into the cavity of a custom tool (i.e., the cavity is in the shape of the part), then allowing the plastic to cool down and solidify, and finally opening the tool to remove the part. Injection molding is used to mass-produce plastic parts in quantities from hundreds to millions of parts. SFF has been widely investigated for fabricating injection mold tools with complex molding surfaces, as well as with conformal internal cooling channels for thermal management. With SDM, even more advanced tools can be fabricated composed of multi-materials such as steel/copper composites. While steel provides strength and wear-resistance, copper's superior heat transfer properties provide quick heat up and cool down of the tool as well as uniform heat-

**Figure 4**
*Example of a part built with an integrated SDM CNC shaping/deposition machine. (a) Green $Si_3N_4$ part. (b) Part after pressureless sintering in $N_2$ at 1750°C.*

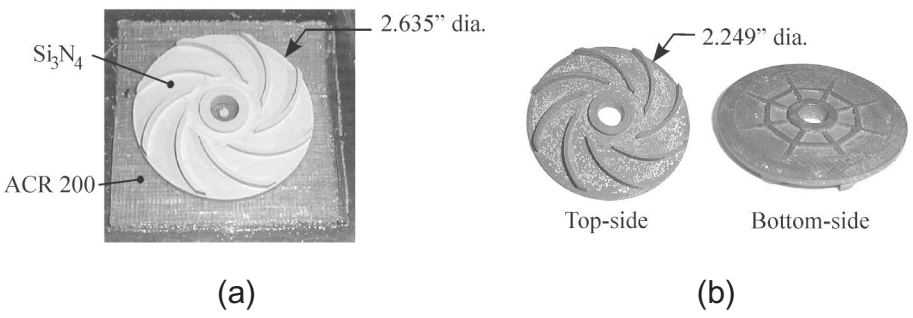


[1]Fadal Engineering, Chatsworth, CA.

[2]The extruder and the feedstock materials are manufactured by Advanced Ceramics Research Corporation, Tucson, AZ.

**Figure 5**
*Multi-material metal structures built with SDM. (a) Multi-material injection mold tool. (b) Schematic of one half of tool. (c) Laser welding process. (d) Microcasting apparatus.*

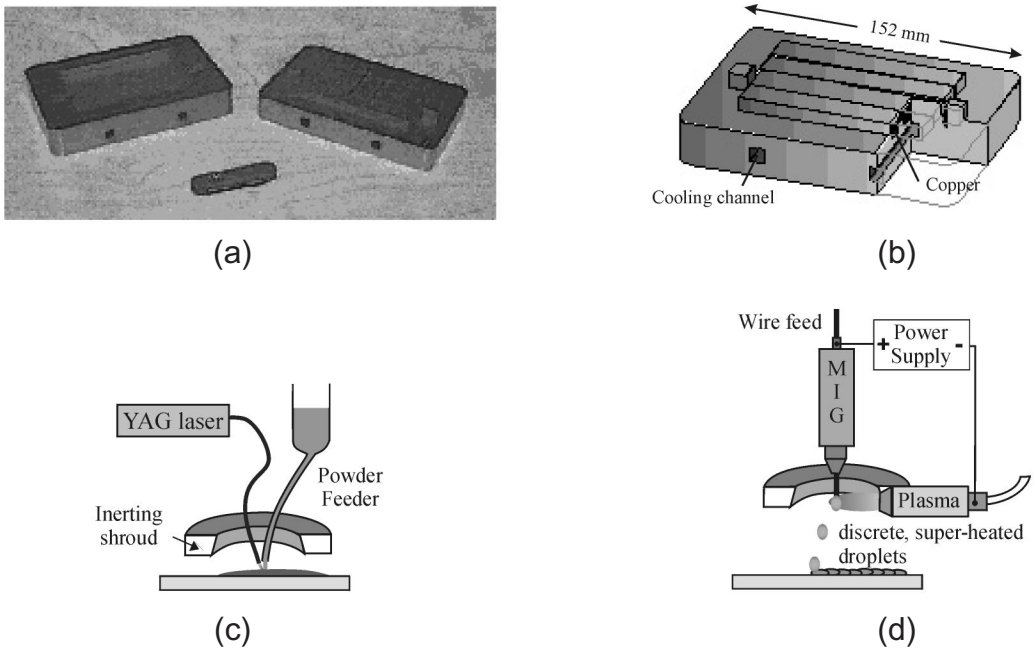


ing. For example, Figure 5a shows a composite 316L stainless steel injection molding tool produced by SDM using robotic-controlled laser welding and microcasting deposition processes (7). One half of the tool, which is shown schematically in Figure 5b, has four internal copper deposits for temperature equilibration. Both halves of the tool have a "U"-shaped channel for water cooling during the molding process. The channels were formed by sacrificial copper, which was removed by etching in nitric acid. Portions of the cavities contained small features that could not be cut with end mills and these were finished with EDM.

In this tool, the steel was deposited with a laser welding process (Figure 5c). A 2.4 kW CW Nd:YAG laser scans over the substrate and a melt pool forms into which metal powder is injected (Figure 5c). The injected powder fuses onto the substrate, leaving a bead of deposited material in its wake. While this laser welding process is very precise, in comparison with conventional welding methods, it cannot effectively deposit copper due to copper's high reflectively. Therefore, microcasting was used to deposit the copper (Figure 5d). Microcasting is a non-transferred welding process that deposits discrete droplets of super-heated molten metal (6).

In addition to creating steel/copper structures, the laser system has also been used to deposit INVARTM, a low coefficient-of-thermal-expansion (CTE) nickel alloy, onto copper that was previously deposited onto steel. Such multi-material structures will have significant advantages in a wide variety of military applications. For example, in dies used for forming composite airfoils (e.g., for airplane and boat bodies), INVAR provides a closer match to the CTE of composite materials, thus resisting deforming the material during molding operations.

Ideally, the transition between different materials should be functionally graded, e.g., having a gradual change in material composition from one material to the next material. The laser system is particularly suitable for producing functional-gradient, multi-material parts because different materials can be continuously alloyed during the build process by simply mixing the powders which are fed to the melt pool.

## 3.2. Embedded Electronics

Another example of a heterogeneous design is an embedded electronic device fabricated by building up a non-conductive housing package and simultaneously embedding and interconnecting electronic components within the housing. With this approach it is feasible to relatively quickly fabricate compact, rugged, customized computer modules in small lot sizes. This capability is particularly well suited for military applications, to manufacture mission-specific, conformal shaped 'smart' devices such as wearable computers tailored for an individual soldier or a small military unit.

**Figure 6**
*Embedded Electronics. (a) 'Frogman' computer. (b) Waterproof application. (c) CAD model of 'Frogman'. (b) Deposition apparatus.*

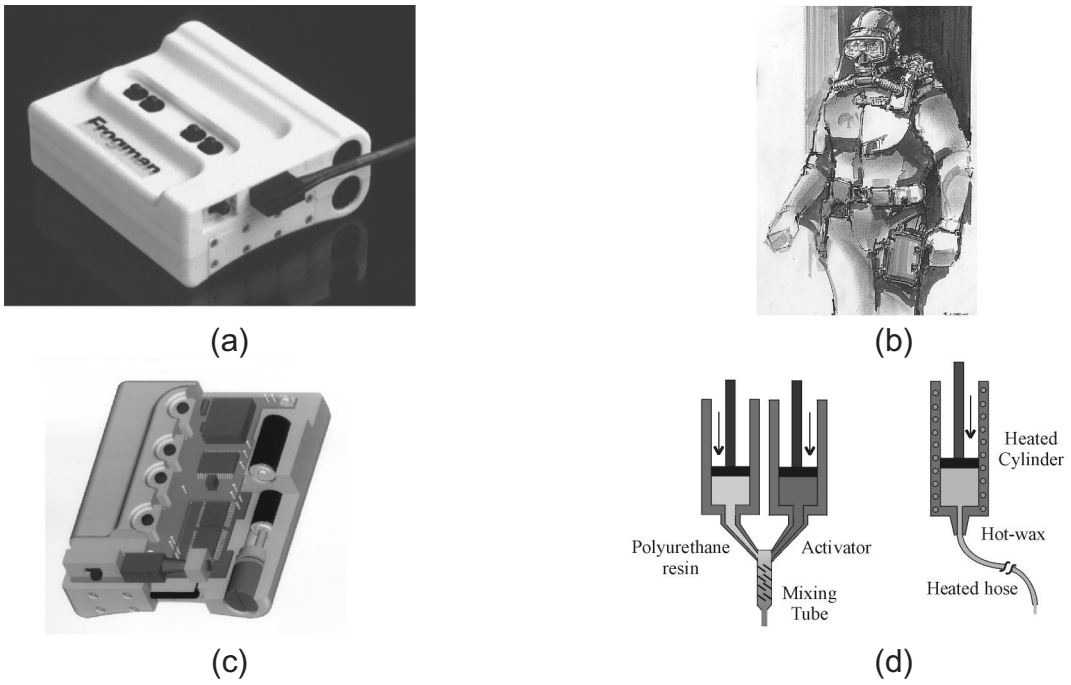


These computers might store maps, equipment descriptions, help to log data, or provide communication links.

For one example, the 'Frogman' shown in Figure 6a and 6b is a waterproof computer that can store maps for navigational aids, or detailed assembly drawings for service, maintenance, or field operations. The graphical information, which is stored on Personal Computer Memory Card International Association (PCMCIA) cards, is displayed on a heads-up display (Figure 6c). A conformal shaped rear surface was also required so that the unit could be comfortably strapped to a diver's leg. The device is built up in layers of polyurethane (PU) and sacrificial wax. The PU is deposited as a 2-part thermoset (left side of Figure 6d). The wax can be extruded with a conventional hot-glue gun (right side of Figure 6d), or thick layers can be poured from a hot-melt pot. The fabrication details, including component embedding and interconnection are described in detail in (8). The important points are that custom tooling was not required to manufacture the Frogman and that embedding facilitates waterproofing.

# 4. Integrated Assemblies

SDM has also been used to build up simple assemblies in a single operation. As an assembly is being built up, its individual components are separated by and encased within sacrificial support material. After the assembly structure has been completely built up, the sacrificial material is removed, freeing the components to move with respect to each other. For example, SDM was used to create the steel crank mechanism shown in Figure 7. In this mechanism, a piston is connected to a crankshaft with a connecting rod. Turning the crank causes the piston to move back and forth in its chamber. The mechanism components are 316L stainless steel, deposited with laser welding, and the sacrificial support material was microcast copper.

The capability to create such integrated assemblies may be particularly useful for producing miniature mechanisms where discrete assembly is difficult, i.e., similar to the micro-electro-mechanical systems (MEMS) methodology. To demonstrate the feasibility of SDM for the fabrication of structures with feature sizes in the range of tens to hundreds of and thousands of microns, several simple artifacts have been built (9). This regime has been recently referred to as the 'mesoscopic regime' which means that characteristic feature dimensions are bigger that those typically achieved using very large scale integration (VLSI) fabrication methods (e.g., used to make integrated circuit chips), yet smaller than parts produced using conventional processing techniques. We believe that mesoscopic assemblies will be particularly important for enabling future DOD applications such as autonomous micro-vehicles and micro-flying machines.

In SDM, mesoscopic structures are built up using sputtering and electro-plating deposition processes, and shaped

**Figure 7**
*Complete assemblies and mechanisms directly built up with SDM. (a) Steel crank and piston mechanism. (b) Schematic of mechanism.*

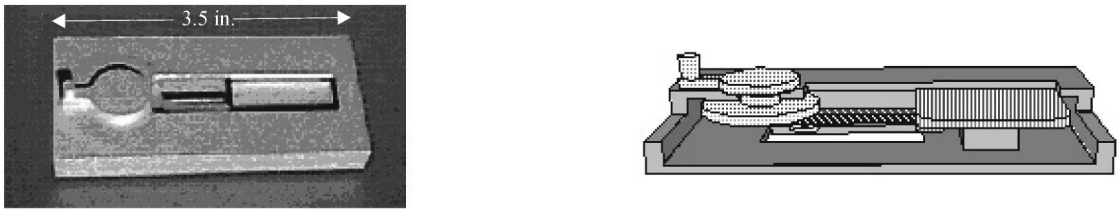


(a) (b)

with micro CNC or EDM machining. For one example, the 1.1mm high nickel structure shown in Figure 8a consists of a wheel (5mm dia., 0.3mm thick) which is permanently mounted on a nickel axle (1mm dia.). The scanning electron microscopy (SEM) photograph in Figure 8b shows a cross-section of the wheel and axle before removal of the copper support structure.

Additional examples of novel SDM mesoscopic integrated assembles are shown in Figure 9. Figure 9a is a nickel substrate carrying nine mesoscopic wheels. This structure suggests the possibility for building massively parallel miniature machinery. Figure 9b shows a 130mm thick microturbine impeller that rotates at high speeds when air is passed through the gas jets. This structure establishes the feasibility of building assembled devices with clearances on the order of less than 20 microns.

# 5. Discussion

SFF has been successfully used within the limited realm of Rapid Prototyping. However, as SFF processes improve and are able to build functional, engineering models, SFF will be used for mass customization, i.e., customers able to order products in small-lots (as small as one) customized for their specific needs. Such 'mass-customization' will be attractive for not only consumer and commercial markets, but also for defense industries as a "dual-use" technology for creating products tailored to individual soldiers needs, as well as for cost effective tooling for manufacturing defense systems. In addition, by opening up the design space, novel designs, inaccessible with conventional manufacturing techniques, will be possible. One class of such novel designs is heterogeneous structures, such as embedded electronics, and another class is integrated assemblies as described in this article. For heterogeneous structures to be practical, however, streamlined CAD systems will be required which enable concurrent representation and manipulation of geometry, material and embedded components. Other possible novel designs will involve functional gradient structures such as ceramic to metal parts or graded metal to metal structures allowing the transition from highly thermally conductive regions, inside, to tough surfaces on the outside of a part. Beyond these novel applications of SFF, it is hard to predict where exactly this will lead to when creative people have access to SFF technology. Undoubtedly, the creation

**Figure 8**
*Mesoscopic nickel wheel on axle built with SDM. (a) Mesoscopic Ni wheel. (b) Cross-section of wheel and support.*

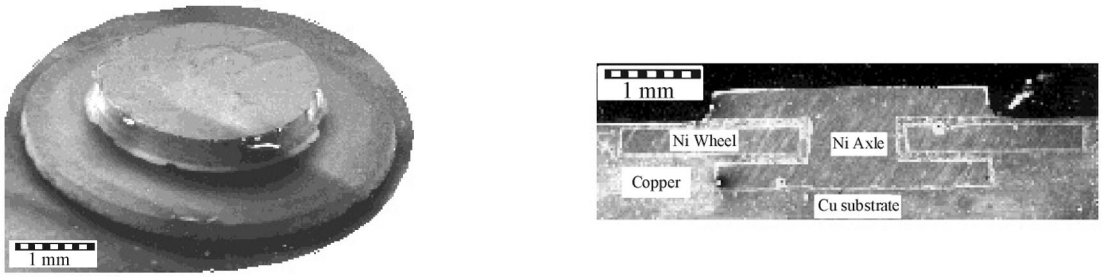


(a) (b)

**Figure 9**
*Examples of mesoscopic assemblies. (a) Assembly of nine mesoscopic wheels. (b) Miniature turbine impeller.*


(a) (b)

of products that no one has even conceived of as yet will be one of the likely outcomes.

# Acknowledgments

This work has been supported by the ONR, DARPA, and NSF. The authors acknowledge the following individuals for their contributions in creating the systems and the parts built with the systems described in this article: Gennady Neplotnik, Larry Schultz, Robert Merz, Alexander Cooper, John Fessler, JohnKeitzman, and John Lombardi.

# Bibliographies

Dr. Weiss is a Principal Research Scientist at the Robotics Institute of Carnegie Mellon University where he directs the Shape Deposition Manufacturing Laboratory. Prior to joining the Robotics Institute in 1979 he designed cardiac pacemakers in industry. He received his Ph.D. in Electrical and Computer Engineering and his Masters degree in Bioengineering from Carnegie Mellon.

Dr. Prinz is the first holder of the Rodney H. Adams professorship in the School of Engineering at Stanford University. Prior to joining Stanford in 1994 he taught Mechanical Engineering at Carnegie Mellon University for fourteen years. He obtained his Ph.D. in Physics and Mathematics from the University of Vienna, Austria.

# REFERENCES

1. Weiss, L.E., Solid Freeform Fabrication Processes Overview, in Japanese Technology Evaluation Center and World Technology Evaluation Center Panel Report on Rapid Prototyping in Japan and Europe, Analytical Chapters, ed. G. M. Holdridge, SME, I, 5, (1997).
2. Merz, R., Prinz, F.B., Ramaswami, K., Terk, M. and Weiss, L.E., Shape Deposition Manufacturing, Proceedings of the 1994 Solid Freeform Fabrication Symposium, The University of Texas At Austin, eds. Harris Marcus, J.J. Beaman, J.W. Barlow, D.L. Bourell and R. Crawford, August, 1, (1994).
3. L.E. Weiss, R. Merz, F.B. Prinz, G. Neplotnik, P. Padmanabhan, L. Schultz, K. Ramaswami, Shape Deposition Manufacturing of Heterogeneous Structures, SME Journal of Manufacturing Systems, 16, 239, (1997).
4. Weiss, L.E., Hartman, K., Krishman, R., Merz, R., Neplotnik, G., Prinz, F.B., Schultz, L., and Terk M., Robotic-Assisted Shape Deposition Manufacturing, in Proceedings of 1994 IEEE International Conference on Robotics and Automation, 2890, (1994).
5. Kietzman, J.W., Cooper, A.G., Weiss, L.E., Schultz, L., Lombardi, J.L., and Prinz, F.B., Layered Manufacturing Material Issues for SDM of Polymers and Ceramics, 1997 Solid Freeform Fabrication Symposium, The University of Texas At Austin, 133, (1997).
6. R. Merz, “Shape Deposition Manufacturing”, PhD. Dissertation, Institut für Allgemeine Elektrotechnik und Elektronik, Technische Universität Wien, (1994).
7. Fessler, J.R., Merz, R., Nickel, A.H., Prinz, F.B., and Weiss, L., Laser Deposition of Metals for Shape Deposition Manufaturing, 1996 Solid Freeform Fabrication Symposium, The University of Texas At Austin, August, 117, (1996).
8. Weiss, L.E., Neplotnik, G., Prinz, F.B., Schultz, L., Padmanabhan, P, Krishnan, R., and Merz, R.., Shape Deposition Manufacturing of Wearable Computers, 1996 Solid Freeform Fabrication Symposium, The University of Texas At Austin, 31, (1996).
9. Merz, R. and Prinz, F.B., Rapid Prototyping of Mesoscopic Structures, Proc. of the 7th International Conference on Rapid Prototyping, ed. A. Lightman, San Francisco, March, 261, (1997).

# Solid Freeform Fabrication (SFF) of Functional Advanced Ceramic Components

*S. C. Danforth and A. Safari, Ceramic and Materials Engineering, M. Jafari, Industrial Engineering, N. Langrana, Mechanical and Aerospace Engineering, Rutgers, The State University, Piscataway, NJ*

## Abstract

Solid Freeform Fabrication (SFF) technologies are now being developed for functional ceramic components. SFF offers unique manufacturing opportunities, free from constraints imposed by the part's external geometric complexity, or the internal complexity resulting from the presence of multiple phases, porosity, etc. This paper gives a brief overview of novel SFF techniques under development for: structural ceramics, bio-ceramics, and electroceramic components. Parts were made directly by Fused Deposition of Ceramics (FDC). Fused deposition modeling (FDM™) and Sanders Prototyping (SPI) methods were used to form a variety of complex shaped molds (some with very intricate graded internal structures) for the indirect (or lost mold) method of fabrication. Current research is directed at developing the processing and manufacturing science needed for layered manufacturing of multi-material, multi-functional ceramic components for electromechanical as well as structural applications.

## Introduction

Solid Freeform Fabrication (SFF) refers to methods that fabricate freestanding solid objects. While many of these techniques do not require the need for tooling or machining, some do. SFF methods are computerized (CAD file driven) material additive processes, originally applied to form and fit polymer applications which allow dramatic reductions in the time and cost of each component design iteration. [1-4] Several SFF technologies are under development at Rutgers University to make structural ceramic, bio-ceramic, as well as electronic ceramic components and devices. The electronic ceramic components under investigation are piezoelectric ceramics and ceramic-polymer composites for use as transducers, actuators, vibration control devices, etc. All SFF tech-

nologies share the same general approach; they start with a surface tessellated .stl file, that is then sliced mathematically into discrete layers, and then sent to a fabricator which builds the object in a layerwise additive fashion. Solid freeform fabrication methods differ in the details of the materials, material deposition, etc. For SFF of ceramics and some SFF techniques for metals, the techniques use powders as the raw material, and therefore require post-SFF processing (binder removal, sintering, or infiltration) of parts to achieve the desired fully dense microstructure and desired properties. Some SFF techniques are able to make fully dense metal parts without the need for post-processing steps.

# Direct & Indirect SFF Processes

Two different approaches are under development for manufacturing functional ceramic components; referred to as the "direct" and the "indirect" technique, Fig.1. In the direct method: Fused deposition of ceramics (FDC), based on fused deposition modeling (FDM™) developed by Stratasys, Inc., uses ceramic (or metal) particle loaded thermoplastic filament wound on a spool as the material feedstock, fed via counter rotating rollers into a heated extruder referred to as a liquefier.[5,6] The filament acts as the piston to extrude the molten ceramic loaded polymer material out of a (250 micron to 635 micron diameter) nozzle onto a z-stage platform, where the material cools rapidly and bonds to adjacent layers, Fig. 2. The material deposition rate and liquefier x-y position, etc., are controlled by the computer. For ceramic (or powder metal) parts, the binder is subsequently removed followed by sintering to full density. In the indirect method, Fig. 1, components are manufactured by first making a polymer or wax mold, using either FDM™ or Sanders Prototyping (SPI) techniques. The FDM™ or SPI mold is then infiltrated with a ceramic (or metal) powder suspension, dried (or gelled), followed by thermal or solvent mold removal, binder removal, and finally sintering. Processing details, as well as further physical and electromechanical characterization of structural and electroceramic components processed via these direct and indirect SFF methods, are reported elsewhere.[7-12]

**Figure 1**
*Schematic of direct and indirect routes of layered manufacturing.*

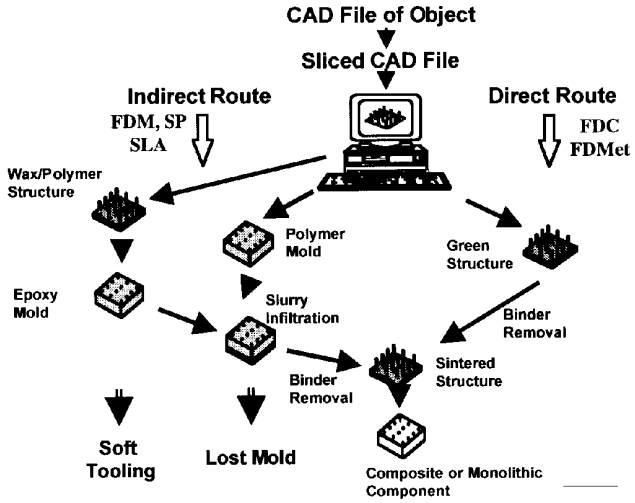


**Figure 2**
*Schematic of the fused Deposition of Ceramics (FDC) SFF process.*

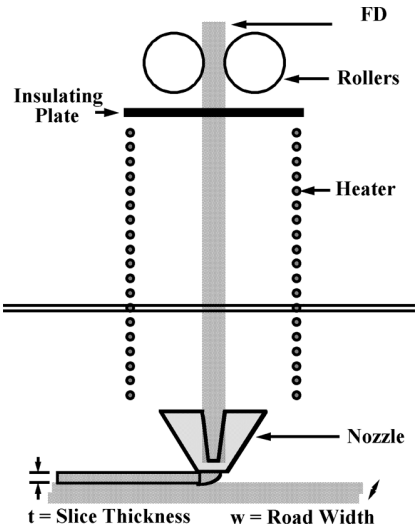


# Structural Ceramics

The FDC process was initially developed for AlliedSignal's GS-44 insitu-reinforced (ISR) silicon nitride (GS-44 $Si_3N_4$). The process steps for FDC of GS-44 $Si_3N_4$ are: ball milling the powder with a surfactant, drying, grinding and sieving, compounding with the multi-component binder system (RU9) in a high shear torque rheometer, followed by cooling and granulation. The material is then extruded into 1778 micron diameter filaments in a single screw extruder fitted with a high shear tip screw and a breaker plate and screen that insure removal of large agglomerates. Parts are built using a liquefier temperature of 185°C in a chamber at 40°C. Typically, 381 micron diameter extrusion nozzles are used, building parts with 254 micron layer thickness. Ceramic part build times have ranged from 1 hr., for small simple shapes, to greater than 16 hr. for large, or very complex shapes. Figures 3 a,b show complex shaped GS-44 $Si_3N_4$ parts, made at Rutgers, by the FDC process. The typical densities of sintered FDC GS-44 $Si_3N_4$ parts are >99 % of theoretical density.[10] The average measured four-point bend

**Figure 3**
*a) Various green ceramic (light) and metal (dark) parts built by FDC process. b) Complex shaped, sintered, machined GS-44 $Si_3N_4$ component built by the FDC process.*

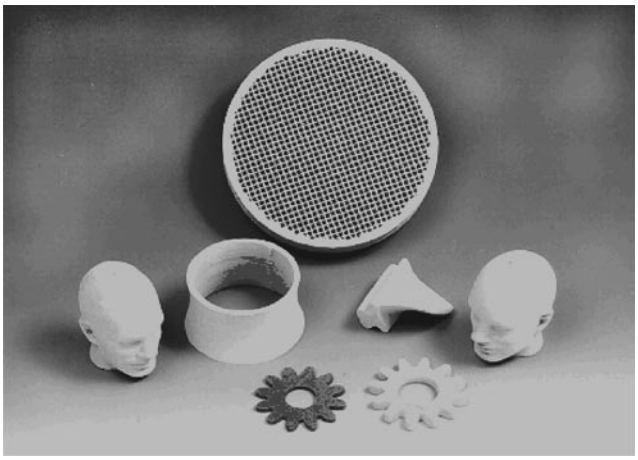

(a)

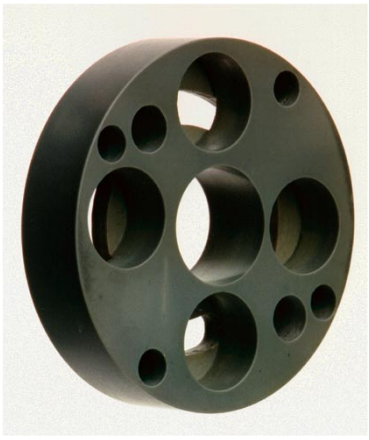

(b)

fracture strength of FDC bars is >900 MPa, similar to values for commercially produced GS-44 $Si_3N_4$ parts. The measured Chevron notch fracture toughness is 8 MPa $m^{0.5}$. While some subtle microstructural features are present which relate to layerwise building, there is little evidence, to date, of any significant difference in the microstructure, fracture strength or fracture toughness in samples where the cracks are driven parallel or perpendicular to the build plane. At present, GS-44 $Si_3N_4$ samples fall into two categories: (1) those with average four-point fracture strengths > 900 MPa, with a Weibull modulus of 15 (which fail from large grains or machining damage), and (2) those which fail from process induced Fe bearing defects and have strengths in the range of 500-700 MPa. The Weibull modulus, m, is a statistical parameter that describes the width of the measured strength distribution. Recent results indicate that the fracture toughness and fracture strength are independent of the crack direction relative to the build plane direction. Feasibility for FDC has also been shown for a wide range of other materials with average particle sizes ranging from 0.5 microns to over 50 microns, including to date: lead zirconate titanate (PZT), $Al_2O_3$, $SiO_2$, WC-Co, and 17-PH stainless steel.

# Porous Hydroxyapatite Ceramics

Hydroxyapatite (HAp) and related calcium phosphate (CP) materials have been widely used as bone implant materials for many years because of their close similarity in composition and high biocompatibility with natural bone. Many researchers have emphasized the importance of controlling the pore size in HAp ceramics, and have claimed that a minimum pore size of 100 microns is necessary for the porous implant materials to function well, and pore sizes > 200 microns are essential for osteoconduction. Many traditional techniques have been used to make porous bone scaffolds. These techniques include the following: (1) the replamine process, which involves coating a polymer foam with a 50 vol. % ceramic slurry and burning out the foam, and (2) pressing HAp powder with polymer beads and then evaporating the spheres during heating, etc. These sintered structures typically have poor strength, because of the discontinuous pore network obtained using these methods. Also, it is nearly impossible to control the pore sizes and shapes for use in

**Figure 4**
*3-D Honeycomb structure with interconnected, regular, cylindrical pore channels.*

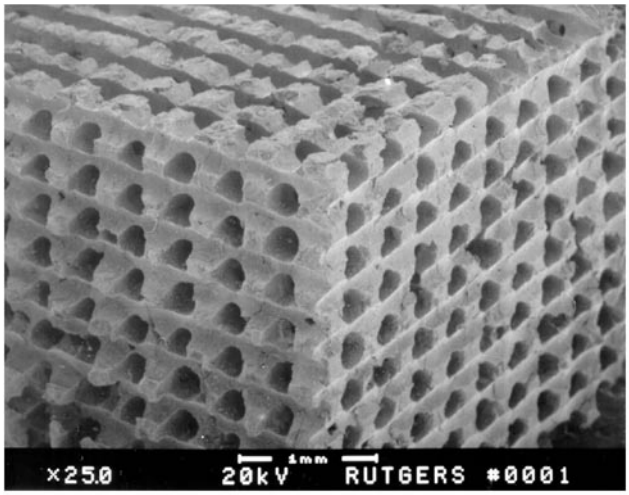

**Figure 5**
*Sintered, HAp bone structures made by indirect SFF technique.*

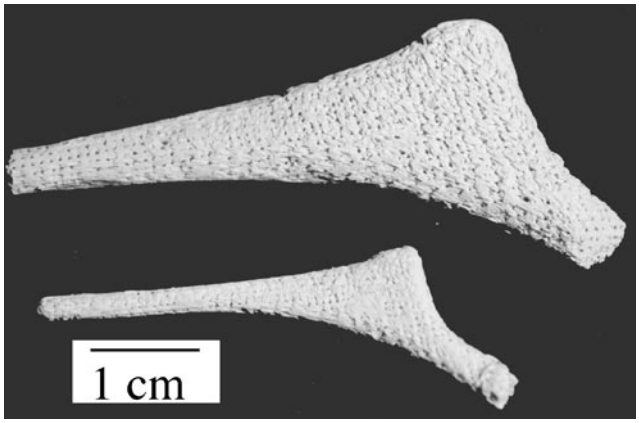


**Figure 6**
*Schematic of the top half of a novel alternate poling design for a Moonie flex-tensional high authority actuator.*

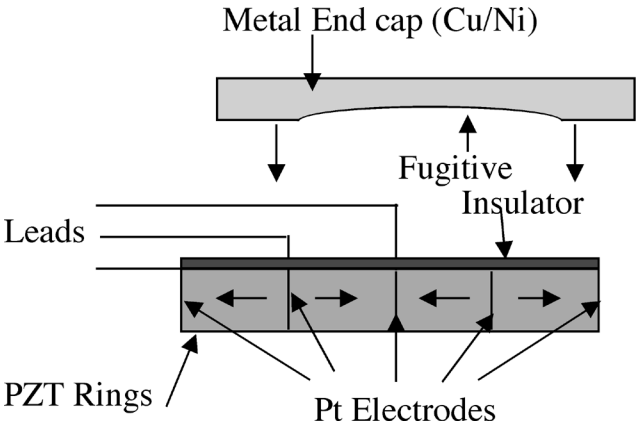


different applications. The FDM™ and SPI indirect SFF methods have been used to make porous bone scaffolds with a controlled porosity. First, the bone implant is designed using AutoCAD or ProEngineer, followed by fabrication of the sacrificial polymer or wax mold, and infiltrating with a HAp aqueous suspension, etc. A variety of porous structures have been fabricated, with porosity ranging from 30 to 70 vol. %. The pore sizes of the structures have also been varied from 200 microns to 750 microns. Figure 4 shows a 3-D honeycomb structure made by the FDM indirect method where the controlled pores are interconnected in three dimensions. This type of 3-D honeycomb structure has never been made using any other method. Figure 5 shows HAp structures with ~ 55 vol. % porosity made by these techniques.

# High Authority Actuators

In the last few years, the technology of using piezoelectric and electrostrictive actuators for applications requiring large displacements such as linear motors, cavity pumps, switches, loudspeakers and noise-canceling devices, has undergone significant development. Such applications require very large displacements (>1000 microns) combined with a moderate force (>10 kg). However, the induced strains in piezoelectric and electrostrictive ceramic discs, regardless of their size, are a few tenths of a micron. Higher displacements and generative force are achievable with these materials by employing strain-amplification techniques. As a result, Multilayer, Bimorph, Moonie, and Rainbow actuators, with magnified output displacement, have been developed. [13-15]. A "Moonie" is an actuator consisting of a thin ceramic disk and two thin metal plates bonded together. Each of the metal plates has a narrow "moon"-shaped cavity in it. A "Bimorph", is an actuator consisting of two thin ceramic plates, which are bonded onto each side of an elastic metal shim. A "Rainbow" is a curved actuator, consisting of an oxide ceramic disk which has been reduced and internally biased.

These components are useful for Naval and other DoD applications. These piezoelectric actuators can be used for active and passive vibration suppression on the space shuttle, missiles and other military as well as commercial vehicles. They can also be used as components of a "smart skin" in a system. For this application, the signal of projectile impact, turbulent flow, or other undesirable vibration, is detected by a transducer, and then fed back to an actuator (in the smart skin), to change its shape, so as to negate, cancel, or minimize the deleterious effects of the event.

The focus of the layered manufacturing (LM) research at Rutgers is on high authority actuators, such as a metal-electroceramic composite flex-tensional transducer termed a "Moonie," and dome shaped actuators, Figs. 6 & 7. Traditional Moonies consist of a monolithic piece of

**Figure 7**
*Photograph of a PZT ceramic dome actuator fabricated by the direct LM (FDC) process.*

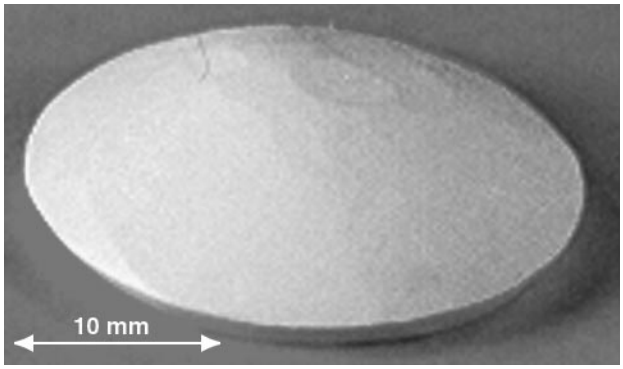

**Figure 8**
*Photograph of green PZT multi-ring ceramic actuator element fabricated by direct LM (FDC) process.*

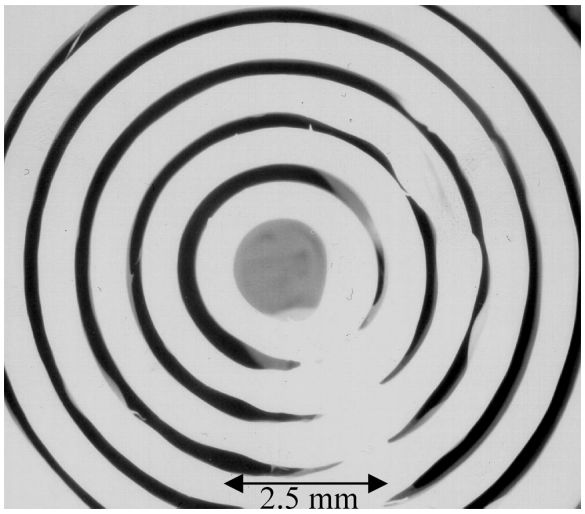


**Figure 9**
*SEM micrograph of a sintered PZT dome actuator element fabricated by direct LM (FDC) process.*

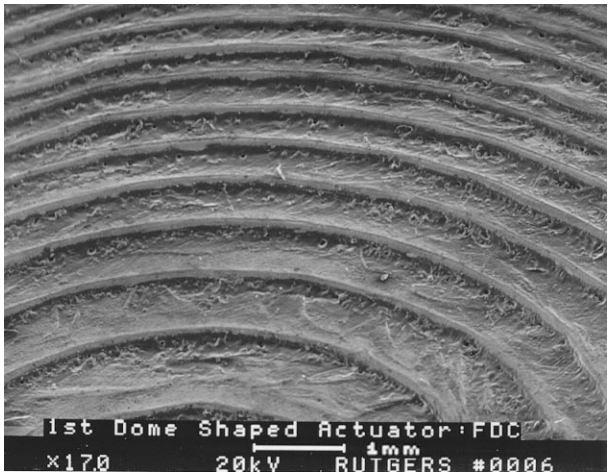


electroceramic (lead zirconate titanate, PZT, lead magnesium niobate-lead titanate, PMN-PT) sandwiched between two metal end caps, where the ceramic is poled in the thickness direction, and upon actuation, extends in the thickness direction. There is an accompanying Poisson contraction in the transverse direction that flexes the metal end caps resulting in an axial displacement, which couples with the axial displacement of the ceramic, thus amplifying the axial motion and transmitting it to the metal end caps (see Fig. 6). These transducers are characterized by values of displacement and force on the order of 20-30 microns and 3 N respectively. Two critical aspects to the successful development of LM of Moonies are: (1) multiple material co-deposition by extrusion, and (2) co-firing (in the range of 1200-1280 °C) of the PZT ceramic with Cu-Ni end caps, and any required electrode and insulator compositions, Fig. 6. This novel Moonie design is based on an alternate poling concept. This was developed via finite element and kinematic electromechanical performance modeling, that predicts twice the displacement compared to a design which uses a monolithic PZT disk. [16,17]. A multi-ring ceramic element, based on this design, has been fabricated at Rutgers via FDC, Fig. 8. PZT made by FDC has been successfully co-fired with Pt at 1285°C in an excess lead atmosphere, and the electromechanical properties of the PZT/Pt structure are: a dielectric constant, K, of 3400, a longitudinal piezoelectric charge coefficient, $d_{33}$, of 620 pC/N, and an electrical dissipation factor, tan δ, of 2%, values which are in excellent agreement with the literature, confirming that these LM techniques can fabricate high quality PZT components. Current research is also directed at development and optimization of co-firing conditions for ceramic, electrode and metal end caps for Moonies.

A new type of high authority, dome-shaped actuator with different curvatures, diameters and thickness, is under development via LM processing. Unlike the conventional techniques used for fabrication of Rainbow actuators with a curved structure, this method has the advantage of precise control of curvature, thickness and geometry. A thermoplastic binder with moderate strength and flexibility, while maintaining low viscosity at the deposition temperature, was developed for FDC with PZT based materials. The powder and binder were compounded, using 60 vol. of PZT ceramic powder (TRS Ceramics, Inc., State College, PA), in a torque rheometer at 135°C and 100 rpm for one hour until a stabilized torque was reached. The compounded mix was granu-

**Figure 10**
*SEM micrograph of a cut cross section of a sintered PZT dome actuator element fabricated by direct LM (FDC) process.*

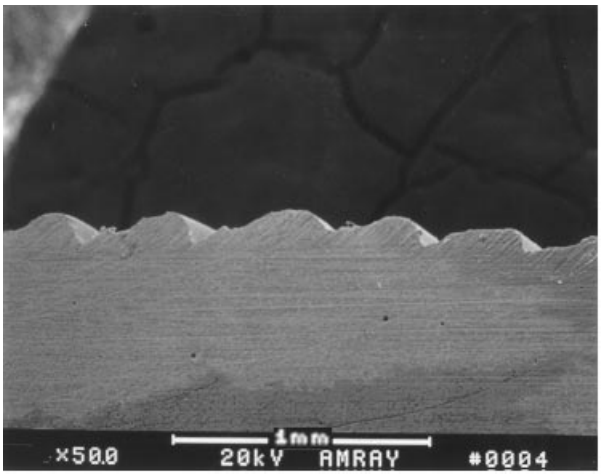

**Figure 11**
*a) SEM micrograph of a polished and etched, sintered PZT dome actuator element fabricated by direct LM. b) SEM micrograph of a polished and etched, sintered PZT element fabricated by conventional means.*

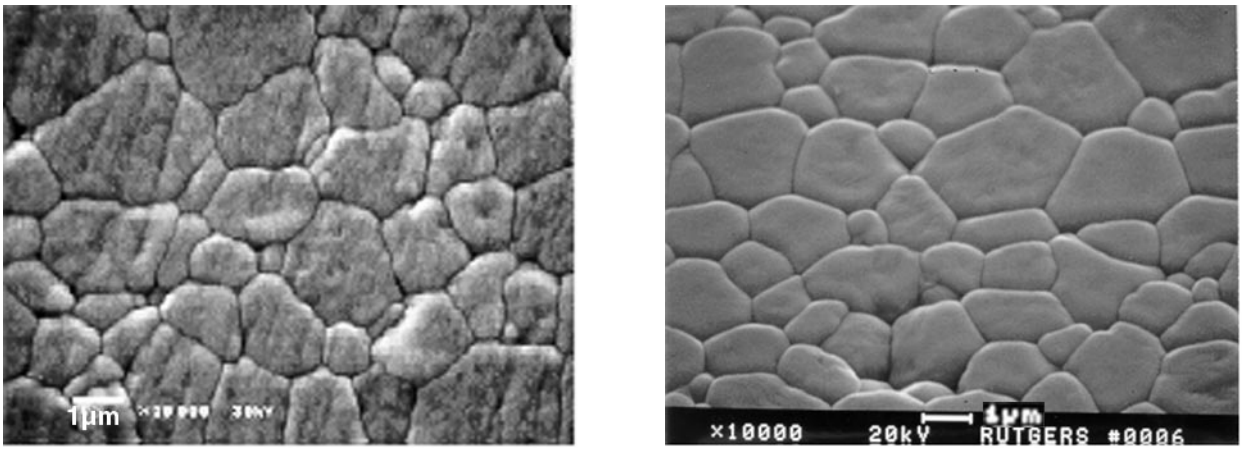


(a) (b)

lated and sieved to use as the feed material for filament extrusion. A capillary rheometer was used for extrusion of short lengths (~ 30 cm) of green PZT filaments. The FDC process was used to manufacture dome shaped parts at a liquefier temperature of 145-170°C, while the surrounding environment temperature was maintained in a range of 35-40°C. After binder removal and sintering a density of up to 94 % theoretical density was reached. Figures 7 and 9 show exterior and interior views of a dome-shaped actuator, fabricated by the FDC process. Examination of sintered parts using electron microscopy techniques showed no sign of delamination for parts made by layered manufacturing techniques, Fig. 10. The samples were thermally etched and their microstructure compared well with that of samples prepared by conventional processing methods, Fig. 11 a and b.

**Figure 12**
*Distribution of $d_{33}$ across the LM dome actuator.*

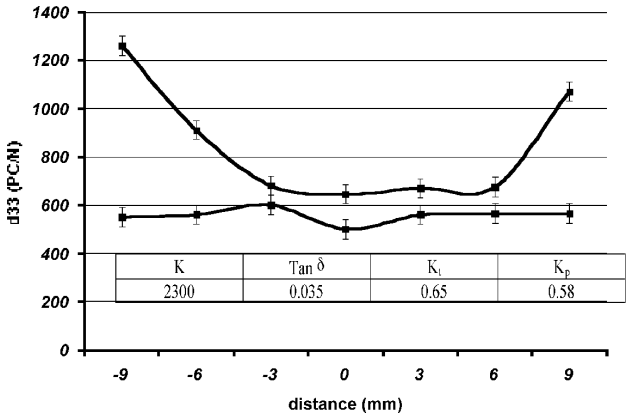


Similar to Rainbows, the dome-shaped actuators have shown a bending mode resonance at about 17 kHz, in addition to radial and thickness mode resonance frequencies. The piezoelectric coefficient, $d_{33}$, of these samples was measured when the samples were unclamped, using a Berlincourt Piezometer. Even though there was a large variation of the $d_{33}$ coefficient across the diameter of these structures, with a minimum $d_{33}$ of 550 pC/N at the center of the dome, a large $d_{33}$ of up to 1270 pC/N was measured at the edges of these samples, using pointed fixtures, Fig. 12. These measured values are comparable with values reported in the literature for Rainbow actuators. These samples also have shown a low dielectric loss (~3.5%) compared to Rainbow samples of the same size (8.5%). It is believed that the higher loss in Rainbows is due to the presence of carbon in the structure as a result of the reduction process.

# Piezoelectric Transducers and Sensors

Piezoelectric transducers and sensors with novel structures and designs have been manufactured by both the direct (FDC) and indirect (FDM™ and SPI) techniques. Figure 13 shows an SEM micrograph of an oriented PZT fiber structure made by the FDC process using a 55-vol. % PZT powder loaded filament as the feedstock, and a 406 micron nozzle in the liquefier. This geometry generates very large piezoelectric charge coefficients, due to the contribution of the $d_{33}$ and $d_{15}$ coefficients. Many other fine scale PZT structures, including volume fraction gradient and a novel radial com-

**Figure 13**
*SEM micrograph of an oriented PZT fiber structure fabricated by direct LM (FDC) process.*

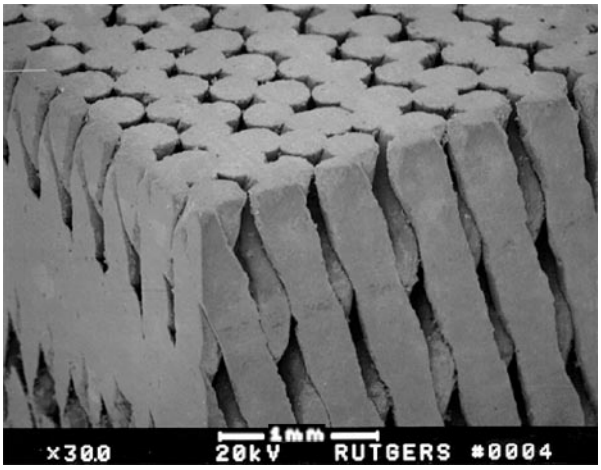


posite design, have been fabricated for use in ultrasonic medical imaging and towed array transducers by the SPI indirect method, Figs. 14 a and b.

# LM Computer Aided Design (CAD)

These and other novel SFF processes are under development for high authority actuator designs that are able to take advantage of the flexibility provided by SFF processes. In one Office of Naval Research Multi-Disciplinary University Research Initiative program at Rutgers (with The University of Delaware and the University of Illinois at Chicago), a new Layered Manufacturing (LM) system is under development. The overall objective of the MURI program is to establish the processing and manufacturing science required for the development of a novel, intelligent LM system for the cost effective fabrication of multiple material, net shape, complex shaped electromechanical components/devices and arrays. The specific objectives of the program are: (1) Develop the necessary machine control systems, and material delivery systems for the deposition of one or more ceramic phases, one metal phase and a fugitive organic support phase for a given component, (2) Develop the science base for accurate process modeling and to achieve a predictive capability both for LM and performance of the complex components, and (3) Develop a system for real time control and a LM CAD system for advanced computer simulation of the entire layered manufacturing process. Figures 15 and 16 show a highly conceptual schematic of a single build layer of a fictional component that could be built by this new type of intelligent SFF process and a conceptual schematic of the multiple material LM system under development.

In currently available FDC based systems (as with most SFF systems), the CAD-manufacturing process is open loop. That is, users cannot predict the quality of the part, and the system itself cannot verify or improve the quality of the part. Therefore, several designs of experiments are needed to improve part quality. [5,9]. Multiple material LM refers to the process of fabricating a part from a three-dimensional CAD model, layer by layer, using more than one material per layer. This complexity increases the chances that the open loop

**Figure 14**
*a) SEM micrograph of PZT structure with volume fraction gradient fabricated by indirect LM (SPI) process. b) Polymer mold, PZT part, and PZT-polymer radial composite structures fabricated by the indirect LM (SPI) process.*

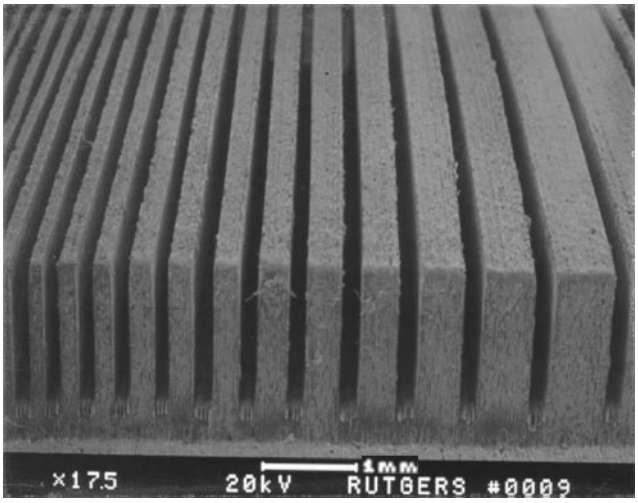


(a)

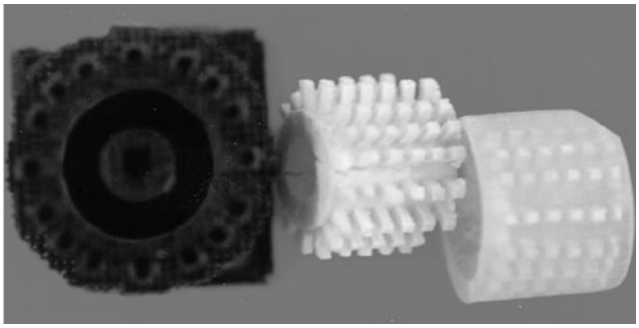

(b)

**Figure 15**
*Schematic of multi-material LM manufacturing system.*

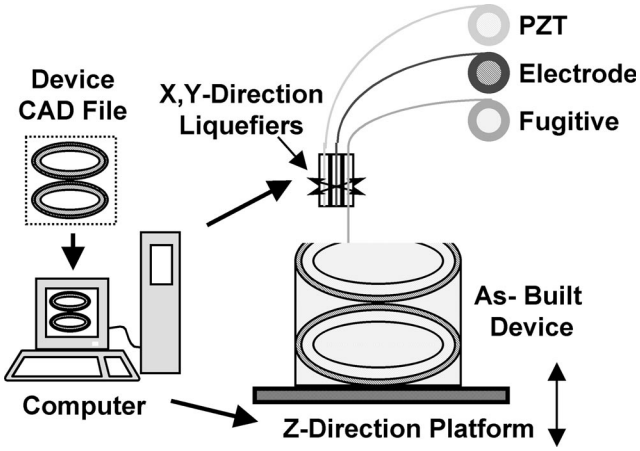


processes will not fabricate high quality parts. A multi-material CAD model consists of several different material blocks connected by interphase boundaries. The LM system will be able to generate CAD models, sliced files, and toolpaths, as well as fabricate a multi-material part in the manufacturing process. Achievement of this goal requires the development of a CAD system that will perform the virtual simulation of the multi-material LM process. SGI OpenGL is used to run a LM simulation, as it provides the necessary flexibility, viewing and animation tools for the designer to verify the LM manufacturability of the component CAD file. The multi-material CAD model is created using commercially available software such as I-DEAS and ProE. Therefore, one .stl and one .sml file per material is generated. The terms .stl and .sml refer to the surface tessellated object model, and the SFF machine tool path files, respectively. This information is then used as the input to the simulation algorithm, which systematically, layer by layer, integrates all .sml files into one tool path build file. This algorithm is written in C++

**Figure 16**
*Schematic of a single, multi-material, multi-functional component built by LM.*

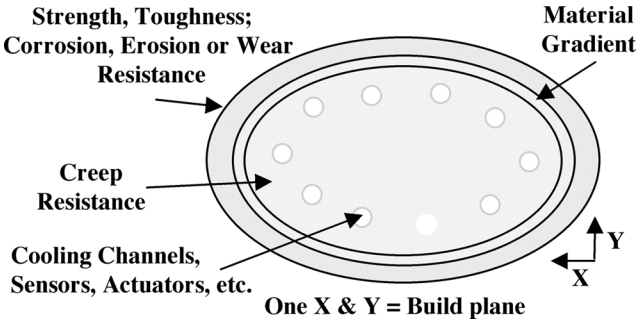


**Figure 17**
*Virtual LM simulation of a 2-material stacked cymbal actuator structure.*

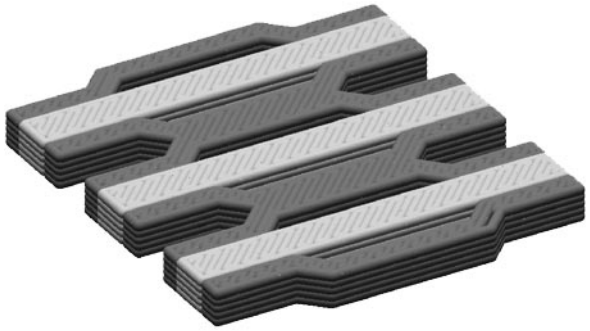

computer language. The results of the multi-material tool path are graphically visualized. The part is stacked layer by layer, and there can be several domains with different materials in each layer. Any defects or voids in each layer can be visualized immediately. The results of actual physically fabricated parts match with our virtual LM simulations, which demonstrates that the simulations provide sufficiently accurate and detailed information. Virtual tool path simulations of multi-material electro-mechanical components have also been created, Figs. 17-19. The LM simulation reduces the time and materials that would otherwise be wasted in manufacturing inaccurate parts.

# LM Machine System Control

As noted above, current FD based technology only supports open loop positioning and deposition control systems. Thus, the first key step in developing the next generation of LM technology is to close the control loop at the

**Figure 18**
*Virtual LM simulation of a multi-material structure.*

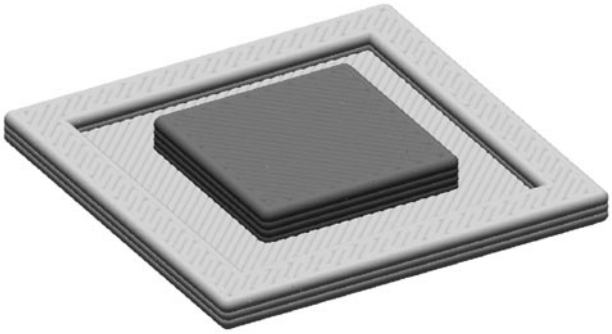

**Figure 19**
*Multi-material structure made by direct LM (FDC) technique.*

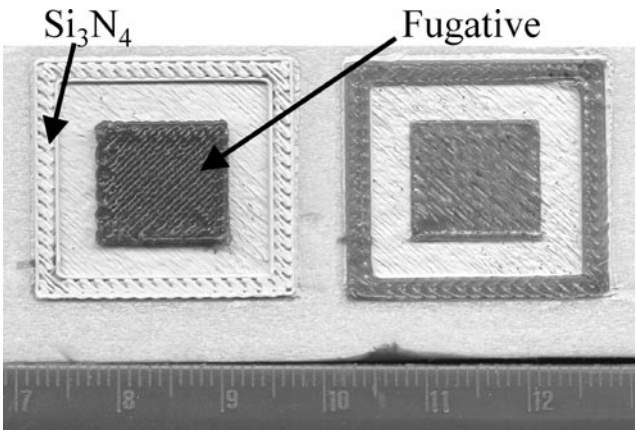


local machine level, so that on-line feedback on the position and velocity of the various axes can be used to minimize potential position relayed part defects, such as internal voids or surface roughness. In terms of trajectory planning (i.e., knowledge of the position and velocity of the deposition system as a function of time) for the positioning system, one should compensate for the fact that only linear interpolation is used with current technology. These inaccuracies in geometric representation contribute to tracking and contour errors in the positioning system, which can translate to over-filling or under-filling at any point in a given layer. Bouhal, et. al. formulated the problem of trajectory planning in Layered Manufacturing, subject to the constraint that the liquefier head must move with constant velocity as much as possible.[18] The main reason for this constraint is that the dynamics of the extrusion deposition system are not sufficiently known at this time. Any lack of synchronization between the deposition and the positioning systems could also result in voids.

The second step in improving the current technology is to provide an on-line process monitoring system so that defects are first detected and then repaired on-line in each given layer, prior to depositing the next layer. Current focus is on a machine vision based, on-line process monitoring and feedback system. This system is envisioned to work as follows. Upon the completion of the fabrication of a given layer, the cameras that are positioned along the same axes as the liquefier head take images of the layer, which is then analyzed through various image-processing techniques to detect the size, nature and position of the defect. Finally, the defects will be eliminated and then the machine would advance to the next layer.

Here, we will briefly discuss the issues that involve the image processing aspects of the above system. Figure 20 illustrates an interior region of a layer of a sample of ceramic part built by the FDC process. On the image we note

**Figure 20**
*Optical image of the surface of a silicon nitride sample built by the direct LM (FDC) process.*

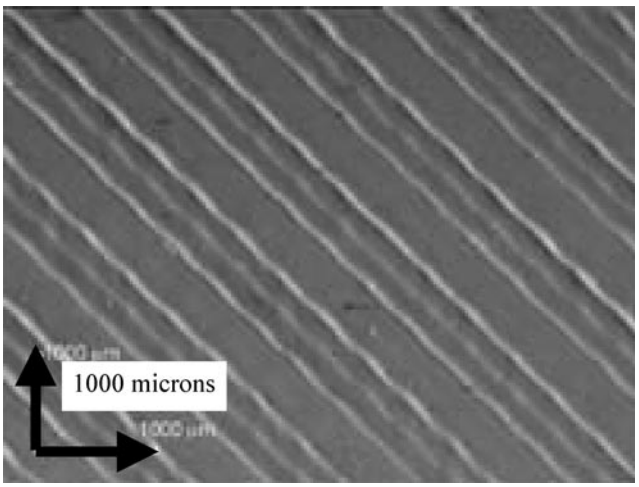


a specific pattern of two thick lines (or edges) with a thinner line in between. Figure 21 illustrates the interior region of a second (different ceramic and binder) sample. In this image, the pattern is different with a flat surface embedded within boundaries that are sometimes cavities. At first glance, the flat surface seems to contain only a single road (material deposited by one pass of the extruder), but by more careful examination, we have determined that it actually contains two adjacent roads. This confirms our belief that the analysis of the image alone would be misleading, and more detailed knowledge of the process, from the parameter settings at the CAD level to material properties, thermal effects and material bonding are needed to assist the image analysis stage. Various elements of the LM process are being modeled that

**Figure 21**
*Optical image of the surface of a PZT sample built by the direct LM (FDC) process.*

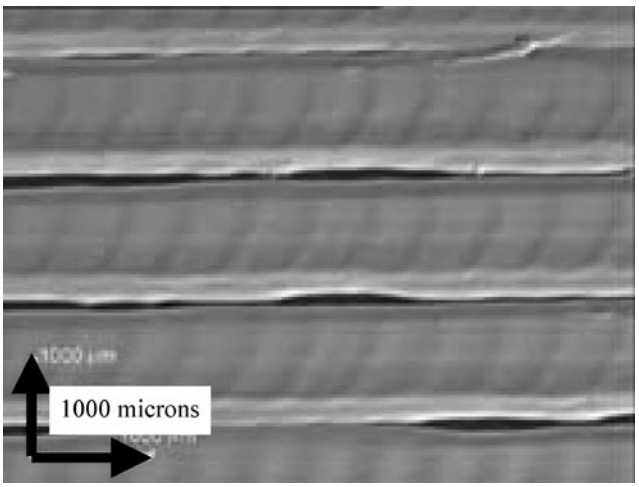

**Figure 22**
*Process signature of the image from Figure 20, of silicon nitride sample made by direct LM (FDC) process.*

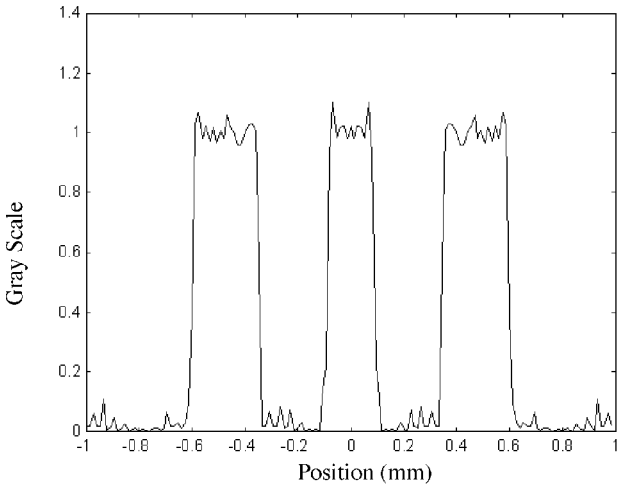


will yield the input data and intelligence tools to assist in image signature determination.[19,20] In particular, one should be able to define an *Ideal Process Signature* that is uniquely defined by a specific LM process and material. At the same time, one can also define *image process signatures* from the image. Figure 22 illustrates the process signature for the sample in Fig. 20. The peaks in Fig. 22 signify the three-edge pattern, that we noted in Fig. 20. For a given layer, there may be several process signatures corresponding to the various uniform segments in that layer. In a perfect FDC process the ideal and the image process signatures must be the same within a given tolerance. Any significant difference between these two sets of signatures will signify potential defects in a given layer, requiring repair.

# Summary & Conclusions

This paper presents a brief summary of recent progress at Rutgers in the development of novel SFF techniques for functional quality advanced structural, bio-ceramic, and electronic ceramic components. For direct fabrication of ceramic components, green ceramic filaments of $Si_3N_4$ or PZT powder loaded thermoplastic binder were used for fabrication of complex ceramic structures by the FDC process, followed by binder removal and sintering. Parts made by FDC exhibit properties that are the same as those of components made by traditional manufacturing methods. Fused Deposition of Ceramics has several advantages as a prototyping and manufacturing technique: (1) the technique can be used with nearly any ceramic, metal or composite powder, (2) the technique produces parts with high density and functional properties, etc. (3) FDC can make complex shaped components with fine features and complicated internal structures, and (4) the technique can be used with multiple materials. Fused deposition modeling (FDM™) and Sanders Prototyping (SPI) methods were used to form a variety of complex shaped molds (some with very intricate graded internal structures) for the indirect (or lost mold) method of fabrication. Once built, the wax molds were infiltrated with a PZT, or hydroxyapatite ceramic slurry, followed by drying, mold and binder removal and sintering. One can readily see the advantages of manufacturing multi-material, multifunctional components, such as Moonie and Dome actuators, where one can now design and manufacture both the component as well as the internal macro- and microstructure for optimized performance. These actuators have great potential as transducers (sonar, vibration sensing) and actuators (motion and vibration control, and smart skin) for Naval and other DoD platforms and systems. Current research is directed at developing the processing and manufacturing science needed for layered manufacturing of multi-material, multi-functional components for electromechanical, as well as structural applications. These novel ceramic manufacturing methods show tremendous potential for affordable manufacturing of functional quality structural ceramics and piezoelectric ceramics (and composites) and bio-ceramics with freedom from the traditional design and manufacturing constraints.

# Acknowledgments

The authors would like to thank DARPA, Dr. W. S. Coblenz, and the Office of Naval Research (ONR) Drs. S. Fishman, W. Smith, R. Wachter, and G. Spanos, for the financial support for this work under contract numbers: N00014-93-1-1059, N00014-94-C-0115, N00014-94-1-0588, N00014-96-1-0959, and MURI Grant No. N00014-96-1-1175. In addition, the authors wish to thank the following for technical and financial support of this research: Dr. P. Whalen and Dr. C. Gasdaska, AlliedSignal, Inc., Dr. L. Bowen, Material Systems, Inc., and Dr. V. F. Janas, Johnson and Johnson, Inc.

# Biographies

Stephen C. Danforth, Ph.D. is a Professor of Ceramic and Materials Engineering, at Rutgers, The State University of New Jersey. His principal fields of interest include: processing of ceramic powders, nanostructured materials, and advanced manufacturing methods for ceramics and metals, specifically solid freeform and layered manufacturing techniques. He is one of the inventors of the Fused Deposition of Ceramics process. He is a Fellow of the American Ceramic Society, and holder of their Karl Schwartzwalder Professional Achievement in Ceramic Engineering (PACE) Award. He has published over 150 papers and given over 100 invited talks at professional meetings around the world.

Ahmad Safari, Ph.D. is a distinguished Professor of the Department of Ceramic and Materials Engineering and a member of the Center for Ceramic Research at Rutgers, The

State University of New Jersey. His main fields of interest include: Layered manufacturing of functional ceramics, electroceramic materials for dielectric, piezoelectric and ferroelectric applications, ferroelectric thin films for non-volatile memories, electroceramic and ceramic - polymer composites for transducers, sensors, and actuators. Professor Safari is a Fellow of American Ceramic Society (1993), a Centennial Fellow of The College of Earth and Mineral Science, The Pennsylvania State University (1996), and honorary professor of Harbin Institute of Technology, Harbin, China (1997). He chaired the US-Japan Meeting on Ferroelectric and Dielectric Materials (1995) and the 10th International Symposium on the Applications of Ferroelectrics (1996). Dr. Safari is the author/co-author of over 190 papers and holds eleven patents. He is one of the inventors of the Fused Deposition of Ceramics process. He has given over 250 lectures on his research at national and international meeting and industries.

Mohsen Jafari received his Ph.D. in Industrial Engineering and an M.S. in Computer Science from Syracuse University. He taught in Syracuse University from 1985-1987, and from 1987 to the present he has been an Associate Professor in the Department of Industrial Engineering at Rutgers, The State University. He has been Principal or Co-Prinicipal Investigator to over $3M research projects funded by various government agencies. He has published over 25 journal articles and has given many invited and contributed talks in international conferences. Seven Ph.D. and over ten M.S. thesis have already been completed or are in progress under his supervision.

Noshir A. Langrana, Ph.D. P.E. is a Professor in Mechanical and Aerospace Engineering, at Rutgers, The State University of New Jersey. His principal fields of interest include: computer-aided design, solid modeling, virtual reality simulation, optimization and finite element analysis, computer controlled compression molding manufacturing process, rapid prototyping technology (SLA, SFF and FDC), mechanical testing of composites, and mechanical behavior in high temperature environment. He is a Fellow of ASME and AIMBE. He is a recipient of Greatest Advances of 1996 (one of 26 major scientific advances in American Universities) recognition by Science Coalition Washington, DC 1997. He is a joint inventor on five patents and has published extensively.

# REFERENCES


1. Proceedings of the Solid Freeform Fabrication Symposium, Vol. 1-8, Ed. Edited by J. J. Beamen, H. L. Marcus, D L. Bourell, and J. W. Barlow, Univ. of Texas at Austin, Austin, TX, 1990-1997.
2. M, B. Hsieh, "Laminated Object Manufacturing (LOM): A simple Process", 123-130, Proc. Solid Freeform Fabrication Proceedings (Austin, TX, August 1991). Edited by H. Marcus, J. J. Beamen, J. W. Barlow, D L. Bourell, and R. H. Crawford, University of Texas at Austin, Austin, TX, 1991.
3. Griffin, J. Daufenbach, S. McMillin, "Desktop Manufacturing: LOM vs. Pressing," Am. Ceram. Soc. Bull., [73], 8, 1994.
4. Cawley, P. Wei, Z. E. Liu, W. S. Newman, B. B. Mathewson, A. Heuer, "Alumina Ceramics Made by CAM-LEM (Computer Aided Manufacturing of Laminated Engineered Materials Technology", 9-16, Solid Freeform Fabrication Proceedings (Austin, TX, August 1995). Edited by H. L. Marcus, J. J. Beamen, D L. Bourell, J. W. Barlow, and R. H. Crawford, University of Texas at Austin, Austin, TX, 1995.
5. M. K. Agarwala, A. Bandyopadhyay, R. van Weeren, V. Jamalabad, P. Whalen, N. A. Langrana, A. Safari,, S. C. Danforth, "Fused Deposition of Ceramics" J. Rapid Prototyping, Vol. 2, 4, 4-19, (1996).
6. M. K. Agarwala, A. Bandyopadhyay, R. van Weeren, V. Jamalabad, P. Whalen, N. A. Langrana, S. C. Danforth and A. Safari "Fused Deposition of Ceramics: Rapid Fabrication of Structural Ceramic Components", Bull. Am. Cer. Soc., 75, 11, 60-5, (1996).
7. S. Rangarajan, G. Qi, A. Bandyopadhyay, C. Dai, J. W. Han, P. Bhargava, S. Wu, A. Safari, S. C. Danforth, "The Role of Processing Variables in the FDC Process," Proceedings of Solid Freeform Fabrication Symposium, University of Texas at Austin, 431-40, 1997.
8. G. Qi, C. Dai, S. Rangarajan, S. Wu, S. Danforth, and A. Safari, "Properties of RU955 $Si_3N_4$ Filament for FDC", Proceedings of Solid Freeform Fabrication Symposium, University of Texas at Austin, Austin, Texas, 421-29, 1997.
9. C. Dai, G. Qi, S. Rangarajan, N. Langrana, A. Safari, and S. Danforth, "High Quality, Fully Dense Ceramic Components Manufactured Using Fused Deposition of Ceramics", Proceedings of the Solid Freeform Fabrication Symposium, The University of Texas at Austin, Austin, TX, August 1997.
10. R. Clancy, V. Jamalabad, P. Whalen, ,. Bhargava, C Dai, G. Qi, S. Rangarajan, S. Wu, S. Danforth, Langrana, and A. Safari, "Fused Deposition of Ceramics: Progress Towards a Robust and Controlled Process for Commercialization", Proceedings of Solid Freeform Fabrication Symposium, University of Texas at Austin, 185-193, 1997.
11. "Processing of Piezocomposites by Fused Deposition Technique," A. Bandyopadhyay, R. K. Panda, V. F. Janas, M. K. Agarwala, S. C. Danforth and A. Safari, J. Am. Cer. Soc., 80, 6, 1366-72, (1997).
12. S. C. Danforth and A. Safari "Solid Freeform Fabrication: Novel Manufacturing Opportunities for Electronic Ceramics", Proceedings of 10th Interna-

tional Symposium on Applications of Ferroelectrics, IEEE 96CH35948, 183-188 (1997).
13. R.E. Newnham, Q.C. Xu, "Metal-Elecroactive Ceramic Composite Actuators," U.S. Patent # 5,276,657, Jan. 4, (1994).
14. A. Dogan, J.F. Fernandez, K. Uchino, R.E. Newnham, " New Piezoelectric composite Actuator Designs for Displacement Amplification," Materials for Adaptive Structural Acoustic Control (Penn State-Annual Report), Vol. IV, Appendix 40, (1995).
15. K. Onitsuka, A. Dogan, J.F. Tressler, Q.C. Xu, S. Yoshikawa and R.E. Newnham, "Metal-Ceramic Composite Transducer, The "Moonie"," Journal of Intelligent Material Systems and Structures, Vol. 6, pp. 447-455, (1995).
16. Ruan, S.C. Danforth, A. Safari, and T-W. Chou, " Design and Analysis of Electromechanical Devices," submitted to Journal of the American Ceramic Society, June 1997
17. Ruan, S.C. Danforth, A. Safari, and T-W. Chou, " Analysis of the Electromechanical Coupling Effect in Linear Piezoelectric Materials," submitted to Journal of Solids and Structures, November, 1997.
18. A. Bouhal, M. A. Jafari, W. B. Han, and T. Fang, "Tracking Control and Trajectory Planning in Layered Manufacturing Applications," August 1997, under review for IEEE Transactions in Industrial Electronics.
19. S. I. Guceri, A. Yardimci, "Process Analysis of Fused Deposition of Ceramics", Final Technical Report under DARPA/ONR Contract Number N00014-94-C-0115, Manufacturing Processes Laboratory, University of Illinois at Chicago, May, 1997.
20. "Part Quality Prediction Tools for Fused Deposition Processing", M. A. Yardimci, S. I. Guceri, S. C. Danforth and M. Agarwala, Proceedings of the 7th Solid Freeform Fabrication Symposium, Edited by H. L. Marcus, J. J. Beamen, D. L. Bourell, J. W. Barlow and R. H. Crawford, University of Texas at Austin, 539-548, 1996.

# Solid Freeform Fabrication of Ceramics via Stereolithography

*G. Allen Brady and J. W. Halloran, Department of Materials Science, University of Michigan, Ann Arbor, MI*

## Abstract

Solid freeform fabrication of ceramics can be accomplished with stereolithography by using a stereolithography apparatus (SLA) to build a ceramic-loaded polymer object from an ultraviolet (UV) curable suspension of ceramic powders in an acrylate monomer. Objects are later sintered in a separate furnace to remove the polymer and densify the ceramic. Fully dense ceramics with excellent microstructure are achieved. Like conventionally fabricated ceramics, dimensional accuracy is limited by sintering shrinkage, which is anisotropic but repeatable within about 0.7%. Higher refractive index materials, which scatter the UV radiation more strongly, require longer build times. Examples are drawn mostly from aluminum oxide, but are related to other ceramics.

This research was supported by the US Office of Naval Research under grant N00014-95-1-0527, through Drs. S. Fishman and R. Wachter.

## Introduction

Solid freeform fabrication (SFF) techniques provide two significant benefits to the engineering design cycle. First, layer-wise fabrication allows unique and otherwise cumbersome and uneconomical designs to be fabricated easily. Second, these designs can be fabricated directly from the computer-aided design (CAD) or other data file, even at remote sites, reducing design time and other costs. The time and cost savings using these processes in the design and manufacturing cycles are evident in the growth of the rapid prototype industry.

Fabrication of ceramics via solid freeform fabrication methods has been an area of active research in the past several years. The ability to directly fabricate ceramic bodies into complex shapes without the time and expense of tooling (which can take months to procure) would be a unique and important advance in solid freeform fabrication techniques. Specifically, the investment casting design cycle is

usually longer and more costly than other manufacturing methods. Direct fabrication of complex molds for investment casting items such as blades for turbine aircraft engines by ceramic SLA without tooling can lead to significant cost savings. In addition, adapting stereolithography (SL) to produce ceramics offers access to a large, experienced market as a potential user base. To this end, this work aims to provide an overview of the advances made in directly producing ceramics in a commercially available stereolithography apparatus (SLA 250/40, Systems, Valencia, CA).

The stereolithography process is based upon photopolymerization of a liquid monomer mixture which, when irradiated with an ultraviolet laser, rapidly polymerizes to form a solid polymer gel. The first step is curing a cross section by drawing the cross section on the surface of the resin with the laser (the part is attached to a platform beneath the surface of the resin by supports). Second, the elevator platform dips into the liquid resin a finite distance allowing the liquid resin to flow over the cured portion of the part. A doctor blade sweeps over the part, leaving a layer of fresh resin that becomes the next cured layer as the laser draws the next cross section. Repeating these steps builds up the three-dimensional part.

Formulating a photocurable ceramic suspension for use in the SLA extends the stereolithography technique. The ceramic suspension consists of fine, alumina powder (Reynolds RC-HC DBM, Malakoff Ind., Malakoff, TX; 0.5 μm mean particle size) suspended in a mixture of acrylate monomers. Addition of a dispersant allows a stable colloidal suspension of at least 50 vol% alumina to be formulated. This suspension has a viscosity of about 200 mPa*s at a shear rate of 100 $s^{-1}$. The low viscosity allows the resin to self-level during fabrication, keeping the top surface very smooth. The suspension is rendered photocurable by addition of a photoinitiator. As the laser traces the part in the resin, the monomer polymerizes and forms a gel that becomes a polymer binder holding the ceramic particles together. After the part is completed in the SLA, the green ceramic body is slowly heated to 500°C to remove the polymerized binder and then sintered to full density at 1580°C [1,2,3]. The binder removal and sintering steps are traditional methods for powder-processed ceramics.

# Fabrication of Ceramics

Several ceramic parts have been fabricated in the SLA using the alumina resin. These parts are shown together in Figure 1. They represent a wide range of complexity and size and serve to illustrate how the SL process can create various shapes in ceramics. These parts are: 1) an 8.5X life size replica of a human trabecular bone (Cerbone), 2) a uniquely designed 3D object displaying "UofM" on one face and "ONR" on the opposite face (UM-ONR), 3) a block letter M (BlockM) and 4) a mechanical testing specimen (Theta). The Theta part and Block M are quite simple, and used to determine the accuracy of the process. Because of its complex shape, the UM-ONR object cannot be produced by conventional molding techniques. The trabecular bone model is another excellent example of an object that could not otherwise be fabricated, as it is a complex random structure with interconnected solid and void phases. Table 1 lists relevant data for each part regarding size, build time and sintering data.

**Figure 1**
*Collection of various ceramic parts fabricated via Stereolithography. The larger copies are as-built and the smaller copies are sintered.*

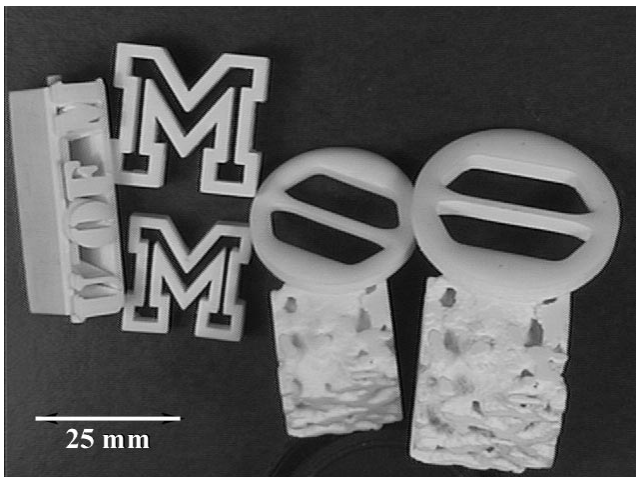


The surface finish of the as-built and sintered parts is excellent. As seen in a close-up view of the UM-ONR part in Figure 2, the top surface has a shiny appearance and the side edges have a scalloped appearance. The scalloping is due to layer by layer build up. Close inspection of the center rod in Figure 3 shows more evidence of the stair-stepping that occurs as the cylinder is approximated by a series of slabs of finite thickness.

On average, the parts exhibited sintering shrinkage of 16.5% in the build-plane and 21.8% in the build direction.

**Table 1**
*Data on various ceramic parts fabricated by Stereolithography.*

| Part Name | Volume, $cm^3$ | Surface Area, $cm^2$ | Build time, hrs | ΔZ/Z, % | ΔX/X, % | Weight Loss, % |
|---|---|---|---|---|---|---|
| Cerbone | 93.9 | 7.12 | 40 | 21.8% | 16.2% | 21.8% |
| UM-ONR | 72.4 | 5.41 | 23 | 22.4% | 16.0% | 21.6% |
| BlockM | 39.8 | 3.32 | 16 | 21.1% | 17.3% | 21.1% |
| Theta | 21.8 | 2.26 | 19 | | | |
| | | | **Averages** | **21.8%** | **16.5%** | **21.4%** |

**Figure 2**
*Close-up top view of as-built UM-ONR part. Note the smooth upfacing surface and scalloped sides.*

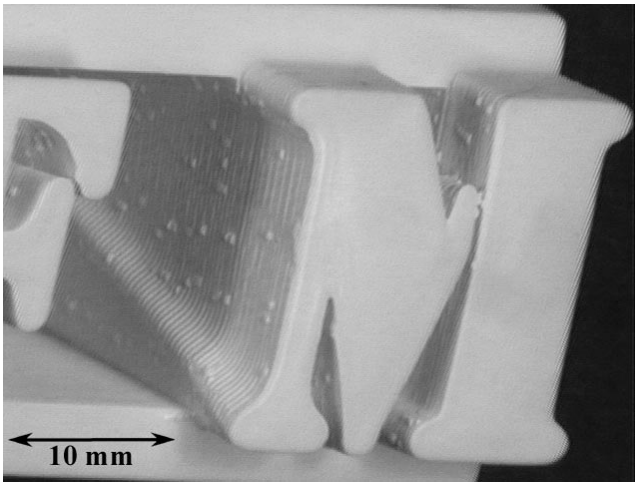


The anisotropy reflects the layered processing route and is similar to what is seen in tape-cast materials. The weight loss is within ±0.2% of the expected value according to the suspension composition. Thermogravimetric data also confirms this result.

The alumina parts were sintered to about 95% theoretical density. Bonding between the layers was observed to be excellent and no trace of layering could be found in fracture surfaces. However, imperfect laminations were localized near the edges emanating from the surface scalloping. Another important property of the finished parts is the smoothness of the upfacing surfaces. This smoothness is due to the fact that the final surface is as smooth as the resin can self level. Profilometry scans shown in Figure 4 illustrate the difference in roughness between the surface and sides. The calculated RMS roughness of the upfacing surface is 4.0 μm and the roughness of the scalloped side surfaces is 27.5 μm.

# Scattering

As the laser scans across the surface of the resin, a region of resin is polymerized. The cure depth of this region is given by the equation [4]

$$C_d = D_p \ln\left(\frac{E_o}{E_c}\right) \qquad (1)$$

where resin parameters $D_p$ and $E_c$ are depth of penetration and critical exposure dose respectively and $E_o$ is the average exposure dose supplied by the laser. This equation was developed assuming the Beer-Lambert behavior for absorption. For typical stereolithography resins, attenuation of the UV radiation intensity occurs almost entirely by absorption. In the photocurable ceramic suspensions used in this work, scattering contributes significantly to the UV radiation intensity attenuation in addition to absorption. It turns out equation 1 also describes the cure depth-exposure dose relationship for photocurable ceramic suspensions [1,3]. Semi-log plots showing the cure depth as a function of exposure dose for a variety of suspensions with different depths of penetrations are shown in Figure 5.

While the alumina particles are transparent to UV and therefore do not increase absorption over that of the photocurable liquid medium, they do serve as scattering centers. The effect of this scattering is reflected in the resin parameter $D_p$ and is given by [5]

$$D_p = \frac{2}{3}\frac{\hat{d}}{\phi\tilde{Q}}\left(\frac{n_o}{\Delta n}\right)^2 \qquad (2)$$

**Figure 3**
*Close-up oblique side view of as-built UM-ONR part. Note the stairstepping effect on the center rod.*

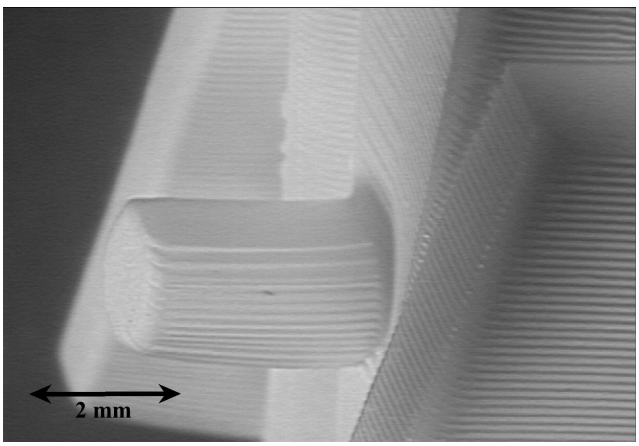


**Figure 4**
*Profilometer scan of side and upfacing surface of an as-built part. Solid line: side scan. Dotted line: upfacing surface scan.*

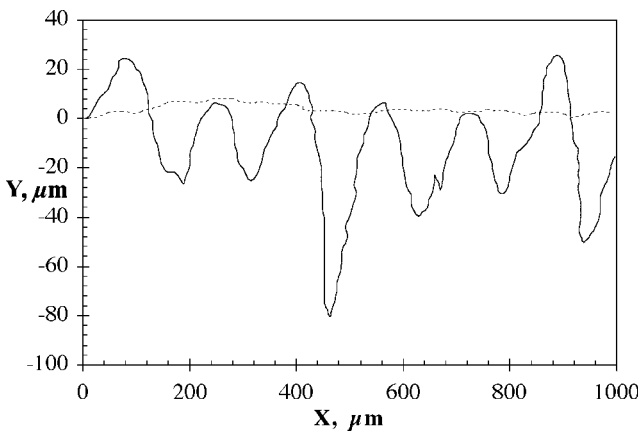

**Figure 5**
*Plot of cure depth as a function of exposure dose for resins with different scattering efficiencies ($1/\Delta n^2$).*

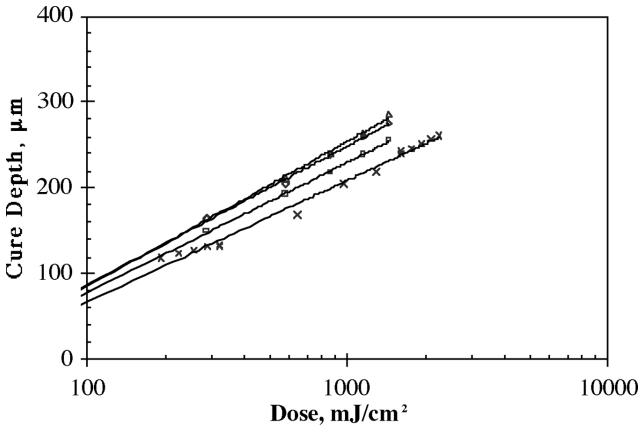


where $\hat{d}$ is the average particle size, $Q$ is the scattering efficiency, $\phi$ is the volume fraction of solids, $n_0$ is the index of refraction of the liquid medium and $\Delta n = (n_0 - n_1)$ where $n_1$ is the index of refraction of the ceramic particles. As a result, the difference in index of refraction between the alumina particles ($n_1$=1.7) and the monomer mixture ($n_0$=1.45 to 1.51) strongly influences $D_p$, and consequently, the cure depth at a given exposure dose. Figure 7 confirms the relationship by showing the linear proportionality between $D_p$ and $1/\Delta n^2$ (data from Figure 6).

**Figure 6**
*Plot of penetration depth for resins with different scattering efficiencies ($1/\Delta n^2$).*

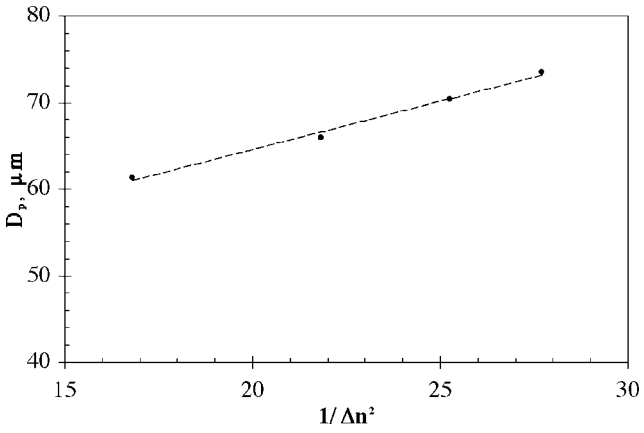


# Build Time

Although the parts shown in Figure 1 are relatively small, the build times are much higher than they would be for typical SL parts. This is mostly due to the low $D_p$ and high $E_c$ of the ceramic resin compared to traditional SL epoxy resin. Identification and quantification of the factors that influence the build time for a given part are essential to reduce the build time. Combining equation 1 and other machine parameters [2], the time to build a given shape can be approximated [4] as

$$t_b \approx n\left(\frac{\pi^2 W_o^2 E_c}{2Ph}\right)\left(\frac{V_s}{z}\right)\exp\left(\frac{C_d}{D_p}\right) \qquad (3)$$

where $n$ is the number of layers in the part, $W_0$ is the beam radius, $P$ is the laser power, $h$ is the hatch spacing, $V_s$ is the volume of the part and $z$ is the height of the part in the build direction. This equation clearly illustrates the influence of part parameters ($n$, $V_s$, $z$), machine parameters ($W_0$, $P$), build style parameters ($C_d$, $h$) and resin parameters ($D_p$, $E_c$) on the time to build a given part.

**Figure 7**
*Comparison between actual, calculated (equation 3) and simulated (Ref. 5) build times for various ceramic parts built by SLA.*

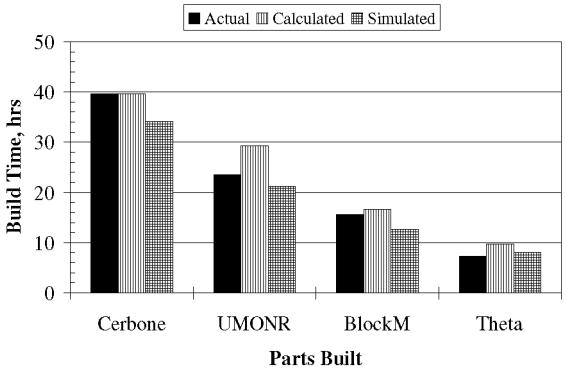


This calculation was used to estimate the build times for each part. The results are compared to a more rigorous build time estimation program[5] that takes information from actual prepared and sliced build files to simulate the build time. The results shown in Figure 7 compare the calculated and simulated build times. The agreement is quite good for all parts, despite the variety of size and complexity. These results indicate Equation 3 is accurate enough to estimate the time to build a single part.

As an illustration, the build time for the Cerbone part was calculated as a function of laser power. This data is shown in Figure 8. The nominal laser power of 25-30 mW was used to build the parts in this study. However, there are other, more powerful UV lasers for use in stereolithography, which have

**Figure 8**
*Build time for "Cerbone" part as a function of laser power. Dotted line: equation 3. Solid line: Build Time Estimator Simulation (Ref.5).*

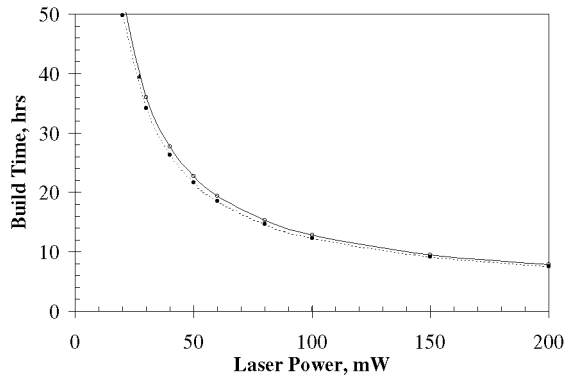


powers of up to and exceeding 200 mW. So, if a 200 mW laser was used, the build time for the Cerbone part would be reduced from 40 hours to about 10 hours.

# Conclusions

Highly loaded ceramic suspensions have been developed to produce ceramic parts via stereolithography. A variety of alumina parts have been successfully fabricated possessing excellent microstructures and very smooth surfaces. The ceramic particles in suspension serve to scatter the UV radiation. The effects of scattering can be understood by a modified Beer-Lambert law and are incorporated into the resin parameters, $D_p$ and $E_c$. Furthermore, the effects of the different resin parameters on the build time for a part can also be accurately quantified.

# Biographies

G. Allen Brady is a research engineer at Allison Engine Company. He competed his PhD thesis on stereolithography at the University of Michigan in 1998. He holds a MS degree from Michigan in Materials Science and a BS degree in Ceramic Engineering from the University of of Missouri-Rolla.

John Halloran is a professor of Materials Science and Engineering at the University of Michigan. He recieved a BS degree from the Univerisity of Missouri-Rolla in Ceramic Engineering in 1973, and a PhD in Materials Science from M.I.T. in 1977. Before coming to Michigan in 1990, he was with an entrepreneurial company (CPS Superconductors and Ceramic Process Systems Corp.) in the Boston area. His previous faculty positions have been at Penn State (1976-1980) and Case Western Reserve University (1980-1985). His current research focuses on ceramic processing, structural ceramics, free form fabrication and novel microfabrication methods.

# REFERENCES


1. Michelle L. Griffith and J. W. Halloran, "Scattering of Ultraviolet Radiation in Turbid Ceramic Suspensions", *J. Applied Physics*, **81** 2538-2546 (1997).
2. G. Allen Brady, Ph.D. Dissertation, "Solid Freeform Fabrication of Ceramics via Stereolithography", University of Michigan, in progress.
3. G. Allen Brady and J. W. Halloran, "Stereolithography of Ceramics", *Rapid Prototyping Journal*, **3** 2 61-65 (1997)
4. Paul F. Jacobs, Rapid Prototyping & Manufacturing-Fundamentals of Stereolithography, 1st ed., Society of Manufacturing Engineers, Dearborn, MI (1992).
5. Joel McClurkin, RPMI Build Time Estimator, v0.1, October 1996, http://risky.marc.gatech.edu/joelm/joel_home.html.

# Direct Photo Shaping of Ceramic Components

*Susanna Ventura and Subhash Narang, SRI International, Menlo Park, California*

## Abstract

This paper describes a new multilayer solid freeform fabrication process ("Direct Photo Shaping") where visible digital light projection is used as a maskless tool to build images on photocurable ceramic dispersions (ceramic powders in photopolymerizable liquid monomers) by flood exposure. For each layer the projected image is changed according to the CAD data describing the object being built and solidification takes place by photocuring of the exposed areas. Multiple layers are dispensed and photocured to fabricate the object of interest. A final rinse with a suitable solvent allows the removal of any uncured ceramic dispersion. The porous free formed "green" ceramic object can then be fired and sintered into a highly dense ceramic part. This ceramic forming process is based on visible-light photo gelcasting. The photocurable ceramic dispersion is prepared from a mixture of ceramic powder and organic monomers containing a visible light photoinitiator. Upon photoexposure the monomers solidify into a polymer thus forming a gelcast green body. Digital Light Processing™ technology (developed by Texas Instruments) enables us to project digital, high resolution, high brightness, high contrast visible light to photocure and form components with a good degree of accuracy. In this paper Direct Photo Shaping is applied to the fabrication of ceramic gas turbine components for military and commercial applications. Silicon nitride specimens with flexural strengths in excess of 1 GPa were fabricated by Direct Photo Shaping. A first-stage silicon nitride turbine vane for the Allison Model 501K industrial gas turbine was fabricated by Direct Photo Shaping and tested in a gas-burner test rig at 1204°C.

## Introduction

The main advantage of desktop manufacturing is the ability to move directly from the design stage on the workstation screen to a physical model, without having to wait

for a machine shop to set up a machine tool to custom-build the model; thus, this approach gives unprecedented power and flexibility to system level designers. By allowing the system level designer to produce an instant functional prototype, desktop manufacturing promises to slash the design cycle time for many applications, thus helping to bring a product from design to production to marketplace faster and more cheaply. In addition, the ability to generate models easily will enable designers to experiment, trying out a variety of design options and comparing them side by side.

Rapid prototyping was initially applied to the fabrication of nonstructural materials by means of computer-aided design/computer-aided manufacturing (CAD/CAM) technology, wherein computer files descriptive of the object were used to create parts made from materials such as UV-curable polymers. The components fabricated in this fashion were considered nonfunctional, and their main application was for iterative design evaluation. During the past few years there has been an increasing demand to extend rapid prototyping technology to the fabrication of functional components with engineering properties and dimensional tolerances comparable to those of conventionally produced components. Today the promise is that advanced solid freeform fabrication (SFF) manufacturing technology will allow the fabrication of functional prototypes from advanced ceramic, metallic, and multiphase materials for structural and electronic applications. The SFF approach to net shape forming holds great promise for rapid prototyping of ceramic components through simplification of the processing cycle, including the elimination of the time consuming steps of pattern making and mold fabrication. SFF of ceramics will allow fast turnaround design validation of new advanced ceramic components for gas turbine engines. In comparison with conventional spark ignition engines, gas turbine engines offer greater fuel efficiency, lower particulate levels, and multiple fuel capability. Turbine engine technology is critical not only to maintaining US military superiority but also to continuing commercial prominence in the aviation, marine and industrial sectors.

Selective laser sintering [1], 3-D ink jet printing [2], laser stereolithography [3], fused deposition [4] and layer object manufacturing [5] are examples of rapid prototyping processes applied so far to the fabrication of ceramic components.

# Direct Photo Shaping

At SRI we have developed a new multilayer fabrication process called Direct Photo Shaping [6]. The process is based on the layer-by-layer photocuring of polymerizable compositions curable by visible light. Each layer is selectively photoimaged by digital light projection via a Digital Micromirror Device (DMD) array that performs the function of an electronic maskless tool. While Direct Photo Shaping promises to be generally applied to the fabrication of polymer, ceramic or metal components, the focus of this paper is to describe its application to ceramics.

We refer to the Direct Photo Shaping ceramic forming process as photogelcasting, since the "green body"[1] is formed by photocuring of a slurry of the ceramic powder in a solution of photopolymerizable monomers. Photogelcasting closely relates to the gelcasting process [7] which is used for forming ceramics from molds and has been shown to produce complex-shaped, near-net-shape parts with high reliability. While in gelcasting a thermal initiator is used to promote polymerization upon heating, in photogelcasting the polymerizable ceramic slurries are cured by exposure to radiation in the presence of a photoinitiator. As in the gelcasting process, the formed green bodies are generally strong and machinable, and after sintering, highly dense ceramic parts are obtained. The potential advantages and enhancements offered by Direct Photo Shaping, relative to other rapid prototyping processes, are described in the next section.

# Process Description

The Direct Photo Shaping process is described in Figure 1. CAD slice images are projected on the photocurable composition which is dispensed and leveled on a build platform. Each layer is photoimaged by digital light projection through a digital micromirror array which modulates the image with a switching time of less than 1 msec. After each exposure, a new layer of photopolymerizable dispersion is applied on the build platform. When the fabrication is complete, the formed ceramic green part is removed from the platform and rinsed with a suitable solvent to dislodge any

**Figure 1**
*Schematic representation of the Direct Photo Shaping process.*

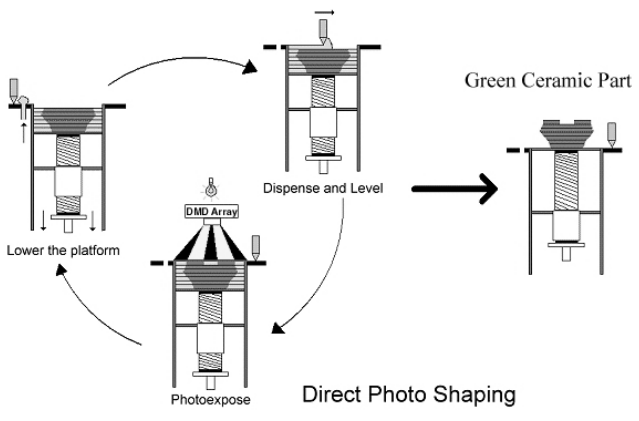


[1]Green body refers to the formed porous ceramic part before densification.

uncured material. The final ceramic part is obtained after binder removal and sintering.

The machine operates in a three-step cycle described as follows (see Fig.1).

**Step 1: Apply Slurry.** The ceramic slurry is dispensed on the build table by means of a peristaltic pump and uniformly applied as a thin layer by a doctor blade. Typically, a layer thickness of 2 mil with a control of +/- 0.5 mil is used. Thicker layers may be fabricated and the layer thickness can be adaptively controlled.

**Step 2: Photoexpose.** The layer is shaped into the desired cross section profile by digital light projection of visible light (the light source is a 270 watt metal halide lamp). The exposure time, which is material dependent, is typically 15 seconds or lower.

**Step 3: Lower Platform.** The photoexposed portion of the layer is cured into a solid film. The platform is then moved to a lower position and a new layer fabrication cycle starts.

The size of the working area is determined by the light projection settings, thus the light can be projected on smaller or larger areas as desired. To optimize resolution, light projection on a small area is desirable. Our current system typically operates on a projected area of 6 x 8 inches down to 2 x 3 inches.

The process makes use of compositions photocurable by visible light. This allows us to achieve good depth of cure especially for highly filled compositions such as ceramic slurries [8]. Other advantages of Direct Photo Shaping include:

- Fast build time because each layer is shaped by flood exposure, thus curing the entire profile at once (unlike the case with a scanning laser); typically for making silicon nitride components, each layer is dispensed and imaged in less than 45 seconds. On the other hand the dispensing and imaging of other ceramics, such as alumina, may take as low as ten seconds.
- Minimum number of steps (no postprocessing after the fabrication of each layer is needed).
- Low cost.
- High resolution (each pixel is a 16-μm-square mirror and DMD arrays with resolution of 1280x1024 and a fill factor of about 90% are available [9]).

Moreover, the use of digital light projection to photocure the ceramic layer offers additional capabilities not available with the traditional laser scanning systems. The DMD-array can be used to project gray images, and the intensity of the gray can be modulated to control light transmission. We expect that the control of the gray scale (i.e, controlled radiation dose) may be used to improve accuracy and surface finish, for example by generating curved layers. Positional control of the photocuring rate allows one to

**Figure 2**
*(a) DMD optical switching principle. (b) Operating DMD arrays.*

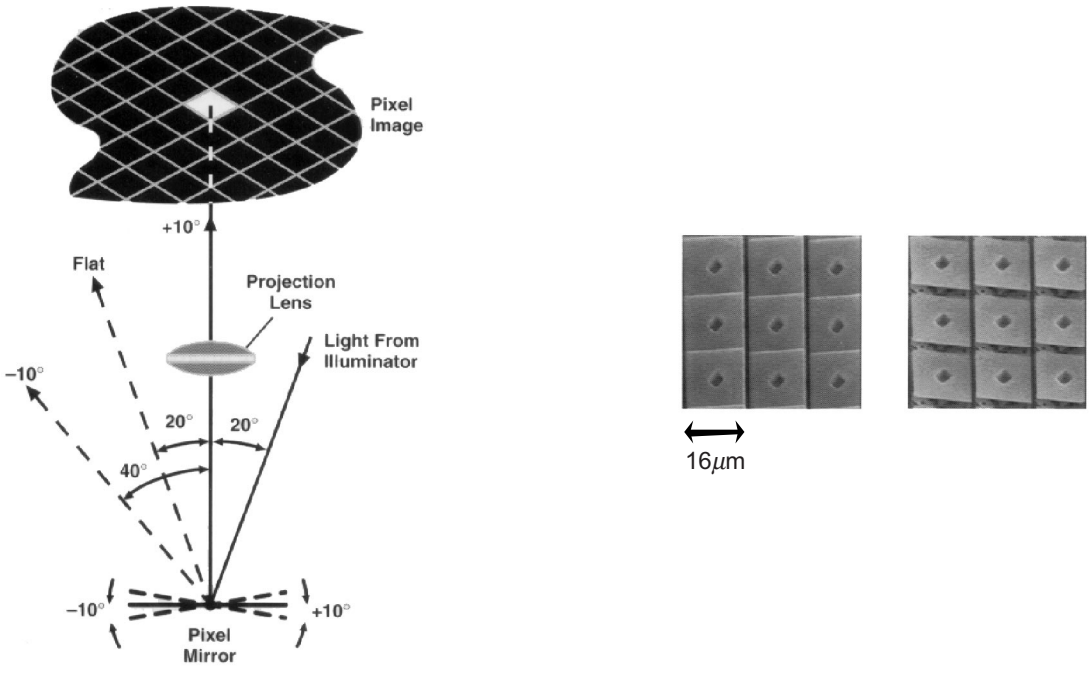

change physical properties in a positional manner and to minimize stresses developed during curing, as well as to generate a robust self-support structure by partial cure of the slurry surrounding the part being built.

## DMD Array - A Maskless Imaging Tool

Digital Light Processing by means of digital micromirror devices is a new light projection technology developed by Texas Instruments [9]. Digital micromirror arrays are constituted by digital light switches, aluminum mirrors, 16 μm square, that precisely control and modulate light. The DMD array is interfaced with a suitable light source and optics, and each pixel mirror is electronically controlled to reflect the incident light in or out of the projection area. Figures 2a and 2b illustrate DMD arrays and their optical switching mode. Because DMD is a reflective digital light switch, its optical efficiency - 62% - is more than ten times higher than that of a liquid crystal display light transmitting pixel (about 5%). This makes DMD arrays a superior tool for maskless imaging of photocurable compositions. Previous attempts of using a LCD programmable mask in combination with UV light to photocure polymers were not successful because of the poor stability of liquid crystal polymers to UV radiation [10].

## Photocurable Composition

We have developed ceramic photocurable compositions that are photoactive in the visible region. This allows us to readily interface the chemistry with the DMD technology and to obtain better depth of curing for the ceramic filled compositions.

Our photocurable compositions contain photoactive monomers, a suitable photoinitiator, a dispersant and the ceramic powder. The ceramic content typically varies from 45 % to 55% on a volume basis. Ceramic slurries are prepared by ball-milling the silicon nitride powder in the photocurable monomers, after addition of a suitable dispersant, a solvent/plasticizer and the photoinitiator. Ceramic slurries with viscosity of 10,000 cps or less are generally used.

The ceramic slurry composition is optimized to improve interlayer adhesion and eliminate any possible delamination during debinderization (see below). This is achieved by reducing the layer stiffness and by using additives to produce a tacky top layer.

## Fabrication and Testing of Silicon Nitride Specimens

Silicon nitride ceramics are of great commercial and military interest because of their excellent mechanical properties, good oxidation resistance and thermal shock behavior both at room and high temperatures.

Silicon nitride specimens of a simple tile shape (3" x 3"x 0.25") were formed from NCX-5102[2] silicon nitride according to three different methods to compare their mechanical properties and to validate the Direct Photo Shaping process. Tile specimens were prepared by (1) Direct Photo Shaping, (2) gel casting in a mold, and (3) powder dry pressing.

**Figure 3**
*Representative microstructures of silicon nitride samples fabricated by (a) Direct Photo Shaping, and (2) dry powder uniaxial pressing.*

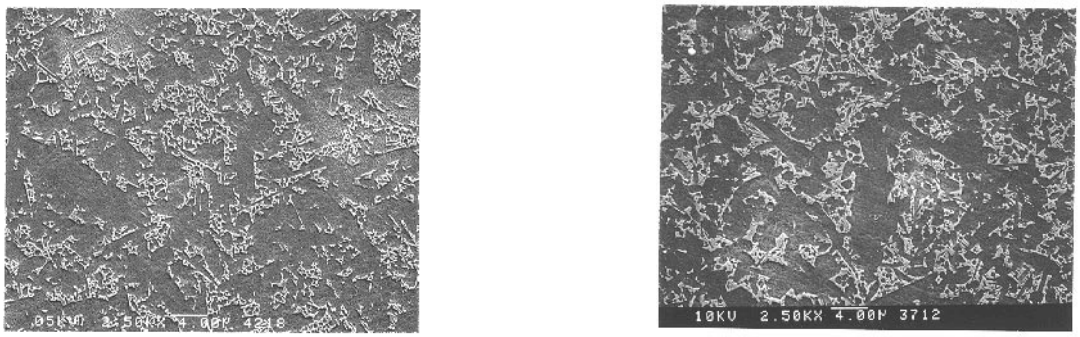


(a) (b)

[2] NCX-5102 refers to a high performance silicon nitride powder processed by Saint-Gobain Industrial Ceramics (Northboro, MA)

**Table 1**
*Summary of Mechanical Property Data for Tiles Formed by Uniaxial Pressing, Thermal Gelation and Direct Photo Shaping*

| Sample | Forming method | Density (g/cc) | Hardness (GPa) | $K_{IC}$ (MPa $\sqrt{m}$) | | Modulus of Rupture (MPa) | | Weibull parameters | |
|---|---|---|---|---|---|---|---|---|---|
| | | | | Indent | Indent Fracture | 3x4x50 mm | 1.5x2x 25 mm | beta | n |
| a | Press | 3.22 | 17.0 | 4.0 | 5.9 | 844 | 937 | 23 | 30 |
| b | Press | 3.22 | 15.5 | 4.0 | 6.1 | 832 | 976 | 24 | 30 |
| c | Gelcasting | 3.22 | - | - | 5.2 | 839 | - | - | - |
| d | Gelcasting | 3.10 | 15.8 | 3.8 | 4.1 | 580 | 779 | 13 | 13 |
| e<br>f | Direct Photo Shaping | 3.21 | 16.5 | 4.5 | - | - | 1018<br>1052 | 16<br>25 | 15<br>15 |

Notes:

1. Specimens e and f were cut from the same sample. Specimens e were cut so that the casting planes were parallel to specimen faces; specimens f were cut so that the casting planes were perpendicular to the specimen faces. In both cases the lamination direction was parallel to the long dimension of the specimen.

2. Some sample properties were not determined because of insufficient number of specimens.

After binder removal, the samples were initially presintered to improve their handling strength and then densified by HIPing using glass encapsulation. After HIPing the samples were >98% dense, as shown in Table 1, and no evidence of the original layers was observed by SEM examination of cross-sectional surfaces of the SFF tiles. Samples for microstructural evaluation were prepared by polishing fracture surfaces and then plasma etching using a 95% $CF_4$/5% $O_2$ carrier gas [11]. This etching technique removes the $Si_3N_4$ and effectively marks the $Si_3N_4$ grain boundaries. Figure 3 shows representative etched surfaces for a sample prepared by the SFF method and for a tile formed by dry pressing. Both samples show a pronounced bimodal distribution of grain sizes and as is typical of *in situ* reinforced $Si_3N_4$, show a pronounced acicular microstructure.

Table 1 summarizes the mechanical property data for tiles formed according to the three different methods. Specimens for flexure testing were machined either to 1.5 mm x 2 mm x 25 mm or 3 mm x 4 mm x 50 mm size. Flexure strength was measured by four-point bending in accordance with ASTM method C1161 [12]. Hardness was measured with a Vickers diamond indenter at a load of 0.5 kg [12]. Fracture toughness was measured by both the indentation method and the controlled flaw method [12]. Sintered densities were measured in deionized water using the Archimedes method [12].

The mold gelcast samples showed lower densities and strengths than the dry pressed and layered samples; this was attributed to slight differences in the HIPing cycles which were used for these samples. The sample formed by Direct Photo Shaping showed similar properties to the dry pressed samples with modulus of rupture (MOR) values slightly in excess of 1 GPa. The flexure strengths for the layered tiles were not dependent on the orientation relative to the casting direction. Fracture toughness measured by Vickers indentation was 4.0 MPa $m^{1/2}$ for the dry pressed samples and 4.5 MPa $m^{1/2}$ for the solid freeform sample. Fracture toughness as measured by controlled indentation was slightly higher, as is typically observed, and was comparable to values previously reported on optimized slip cast material of the same composition [7].

# Fabrication of Complex Shape Silicon Nitride Components

A first-stage silicon nitride turbine vane for the Allison Model 501K industrial gas turbine was fabricated by Direct Photo Shaping. The component, which is approximately 40 mm high with a chord length of 34 mm, was chosen to demonstrate the feasibility of the Direct Photo Shaping process to build complex geometry components. Three vanes were built at the same time on our build platform. The vanes were fabricated from 523 layers, each 50 μm thick. This layer thickness was found optimal to ensure good interlayer adhesion and to generate smooth curved layers. The total time required for the fabrication of the three green vanes was about seven hours, thus just over two hours per vane.

After binder removal, the silicon nitride vanes were densified to more than 98% theoretical density by HIPing. The vanes were approximately 20% linearly undersized due to the shrinkage during the densification process. Figure 4 illustrates a green silicon nitride turbine vane sample next to a sintered one.

**Figure 4**
*"Green" (left) and sintered (right) silicon nitride turbine vanes.*

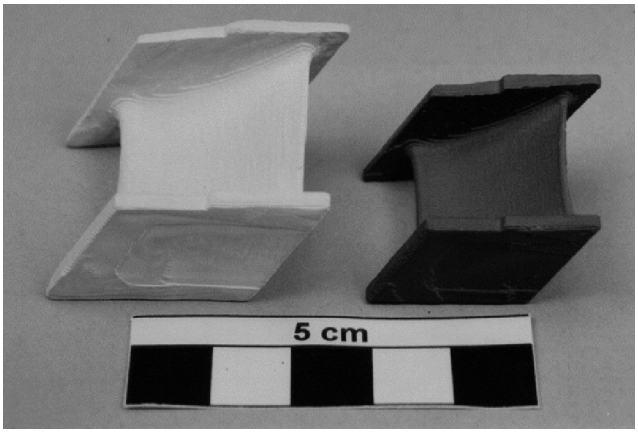


One silicon nitride vane was evaluated in a gas-fired burner test rig and subjected to a total of 20 thermal cycles at an average gas temperature of 1204°C. Nondestructive inspection of the component after testing was performed by fluorescent penetrant inspection and real-time microfocus X-radiography. As indicated in Figure 5, no cracks or defects were found on the part after the test.

**Figure 5**
*Microfocus x-ray photographs of silicon nitride vane after testing at 1204°C.*

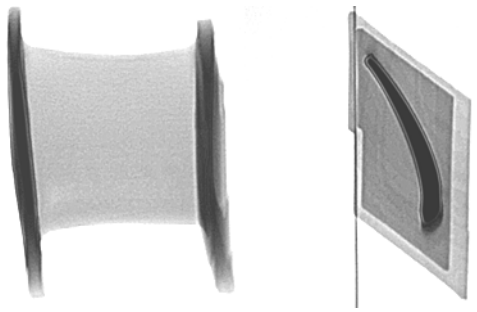

# Conclusions and Outlook

We have presented a new multilayer solid freeform fabrication process, Direct Photo Shaping, where visible digital light projection is used as a maskless tool to photocure cross sections from CAD data. We have described the application of this process to the fabrication of silicon nitride ceramic components. Tile specimens (3"x3"x0.25") were found to be more than 98% dense and to have flexure strengths slightly in excess of 1 GPa and comparable mechanical properties to those of tiles formed by conventional powder processing techniques. Silicon nitride turbine vanes were fabricated and validated for their mechanical properties by subjecting them to repeated thermal cycling at 1204°C. While Direct Photo Shaping has been here described for the fabrication of silicon nitride components, the process has been shown to be feasible for the fabrication of other ceramic (e.g, alumina), polymer and metal parts.

Direct Photo Shaping is a low cost solid freeform fabrication process based on inexpensive visible light projection through a digital micromirror array used as a maskless tool. Because the photocuring takes place by flood exposure, the build time for each layer is fast, a minimum number of steps are required and good resolution is achievable.

Direct Photo Shaping is a flexible fabrication tool which allows us to dispense materials with positional and compositional control and to fabricate functionally gradient materials, microcellular materials, and in general materials with controlled microstructure. The added feature of projecting gray scale light by Direct Photo Shaping further allows us to control the radiation dose in a positional fashion for improved accuracy and surface finish. We are currently applying Direct Photo Shaping to the fabrication of meso and micro mechanical and electromechanical devices containing multiple ceramic/polymer/metal interfaces.

# Acknowledgments

This work was supported by the Defense Advanced Research Projects Agency (DARPA) and the Office of Naval Research (ONR). We thank Dr. William Coblenz and Dr. Steven Fishman for their continuous support and valuable suggestions. We thank our colleagues and collaborators for their essential contributions to this work: John Stotts and Philippe Guerit at SRI for the fabrication of ceramic green parts, Anne Hardy and Mike Mangaudis at Saint Gobain Industrial Ceramics for supplying the silicon nitride powder and for performing the post processing steps, and Lance Groseclose at Allison Engine Company for the design and testing of the silicon nitride turbine vane.


# Biographies

Dr. Susanna C. Ventura received her Doctorate in Chemistry from the University of Padova, Italy, in 1981. From 1982 to 1984, she worked as postdoctoral fellow at Politecnico in Milan where she studied synthetic applications of free radical reaction. In 1986 she joined the Polymer and Technology Department in SRI International where she is currently responsible for the solid freeform manufacturing program and polymer development.

Dr. Subhash C. Narang received his M.S. in chemistry in 1970 from Panjab University, India, and his Ph.D. in chemistry in 1975 from Flinders University, Australia. From 1975 to 1976 he was postdoctoral fellow with Professor Sir Derek Barton at Imperial College in London. From 1977 to 1981 he was postdoctoral fellow with Professor George Olah at University of Southern California. Before joining SRI in 1985, he was assistant professor at Polytechnic Institute of New York, Brooklyn. Present research interests include polymer synthesis, battery technology, rapid prototyping and material science.

# REFERENCES


1. J.V. Tompkins, B.R. Birminghan, and H.L. Marcus, "Solid Freeform Fabrication Using Gas precursors"; Ceramic Transactions, proceedings of the First International Symposium on Advanced Synthesis and Processing, Cocoa Beach, FL, January 1995.
2. J. Grau, J. Moon, S. Uhland, M. Cima, and E. Sachs, "High Green Density Ceramic Components Fabricated by the Slurry-Based 3DP Process"; Proceedings of the Solid Freeform Fabrication Symposium (Austin, TX, August, 1997), pp.371-8.
3. M.L. Griffith and J.W. Halloran, "Freeform Fabrication of Ceramics via Stereolithography"; J. Am. Ceram. Soc., 79(10), 2601-8 (1996); T. Himmer, T. Nakagawa and H. Naguchi, "Stereolithography of Ceramics", pp. 363-370.
4. R. Clancy, V. Jamalabad, P. Whalen, P. Bhargava, C. Dai, R. Rangarajan, W. Wu, S. Danforth, N. Langrana and A. Safari, "Fused Deposition of Ceramics: Progress Towards a Robust and Controlled Process for Commercialization"; Proceedings of the Solid Freeform Fabrication Symposium (Austin, TX, August, 1997), Proceedings of the Solid Freeform Fabrication Symposium (Austin, TX, August, 1997), pp. 185-194.
5. D. Klosterman, R. Chartoff, N. Osborne, G. Groves, A. Lightman and G. Han, "Laminated Object Manufacturing of Advanced Ceramics and Composites"; Proceeding of the Seventh International Conference on Rapid Prototyping, San Francisco, CA, April 1997, pp.43-50.
6. S. Ventura, S. Narang, S. Sharma, J. Stotts, D. Annavajula, L.Ho, S. Lombardo, A. Hardy, M. Mangaudis, and L. Groseclose "Direct Photo Shaping: A new SFF Process for Ceramic Components"; Proceeding of the Seventh International Conference on Rapid Prototyping, San Francisco, CA, April 1997, pp.271-8.
7. O.O. Omatete, M.A. Janney, and R.A. Strehlow, "Gel casting - A New Ceramic Forming Process", Ceram. Bull. 70(10), 1991.
8. G.A. Senich and R.E. Florin, J. Macro. Sci., Rev. Macromol. Chem. Phys., C24(2), pp. 239-324 (1984).
9. L.J. Hornbeck, "Digital Light Processing for High Brightness, High-Resolution Applications", Presented at "Electronic Imaging, EI '97", 10-12 February 1997, San Jose', California; L.J. Hornbeck, "Digital Light Processing and MEMS: Timely Convergence for a Bright Future"; Presented at Micromachining and Microfabrication '95, 23-24 October 1995, Austin, Texas.
10. M. Burns, "Automated Fabrication: Improving Productivity in Manufacturing"; Prentice Hall, Englewood Cliffs, NJ, 1993.
11. K. N. Seibein and W. M. Lovington, "Plasma Etching of $Si_3N_4$"; pp. 319-329 in "Microstructural Science", vol. 16. Edited by H.J. Cialoni, M.E. Blum, G.W.E. Johnson, and G.F. VanderVoort, ASM International, Metals`Park, OH, 1985.
12. "Ceramics and Glasses", Vol. 4, Engineered Materials Handbook.

# Gas Phase Solid Freeform Fabrication and Joining of Ceramics

*K.J. Jakubenas, J.E. Crocker, S. Harrison, L. Sun, L. Shaw, H.L. Marcus, Institute of Materials Science, University of Connecticut, Storrs, CT*

## Abstract

Structural ceramic materials are finding growing use in a wide range of applications, particularly advanced power generation and propulsion systems. Yet, applications of ceramics are being limited by the very properties that make them desirable, high temperature stability and high hardness. Conventional forming techniques are severely tested by materials that do not melt, are harder than tool bits, and are not ductile. Even techniques specifically devised for forming ceramics, such as hot isostatic pressing, have strong limitations. Gas phase Solid Freeform Fabrication (SFF) technologies offer the potential to form complex shapes from ceramics and other materials without the restrictions of conventional forming techniques.

Two similar yet distinct gas phase SFF techniques are being investigated as well as a related spinoff technology that complements both SFF and conventional forming techniques. The techniques are Selective Area Laser Deposition (SALD), SALD-Vapor Infiltration (SALDVI), and SALD Joining. The common thread linking the techniques is the use of a laser to create a localized reaction zone which decomposes a reactant gas to deposit material in a spatially controlled manner.

Development and control of gas phase SFF techniques, including shape, composition, and material properties, requires an understanding of the governing physical processes. This paper begins with a description of the underlying physical processes of thermodynamics, kinetics, and heat / mass transport and then shows the experimental effects of these processes. The goals and continuing development of gas phase SFF technology are discussed in light of the governing physical process and experimental results.

## Introduction

The advantages of structural ceramic materials in high temperature, high wear, corroding environments such as gas

turbines and jet engines in warships and aircraft have been widely reported[1-2]. Application of the high temperature stability and high hardness properties of ceramics have often been limited by the difficulty these properties present in forming operations. Gas phase Solid Free-Form Fabrication (SFF) techniques are being developed as alternative shape forming technologies for ceramics[3-10]. These approaches are also relevant to metals.

SFF techniques in general view complex three-dimensional shapes as being built of thin, two-dimensional layers. The shape forming strategy of SFF is to add a thin layer of defined contour to previously formed layers of the same or different contour, thus building up a fully three-dimensional shape. A wide range of techniques has been developed following this method. Several of these techniques are proving commercially successful, especially for complex shapes made from polymers. Significant work has also been done by many groups on SFF of metals and ceramics[11]. Most of the approaches to ceramics have been targeted at making "green" shapes, that is parts with high porosity that are densified in post-SFF processing by firing and/or pressing as is done in conventional ceramic forming. Unfortunately, such post-processing may void many of the advantages of SFF because of problems with shape retention due to non-uniform shrinkage during densification.

Gas phase SFF techniques seek to avoid most, if not all, of the post processing steps currently necessary for forming ceramics. Gas phase SFF approaches differ from most other techniques in that layers are formed as a result of a chemical reaction rather than a phase change such as solidification. The governing processes involved are therefore different, creating significant flexibility. For example, typical post processing for silicon carbide requires firing temperatures of ~1500°C for several hours, while deposition of bulk amounts of dense silicon carbide from a decomposition reaction is possible at ~1000°C. Thus gas phase approaches offer unique routes to fabricate difficult to form materials.

Three gas phase SFF techniques are described in this paper: Selective Area Laser Deposition (SALD), SALD-Vapor Infiltration (SALDVI), and SALD Joining. In all three techniques, material is deposited in a localized, laser heated reaction zone in which decomposition of a reactant gas occurs. Figure 1 explains each of the three techniques. Initial efforts were carried out at the University of Texas at Austin[3-6]. More recent research has been done at the University of Connecticut.

**Figure 1**
*SALD, SALDVI, and SALD Joining. a) SALD - A scanning laser beam creates a localized reaction zone on a substrate. Within the reaction zone, a reactant gas decomposes to produce a solid deposit. The part is built up by repeated scanning of the beam in a controlled pattern. b) SALDVI - Similar to SALD except that the substrate is a porous powder bed into which material is deposited to create a dense layer. The part is built up by spreading a fresh layer of powder and repeating the scanning. c) SALD Joining - Similar to SALD except that the substrates are the two parts to be joined. The material deposited from decomposition of the reactant gas serves as the filler material.*

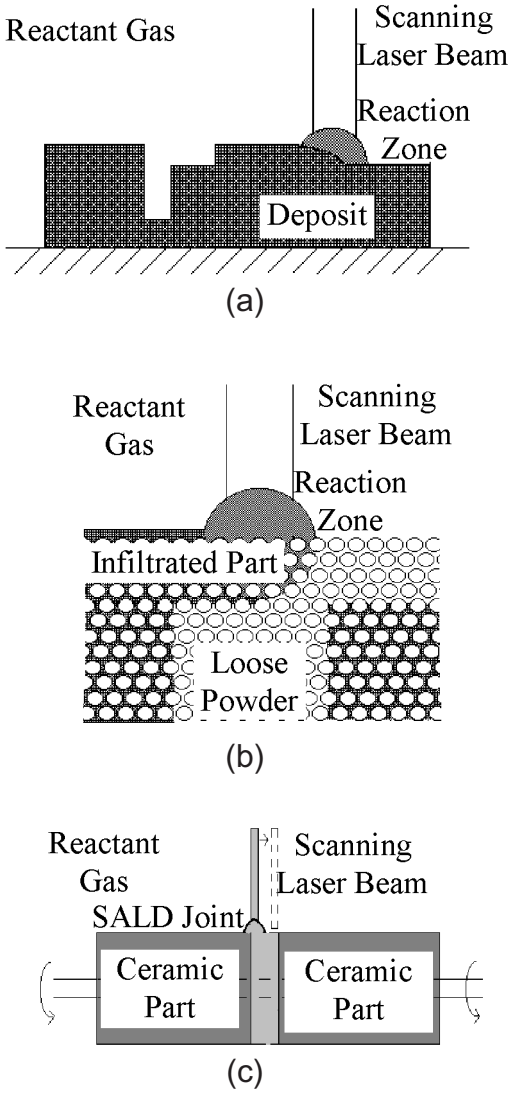


# Physical and Chemical Factors in SALD

SALD techniques are controlled by a number of physical and chemical factors that are heavily interrelated. In order to understand SALD, not only must each contributing factor be understood by itself, but the connections among the factors must also be understood. The properties of SALD deposits and the associated determining factors are listed in Table 1.

For the purposes of discussion in this paper, the factors have been grouped into three areas: heat transport, mass

**Table 1**
*Relationship between SALD Properties and Physical and Chemical Processing Factors*

| SALD Property | Determining Factor |
|---|---|
| Composition | Reactant Gas Composition<br>Thermodynamics<br>Chemical Kinetics<br>Temperature<br>Species Deposition Rate |
| Deposition Rate | Chemical Kinetics<br>Temperature<br>Diffusion<br>Convection |
| Microstructure and Morphology | Species Deposition Rate<br>Temperature Distribution<br>Diffusion<br>Convection |
| Electrical and Mechanical Properties | Composition<br>Microstructure<br>Morphology<br>Interlayer Bonding |

transport, and chemical reactions. This grouping scheme is far from ideal because of the high level of interconnectedness among groups, but the scheme does provide an overview of the salient factors. The groupings are also useful in evaluating the effects of changes in the controllable process parameters as summarized in Table 2. Each of the groups is described briefly in the following sub-sections.

**Table 2**
*Externally Controllable SALD Parameters and the Associated Affected Physical and Chemical Factors*

| Externally Controllable SALD Parameter | Affected Factors |
|---|---|
| Reactant Gas Mixture<br>• Composition<br>• Pressure | Heat Transport<br>• Absorption of Laser Wavelength<br>• Gas Thermal Conductivity<br>Mass Transport<br>• Diffusion Rates<br>• Convection Effects<br>Chemical Reactions<br>• Thermodynamics<br>• Kinetics |
| Laser Beam Properties<br>• Power<br>• Intensity Distribution<br>• Wavelength<br>• Spot Size/Shape | Heat Transport<br>• Heat Flux Intensity<br>• Heat Flux Distribution<br>• Absorption of Laser Wavelength<br>• Reflection, Absorption, Transmission<br>Mass Transport<br>• 1-D vs. 3-D Diffusion<br>• Temperature Gradient Driven Flow<br>Chemical Reactions<br>• Rates<br>• By-products<br>• Potential Photolytic Reactions |
| Laser Beam Scanning<br>• Speed<br>• Pattern | Heat Transport<br>• Transient Effects<br>• Boundary Conditions<br>Mass Transport<br>• Boundary Layers<br>• Diffusion Distances |

## Heat Transport in SALD

The effects of the temperature distribution caused by a laser beam directed incident to a substrate are key to understanding SALD. The temperature distribution underlies the occurrence and extent of chemical reactions and controls convection in the reactant gases. As a result, the composition, morphology, microstructure, and deposition rate of SALD deposits are directly linked to heat transport.

In many conventional thermal processing operations, the part being manufactured is isothermal for time periods of hours. In SALD, temperatures can vary from more than 1500°C to room temperature over fractions of a millimeter and change over that range in seconds. This variation in temperature is inherent and essential to the process for spatial selectivity. Therefore it is clear that an understanding of the determining factors of the temperature distribution is necessary. Existing models of laser induced temperature distributions are being enhanced using a finite element approach for use in SALD process planning, incorporating substrate and reactant gas properties.

## Mass Transport in SALD

Mass transport in SALD involves the motion of reactant gas molecules into the localized reaction zone created by the laser and the motion out of that zone of by-product gases. Diffusion in and out of a small localized reaction zone has been modeled using a range of techniques[12]. All of the techniques emphasize the difference between one-dimensional mass transport seen in conventional wide area chemical vapor deposition (CVD) and the three-dimensional mass transport occurring in highly localized processes such as SALD. In conventional CVD, reactions occur throughout an entire plane of deposition. This means that mass transport that is uniform over the plane can only occur perpendicular to the plane and thus in only one dimension. SALD reactions occur only in a small, localized area, so mass transport can occur over a fully 3-D hemisphere.

The three-dimensional effect occurs when the reaction zone size is of the same order as the characteristic diffusion distance of the reactants. A 1000-fold increase in deposition rates is seen for localized processes such as SALD in comparison to conventional chemical vapor deposition. This phenomenon is attributed to the difference between the 3-D mass transport in localized deposition and the 1-D, wide-area mass transport of conventional CVD.

## Chemical Reactions in SALD

Chemical reactions in SALD are viewed in two terms, reaction kinetics and thermodynamics. Kinetics describe the rate at which various reactions occur to deposit material from the reactant gas. Kinetic calculations are applicable over a wide range of SALD conditions. Unfortunately, reliable ki-

netic data is not widely available, especially for the reactant gases used in SALD. Kinetic data can also be difficult to obtain experimentally. For that reason, thermodynamic equilibrium calculations are often used in modeling SALD reactions. Thermodynamic data is much more widely available than kinetic data, but thermodynamic calculations are limited by an equilibrium assumption and do not convey deposition rates. Equilibrium may be reached in all, part, or none of the SALD reaction zone depending on the temperature distribution. Therefore, thermodynamic equilibrium calculations can only provide a limit on the potential reactions occurring.

Equilibrium calculations for SALD are carried out to create "deposition maps" which show potential solid phases as a function of the externally controllable parameters of temperature and gas mixture. Figure 2 shows an example deposition map. The deposition maps are useful in planning strategies for depositing various materials such as pure materials and composites. Their usefulness has been verified in reducing excess carbon in silicon carbide deposits by the addition of hydrogen and in varying the fraction of silicon nitride in silicon nitride-silicon carbide composites.

**Figure 2**
*Deposition Map for Tetramethylsilane (TMS) ($Si(CH_3)_4$) - Ammonia ($NH_3$) System showing the regions for which various deposits are expected. Calculated using CET89[12].*

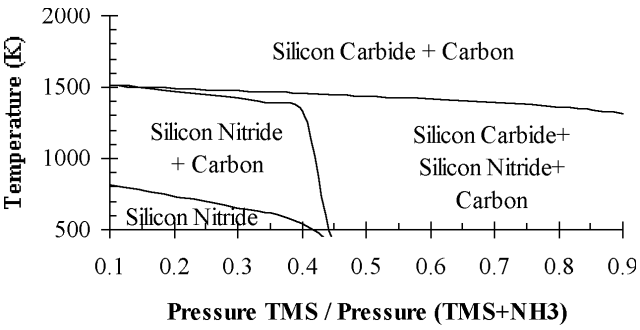


# Experimental Results

## SALD Results

Deposition by SALD has been demonstrated for a number of oxide and non-oxide ceramics as shown in Table 3. Both pure compounds and composites have been formed. SALD processes are not limited to the compounds listed in Table 3. Other SALD researchers have reported deposition of additional ceramics and metals[13-15]. Additionally, approximately 80 elements and compounds spanning the periodic table have been identified as potential SALD/SALDVI materials[16-17]. The governing factors of SALD discussed above are applicable to all of these compounds.

**Table 3**
*SALD Materials*

| Material Deposited | Gas Reactions |
|---|---|
| Carbon | $CH_{4(g)} \rightarrow C_{(s)} + 2\ H_{2(g)}$<br>$C_2H_{4(g)} \rightarrow 2\ C_{(s)} + 2\ H_{2(g)}$<br>$C_2H_{2(g)} \rightarrow C_{(s)} + H_{2(g)}$ |
| Silicon Carbide / Carbon | $Si(CH_3)_{4(g)} \rightarrow SiC_{(s)} + C_{(s)} + CH_{4(g)} + H_{2(g)}$<br>$Si(CH_3)Cl_{3(g)} + 3/2\ H_{2(g)} \rightarrow SiC_{(s)} + 3\ HCl_{(g)}$ |
| Silicon Nitride | $3\ Si(CH_3)_{4(g)} + 4\ NH_{3(g)} \rightarrow Si_3N_{4(s)} + 12\ CH_{4(g)}$ |
| Silicon Carbide / Silicon Nitride | $4\ Si(CH_3)_{4(g)} + 4\ NH_{3(g)} \rightarrow Si_3N_{4(s)} + SiC_{(s)} + 15\ CH_{4(g)}$ |
| Cobalt | Cyclopentadienyl Cobalt Dicarbonyl |
| Silicon | $SiCl_{4(g)} + 2\ H_{2(g)} \rightarrow Si_{(s)} + 4\ HCl_{(g)}$ |
| Silicon Oxide | $SiCl_{4(g)} + O_{2(g)} \rightarrow SiO_{2(s)} + 2\ Cl_{2(g)}$ |
| Titanium Oxide | $TiCl_{4(g)} + O_{2(g)} \rightarrow TiO_{2(s)} + 2\ Cl_{2(g)}$ |
| Silicon Oxide / Titanium Oxide | $SiCl_{4(g)} + TiCl_{4(g)} + 2\ O_{2(g)} \rightarrow SiO_{2(s)} + TiO_{2(s)} + 4\ Cl_{2(g)}$ |

One of the most interesting capabilities of SALD is the ability to mix reactant gases to modify the material deposited. This is especially useful in forming composites. In order to understand composite deposition from gas mixtures, the interrelationships outlined in Tables 1 and 2 must be understood. One example of this is the microstructure that develops from SALD of a mixture of $TiCl_4$, $SiCl_4$, and $O_2$ reactant gases. The deposit is a layered mixture of silicon oxide and titanium oxide as depicted schematically in Figure 3. The layers are the result of both the temperature distribution created by a scanning laser beam and the chemical reaction occurring over a range of temperatures. The leading and trailing edges of the beam create a temperature sufficiently high to form silicon oxide but insufficient to deposit titanium oxide. At the center of the beam, the temperature is sufficient to deposit both oxides resulting in a composite layer sandwiched between the silicon oxide layers. A three-layered microstructure is therefore created by a single pass of the laser beam[18]. The layer thickness can be controlled by varying the beam scan speed, reactant gas ratios, and laser

**Figure 3**
*Multi-layered titanium oxide - silicon oxide composite resulting from a mixture of reactant gases and the temperature distribution caused by a scanning laser beam.*

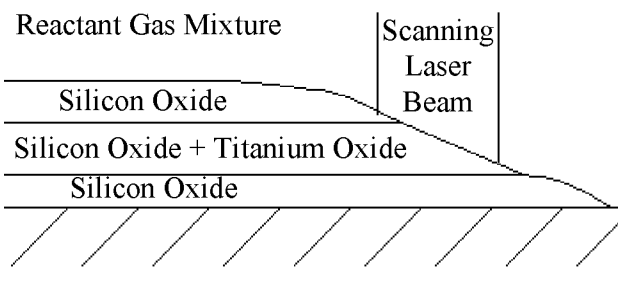

power. Although the titanium oxide-silicon oxide system is of limited engineering interest, the basic principle is applicable to any SALD mixed gas system.

## SALDVI Results

As with SALD, SALDVI has been demonstrated with a number of materials systems as shown in Table 4. As with SALD, the listed systems in no way exhaust the potential materials list. The same range of compounds possible for SALD are also applicable to SALDVI.

**Table 4**
*SALDVI Materials*

| Substrate Powder | Deposited Material | Gas Reactions |
|---|---|---|
| Silicon Carbide | Silicon Carbide | $Si(CH_3)_{4(g)} \rightarrow SiC_{(s)} + 3\ CH_{4(g)}$ |
| Silicon Carbide | Silicon Nitride | $3\ Si(CH_3)_{4(g)} + 4\ NH_{3(g)} \rightarrow Si_3N_{4(s)} + 12\ CH_{4(g)}$ |
| Diamond | Silicon Carbide | $Si(CH_3)_{4(g)} \rightarrow SiC_{(s)} + 3\ CH_{4(g)}$ |
| Tungsten Carbide | Cobalt | Cyclopentadienyl Cobalt Dicarbonyl |

The greatest amount of work has been done on the silicon carbide - silicon carbide system. A number of shapes have been made in this system including those shown in Figure 4. Much effort has gone into optimizing the microstructure of the deposit with particular attention to achieving high density. A cut and polished cross-section showing the level of infiltration so far achieved is shown in Figure 4b. The density has been markedly improved recently through a greater understanding of the role of reactant gas mixture and pressure and the temperature distribution used. For example, the deposition must be carried out within a temperature range that is sufficiently high to decompose the reactant gas and deposit material throughout a powder layer depth of ~100-250 μm, but low enough that excessively rapid deposition does not create a sealed surface, thus preventing infiltration. A different effect is seen with varying pressure of the reactant gas; at reactant gas pressures less than 5 torr, infiltration is hampered by a lack of deposited material while at pressures greater than 50 torr, temperature gradient driven gas motion is sufficient to macroscopically disrupt the powder bed[19]. The interrelated roles of heat/mass transport and chemical reactions have been shown to drive the final results of SALDVI.

## SALD Joining Results

Since SALD Joining relies on SALD for the material to form the joint, the same materials possibilities are available. This is particularly advantageous for matching joint material to the objects to be joined to create a monolithic joints. Gradient joints are possible to connect two objects of different materials, thus minimizing problems such as thermal expansion mismatch[20].

**Figure 4**
*Silicon Carbide SALDVI. a) SALDVI Silicon Carbide "ONR" Letters. b) Microstructure of SALDVI Silicon Carbide*

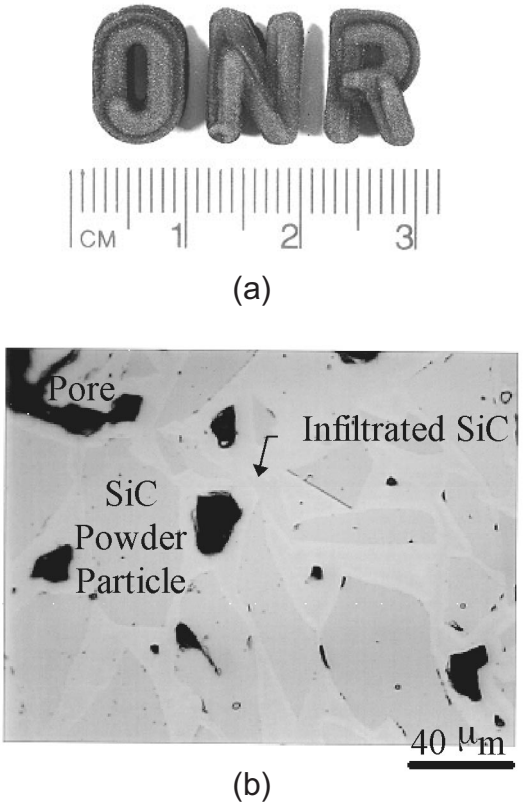


Analysis of SALD joining experiments with silicon carbide objects joined using silicon carbide as the filler have shown that high deposit density and good deposit-to-substrate bonding has been achieved. Figure 5 shows the high density of a deposit and the high quality of bonding possible. Further microstructural control is necessary, however, because excess carbon present in the joints has led to unsatisfactorily low joint strengths. When robust joints can be made repeatedly, SALD joining will promote the utilization of structural ceramics in all settings. For instance, if a ceramic component fails on a ship at sea, the repair process will be as straightforward as a typical welding procedure on a metal structure.

# Application of SALD Techniques - Embedded Devices

Several applications for SALD techniques are under development. SALD, SALDVI, and SALD Joining have great potential for forming shapes from ceramic materials,

**Figure 5**
*Interface between SALD Joining deposit and a substrate object being joined.*

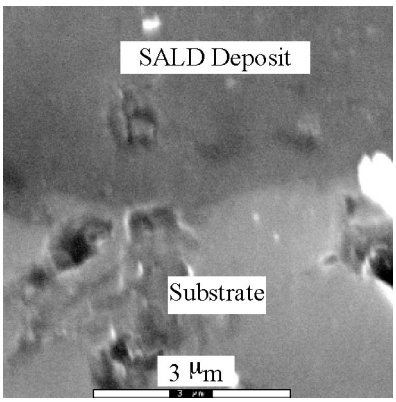


but the most exciting applications are the ones that take advantage of the flexibility of SALD techniques in depositing materials with microstructural control.

The in-situ fabrication of embedded sensors is an example of how SALD processes can be combined to form complex, functional structures. The process begins with SALDVI of a portion of the part composed of several layers. At the desired location for the embedded sensor, a thin, electrically insulating layer is deposited by SALD. The sensor, for example a thermocouple, is then deposited by SALD followed by another SALD insulating layer. The rest of the part is then completed by SALDVI. All of this is done in one processing chamber without need to remove the part between steps. Figure 6 shows a schematic of the process, a silicon carbide piece with a functioning silicon carbide-carbon thermocouple embedded, and the response of the embedded thermocouple to a modulated external heat source. Potential uses for these in-situ thermocouples involve monitoring the internal temperatures of high temperature application parts, such as a jet's engine components or wing panels.

# Summary

SALD techniques offer a set of gas-based SFF techniques for ceramic materials. The two primary advantages of gas phase approaches are that the processes minimize or even completely avoid post-processing and have great flexibility in materials and applications. Research on these techniques has focused on developing a clear understanding of the dominant influences of heat transport, mass transport, and chemical reactions. The roles of each of these has been clarified by a wide range of experimentation. The additional research and development needed to bring the approaches to engineering reality is ongoing.

**Figure 6**
*Embedded thermocouple formed by SALD/SALDVI. a) Schematic of Embedded Thermocouple Process. b) SiC-C thermocouple embedded in SiC. c) Temperature response of the embedded thermocouple shown in b)*

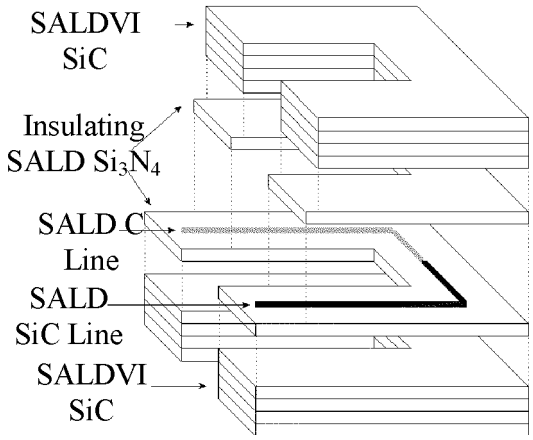


(a)

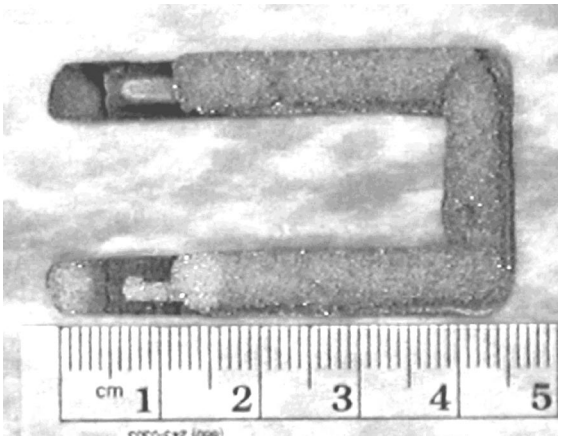


(b)

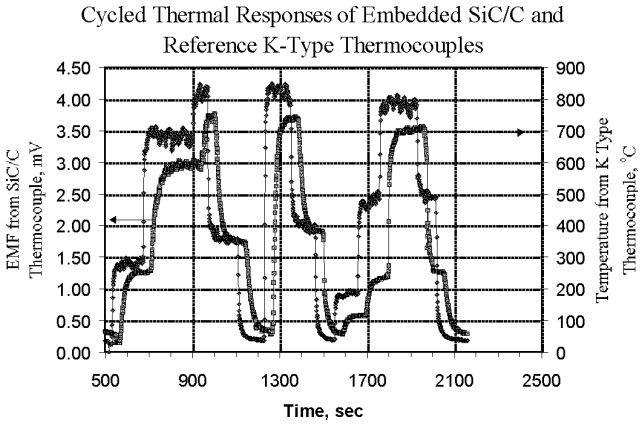


(c)

# Acknowledgements

The University of Connecticut research reported here was supported by the Office of Naval Research Contract #N00014-95-1-0978 and ONR/DARPA Contract #N00014-96-1-1299.

# Biographies

Shay Harrison is a graduate student in the Metallurgy and Materials Engineering program at the University of Connecticut. With a BS degree in materials science and engineering from Rice University, he expects to finish his Ph.D. studies in gas-phase ceramic joining in early 1999.

James Crocker is a graduate student in the Metallurgy and Materials Engineering department at the University of Connecticut. Having completed Masters Degree requirements in 1997, he is currently pursuing Ph.D. studies.

Kevin Jakubenas is a University Post-Doctoral Fellow at the University of Connecticut. He received his Ph.D. in Materials Science and Engineering from the University of Texas at Austin.

Harris L. Marcus is Director, Institute of Materials Science and Professor of Metallurgy and Materials Engineering at the University of Connecticut. His research areas are in fatigue and fracture of structural materials, materials science of surfaces and interfaces, materials processing and solid freeform fabrication.

Leon L. Shaw earned his Ph.D. in Materials Science and Engineering at the University of Florida in 1992. He is currently an assistant professor in the Department of Metallurgy and Materials Engineering at the University of Connecticut.

Lianchao Sun is a graduate student at the University of Connecticut working towards his doctoral degree in ceramics and ceramic processing.

# REFERENCES

1. D.W. Richerson, *Modern Ceramic Engineering*, 2nd Edition Revised and Expanded, New York: Marcel Dekker, Inc., 1992.
2. *Carbide, Nitride, and Boride Materials Synthesis and Processing*, A.W. Weimer, ed. New York: Chapman & Hall, 1997.
3. G.S. Zong, *Solid Freeform Fabrication Using Gas Phase Selective Area Laser Deposition*, Ph.D. Dissertation, The University of Texas at Austin, August, 1991.
4. W.R. Thissell, *Processing and Control of Selective Area Laser Deposition from Methane and Hydrogen*, Ph.D. Dissertation, The University of Texas at Austin, 1994.
5. J.V. Tompkins, R. Laabi, B.R. Birmingham, and H.L. Marcus, *Solid Freeform Fabrication Symposium Proceedings*, The University of Texas at Austin, 1994, pp. 412-421.
6. B.R. Birmingham, *Laser Based Solid Freeform Fabrication Techniques for the Direct Production of Ceramic and Metal/Ceramic Shapes*, Ph.D. Dissertation, The University of Texas at Austin, 1995.
7. S. Harrison, J.E. Crocker, T. Manzur, and H.L. Marcus, *SFF Symposium Proceedings*, UT-Austin, 1996, pp. 345-348.
8. J.L. Maxwell, J. Pegna, D. Messia, and D. DeAngelis, *SFF Symposium Proceedings*, UT-Austin, 1996, pp. 227-237.
9. O. Lehmann and M. Stuke, *Science*, Vol. 270 (8 Dec. 1995), pp. 1644-1646.
10. F.T. Wallenberger, *Science*, Vol. 267(3 Mar 1995), pp.1274-5.
11. J.J. Beaman, J.W. Barlow, D.L. Bourell, R.H. Crawford, H.L. Marcus, and K.P. McAlea, *Solid Freeform Fabrication: A New Direction in Manufacturing*, Kluwer Academic Publishers, Norwell, Massachusetts, 1997.
12. S. Gordon and B.J. McBride, NASA Lewis Research Center, NASA SP-273, March 1976.
13. D. Bauerle, *Chemical Processing with Lasers*, Spring-Verlag, New York, 1986
14. J.L. Maxwell, J. Pegna, and A.G. Ostrogorsky, *SFF Symposium Proceedings*, UT-Austin, 1993, pp. 253-270
15. J.L. Maxwell, J. Pegna, and E. Hill, *SFF Symposium Proceedings*, UT-Austin, 1995, pp. 143-150
16. K.J. Jakubenas, J.M. Sanchez, and H.L. Marcus, *Materials & Design*, accepted and to be published in 1998.
17. K.J. Jakubenas, *Precursor Selection for Selective Area Laser Deposition*, Ph.D. Dissertation, The University of Texas at Austin, December 1996.
18. K.J. Jakubenas, Y.L. Lee, M.S. Shaarawi, H.L. Marcus, and J.M. Sanchez, *Rapid Prototyping Journal*, Vol. 3, No. 2, 1997, p. 66-70.
19. J.E. Crocker, *Making Silicon Carbide Shapes by Selective Area Laser Deposition Vapor Infiltration (SALDVI)*, M.S. Thesis, University of Connecticut, Dec. 1997.
20. J.V. Tompkins, B.R. Birmingham, and H.L. Marcus,*SFF Symposium Proceedings*, UT-Austin, 1995, pp. 409-416.

# Process Planning Issues in the Layered Manufacture of Heterogeneous Objects

*Debasish Dutta, Prashant Kulkarni and Vinod Kumar, Department of Mechanical Engineering and Applied Mechanics, The University of Michigan, Ann Arbor, MI*

## Abstract

A novel feature of Layered Manufacturing, an emerging manufacturing technology, is that it enables fabrication of heterogeneous objects – multi-material and functionally graded interiors – directly from a CAD model. To fully exploit this capability, it is necessary to create CAD models which capture both geometry and material information. We describe our ongoing research in this area. Also, we consider process planning issues and provide details on adaptive slicing, a fundamental process planning task.

## 1.0 Introduction

Layered manufacturing (LM) is a new method of fabrication. Unlike the traditional manufacturing techniques, in LM a part is fabricated directly from a computer model by successively depositing raw material in layers. A distinct advantage of creating a part layer-by-layer is that its geometric complexity has significantly less impact on the fabrication process. Furthermore, different materials, in varying proportions, can be deposited to form a single layer. Such heterogeneous objects, made from materials such as tough ceramics, advanced metallized ceramic composites, and materials with graded chemistries and microstructures, are being designed to provide enhanced structural and mechanical properties in naval systems as well as in other commercial applications. Figure 1(a) shows the cross-section of a model of a turbine blade reinforced with a hard material (in gray) to improve the structural strength of the thin part of the blade. Figure 1(b) shows a simplified model of a valve seat composed of three regions – Aluminum (outer), Brass (inner) and a graded composition in between. While commercial LM systems today are used for rapid prototyping applications, fabrication of heterogeneous objects represents the true potential of layered manufacturing.

**Figure 1**
*Heterogeneous objects.*

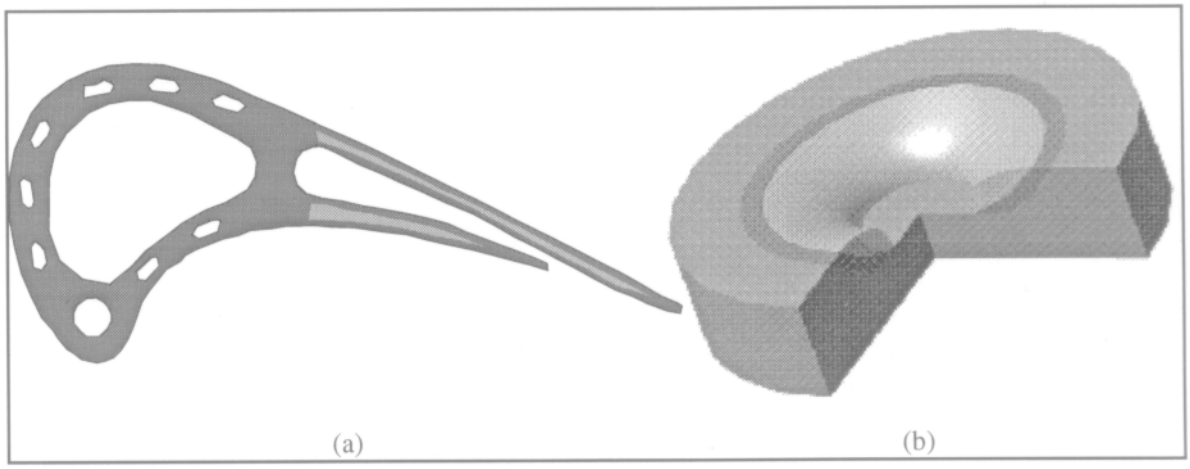


## 1.1 Solid Modeling

The CAD industry has progressed from simple automated drafting/wireframe systems and complex surface modelers to the current state-of-the-art solid modelers. From CAD/solid models, information can be generated about part functionality, manufacturing, assembly and inspection. Hence, solid models have been the key to automation in manufacturing process planning, assembly planning, engineering analysis, etc. Solid modeling has emerged as a key area of research in computer science and several engineering disciplines.

Currently, the solid model of an object contains geometry information stored as data and topology information (e.g. adjacency of faces, edges, vertices) incorporated in the data structure. Typically, there is no information in the solid model regarding the object interior (material, density or other heterogeneities). Without this information, fabrication of heterogeneous objects by LM cannot be fully automated.

## 1.2 Process Planning for Layered Manufacturing

Conventional manufacturing process planning tasks involve determining machining operations (turning, drilling, etc.), parameters (feed, speed, depth of cut) and tools/fixtures necessary to convert a workpiece to the final part. In LM, process planning tasks include defining the build orientation, determining supports, slicing the CAD model (to determine the layers) and the generation of toolpaths and other process information. A block diagram of the key process planning tasks for LM is shown in Figure 2.

Conceptually, process planning tasks for layered manufacturing can be decomposed into tasks that are performed in the *model* domain and ones that are performed in the *layer* domain. In the model domain, the process planning tasks (e.g., part orientation) require geometric information from the CAD model and they output data pertaining to the whole model. The process of slicing converts the model domain into the layer domain. The process planning tasks pertaining to the layer domain (e.g., path planning) are concerned with generation of data for manufacture of individual layers.

Slicing is a fundamental process planning task since all LM processes require it. It is a procedure in which parallel horizontal planes are intersected with the CAD model of the part to determine contours on which material is to be deposited. LM machines are being developed where additional degrees of freedom are being added to the machine, by either pivoting the nozzle or pivoting the platform. In such a case, the planes referred to above are no longer horizontal, but perpendicular to the build direction. Slicing affects the surface accuracy of the manufactured part and the time to manufacture.

In this paper, we provide an overview of our research focusing on the development of computational methods necessary for automated layered manufacturing. In particular, we describe a method for modeling heterogeneous solids in Section 2 and slicing such models in Section 3. We conclude with a brief mention of our research in other process planning tasks.

# 2.0 Heterogeneous Solid Modeling

In traditional geometric/solid modeling, techniques have been developed to model (homogeneous) objects to capture their geometry and topology [1][2]. Such solids can be modeled as r-sets, a regular, compact, semi-analytic subset of the Euclidean space. It captures the notion of solidity (rigidity) of an object having a deterministic boundary.

**Figure 2**
*Process Planning for Layered Manufacturing.*

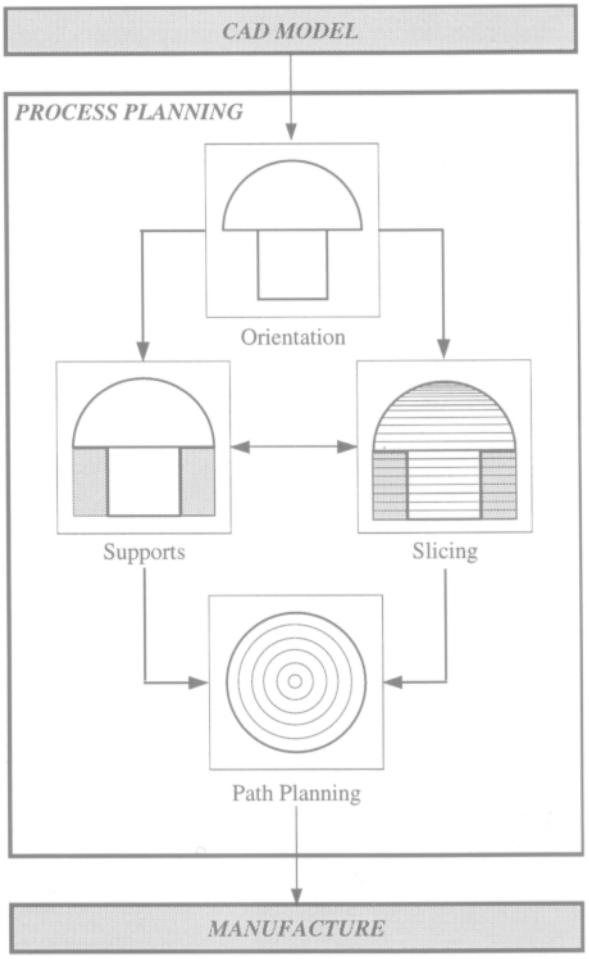


However, in order to represent objects having heterogeneous material domains, the modeling space must be modified. We first consider the simple case where an integer attribute is attached to the model to represent objects made up of a finite number of (homogeneous) material regions. We then extend this idea to model the geometry and material information for a point inside a domain that contains continuously varying materials. This is achieved by considering the volume fraction of each material at the point. A mathematical space of volume fractions is used to represent this information. We extend the conventional r-set to $r_m$-set (and $r_m$-object) to model a heterogeneous object whose geometry is defined via r-set and the material defined by means of volume fractions.

## 2.1 Theory

In order to model heterogeneous objects, the modeling space **T** must include a material dimension (**M**) apart from the spatial dimension $\mathbf{R}^3$ that captures its geometry and topology. If we consider objects made of a finite number of discrete materials [3], the simplest choice for the material dimension **M** would be the set of integers **Z**. However, to model more complicated objects with continuous material distribution, the material space **Z** must be further expanded. It should allow for the representation of a finite set of materials (referred to as primary materials) and also their combinations.

We consider the space $\mathbf{T} = \mathbf{R}^3 \times \mathbf{R}^n$, n being the number of primary materials, as the suitable modeling space. In $\mathbf{R}^3$, the geometry and topology of the object are defined. $\mathbf{R}^n$ is the material space with each dimension representing one primary material. Since a point in the object *S* can be composed of any of the primary materials or their combinations, the composition of material at a point can be quantified by the volume fractions of each of the primary materials. Noting that these volume fractions must sum to 1, we can define the space of volume fractions **V** as:

$$\mathbf{V} = \left\{ \underline{v} \in \mathbf{R}^n \,\middle|\, \|\underline{v}\|_1 \equiv \sum_{i=1}^{n} v_i = 1 \text{ and } v_i \geq 0 \right\} \qquad (1)$$

where $v_i$ (i-th component of $\underline{v}$[1]) represents the volume fraction of material i. Thus, any point $\underline{v} \in \mathbf{R}^n$ can represent a material composition only if it lies on the subspace (or surface) $\mathbf{V} \subset \mathbf{R}^n$. The porosity of a local region can also be modeled by including void as one of the primary materials. Thus, any subset $B \subseteq \mathbf{V}$ can describe the material composition of a heterogeneous object, S. For each point $p \in S$, the geometrical point $\underline{x}$ is associated with its corresponding material point $\underline{v}$ by a mapping from $\mathbf{R}^3$ to $\mathbf{R}^n$:

$$F: \mathbf{R}^3 \rightarrow \mathbf{V} \mid \|F(\underline{x} \in \mathbf{R}^3)\|_1 = 1$$
$$F(x) \equiv \underline{v}(\underline{x}) = \{v_i(\underline{x})\} \qquad (2)$$

Therefore, F is the material function. Additional constraints can be placed on the material function F when defining an appropriate model for *S*.

In summary, for the heterogeneous object S, each point $p \in S$ can be modeled as ($\underline{x} \in \mathbf{R}^3$, $\underline{v} \in \mathbf{V}$) in **T**, where $\underline{x}$ and $\underline{v}$ (or equivalently, $F(\underline{x})$) are the *geometrical* and *material* points respectively. The conventional r-set is now extended to a material r-set which we denote $r_m$-set.

***Definition:*** **$r_m$-set –** A subset (P, B) of **T** where $P \subset \mathbf{R}^3$ is an r-set and $B \subseteq \mathbf{V}$ assigns material to P.

To model multi-material objects and objects with abrupt variations in material composition, we require a set of $r_m$-sets as a generic mathematical model. More precisely, we define:

***Definition:*** **$r_m$-object –** A material object defined as a

[1]An underline in $\underline{v}$ is used to denote a vector in the corresponding space, **V**.

finite collection of $r_m$-sets $(P_j, B_j)$ satisfying conditions C1 and C2:

• **C1:** The $r_m$-sets are geometrically interior-disjoint (i.e., the r-sets are interior-disjoint).

• **C2:** The $r_m$-sets are minimal (i.e., there do not exist two $r_m$-sets whose $C^\infty$ material functions can be combined into a single $C^\infty$ function).

Mathematically, an $r_m$-object, S, can be defined as (EQ-3):

$$S = \{P_j \in \mathbf{A}, B_j \subseteq \mathbf{V}\}, j \in J \text{ (finite)}$$
$$P_i \cap^* P_k = \phi, i \neq k, \forall i, k \in J \qquad (3)$$
$$B_j = F_j(P_j)$$

Our method for modeling heterogeneous solids is based on $r_m$-objects. In addition, our research includes the development of new functionality and operations in CAD systems for the synthesis and manipulation of heterogeneous objects. The methods described above have been implemented and details can be obtained from [3].

# 3.0 Slicing of Heterogeneous Solid Models

Processing of heterogeneous models for layered manufacturing involves considering the geometry as well as the material distribution within the model. We first look at the processing of geometry; the complications introduced as a result of considering the material information are discussed in section 3.2.

## 3.1 Adaptive Slicing

In slicing, a CAD model of the object is intersected with parallel horizontal planes. Each plane generates contours, which we refer to as a *slice* of the model. Depositing material on a slice creates a *layer*. Slicing can either be uniform, where the thickness of successive layers is constant, or adaptive, where the layer thickness varies based on the curvature of the bounding surfaces of the model. In industry, uniform slicing is currently used. Layers generated by uniform slicing for a circular profile are depicted in Figure 3(a). Note, this is a simple abstraction of the layer manufacturing process and each layer is generated by extruding the slice upwards. Depending on the LM process used, the vertical walls of the layers in Figure 3 will be curved. In Figure 3(b), $B_{OR}$ refers to the boundary of the original object (in dark shading) and $B_{LM}$ is the boundary of the corresponding layer manufactured object (in lighter shading). Depositing material in layers will naturally create cusps denoted $\delta_1$, $\delta_2$, and $\delta_3$ in Figure 3(c). The aim of adaptive slicing is twofold:

• **Dimensional Control:** Achieve user specified surface quality in the least build time by maintaining the cusp-height of each layer to be the same.

• **Positional Control:** Ensure that the cusps either lie completely within the CAD model (deficient deposition, Figure 3(b)) or the cusps lie completely outside the CAD model (excess deposition, Figure 3(c)),

In [4], we presented methods for generating layers that satisfy the above two criteria for homogeneous objects. The basic steps in our slicing procedure include: (i) slice contour generation, (ii) layer thickness determination, and (iii) layer generation. We expand on each briefly.

### Slice Generation

An orientation is chosen for the object (corresponding to the build). A slice is generated by intersecting the CAD model with a horizontal plane at a specified height. This is a standard operation supported by every CAD system. A slice can contain several contours depending on the complexity

**Figure 3**
*Different Deposition Strategies.*

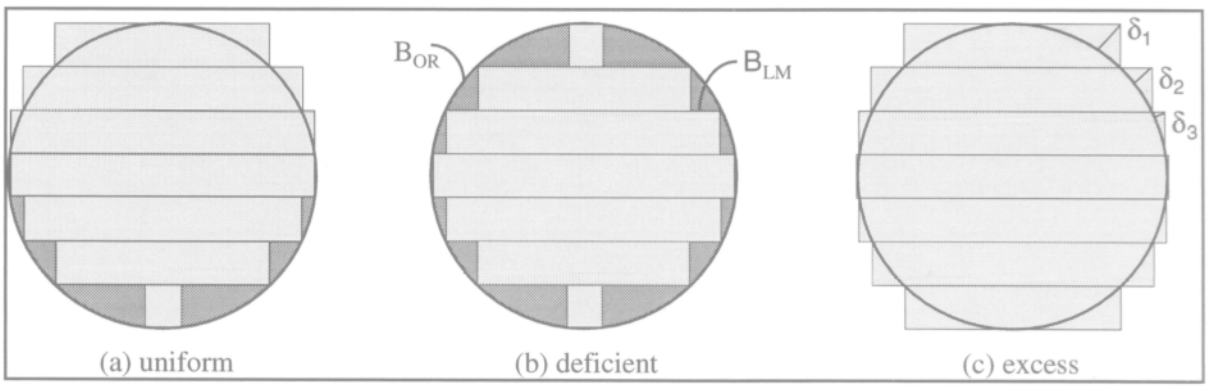

**Figure 4**
*Circular approximation to determine layer thickness.*

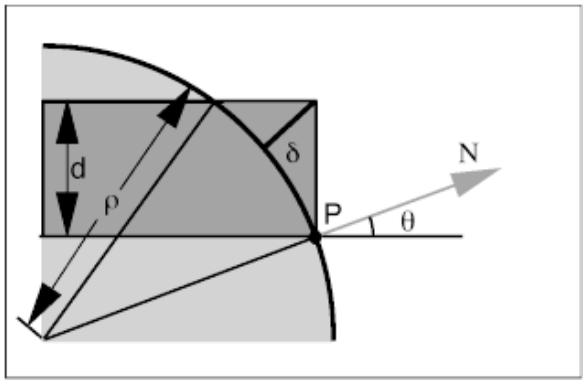


of the object. For example, convex objects will always yield a single contour while non-convex objects are likely to yield multiple contours.

## Layer Thickness Computation

Let us assume a slice contour has been generated. We need to determine the increment for the next slice. This increment is the thickness of the layer of (material to be deposited on) the current slice contour. Recall, in adaptive slicing, the layer thickness will vary based on the surface curvature and the user specified cusp height, $\delta$ (i.e., the dimensional control parameter).

Let us assume we are at a point P on the current slice contour. The layer thickness at P can be computed by taking into account the curvature of the corresponding surface along the build direction. We locally approximate the surface by the circle of curvature along the vertical direction on the tangent plane. Based on this circular approximation and the user specified allowable cusp height $\delta$, we compute the layer thickness d at the point P.

In Figure 4, N denotes the surface normal at point P, $\theta$ is the angle between N and the horizontal, $\rho$ is the radius of curvature of the circular approximation at P, $\delta$ is the cusp height specified by the user and d is the layer thickness to be computed. Let $s(\kappa)$ denote the sign of the curvature, s(c) denote whether the point P lies on the upper or lower part of the circle, and s(d) denote the choice of deposition in positional control (excess or deficient). The layer thickness d is then given by (EQ-4).

$$d = -s(\kappa)\rho\sin\theta + s(\kappa)\sqrt{\rho^2\sin^2\theta + 2s(\kappa)\delta\rho + s(\kappa)s(c)s(d)\delta^2}$$

$$s(\kappa) = \begin{cases} 1 \\ -1 \end{cases} \text{ if } \begin{matrix} \text{Convex (positive curvature)} \\ \text{Concave (negative curvature)} \end{matrix}$$

$$s(c) = \begin{cases} 1 \\ -1 \end{cases} \text{ if } \begin{matrix} \text{P lies on the upper circle} \\ \text{P lies on the lower circle} \end{matrix} \qquad (4)$$

$$s(d) = \begin{cases} 1 \\ -1 \end{cases} \text{ if } \begin{matrix} \text{Excess} \\ \text{Deficient} \end{matrix}$$

There are eight possible forms of (EQ-4) using all combinations of values for the three parameters $s(\kappa)$, s(c), and s(d). Refer to [4] for a detailed description of these eight combinations. Figure 4 illustrates the situation for excess deposition, P in the upper semicircle and $\kappa > 0$.

In general, the CAD model of an object will contain several surface patches joined together. Hence, each slice contour is made up of multiple curves. We process each curve individually in that different points on it would yield different layer thickness values. The minima of layer thickness values computed over all points is the minimum layer thickness for that curve. This can be posed as an optimization problem:

$$\begin{matrix} \text{Minimize } d(u,v) \\ \text{subject to: } z(u, v) = \text{constant} \end{matrix} \qquad (5)$$

This optimization problem is solved for each curve segment comprising slice contour. The minima of all the layer thickness values is the minimum layer thickness for the slice. If the layer thickness is less (greater) than the minimum (maximum) manufacturable thickness, the minimum (maximum) manufacturable thickness value is used.

## Layer Generation

The satisfaction of the user specified positional control (excess/deficient deposition) requires analysis of the layer generation step. A layer can be generated by two different approaches – bottom up or top down. In the bottom up approach, the lower slice (at the current z-level) is extruded upwards. In the top down approach, the upper slice (at a distance d from the current z-level) is extruded downwards. Under the assumption that the z-component of the surface normal will either be positive or negative for the entire contour, the appropriate approach for a layer is determined by the user's choice of the positional control criterion (excess or deficient). The assumption about the normal sign can be easily verified by projecting one slice onto the other and checking for the null intersection [4].

Figure 5 illustrates a simple situation in the layer generation process. Consider Figure 5(a) (middle) where the 3D

**Figure 5**
*Positional control when normal sign assumption is satisfied.*

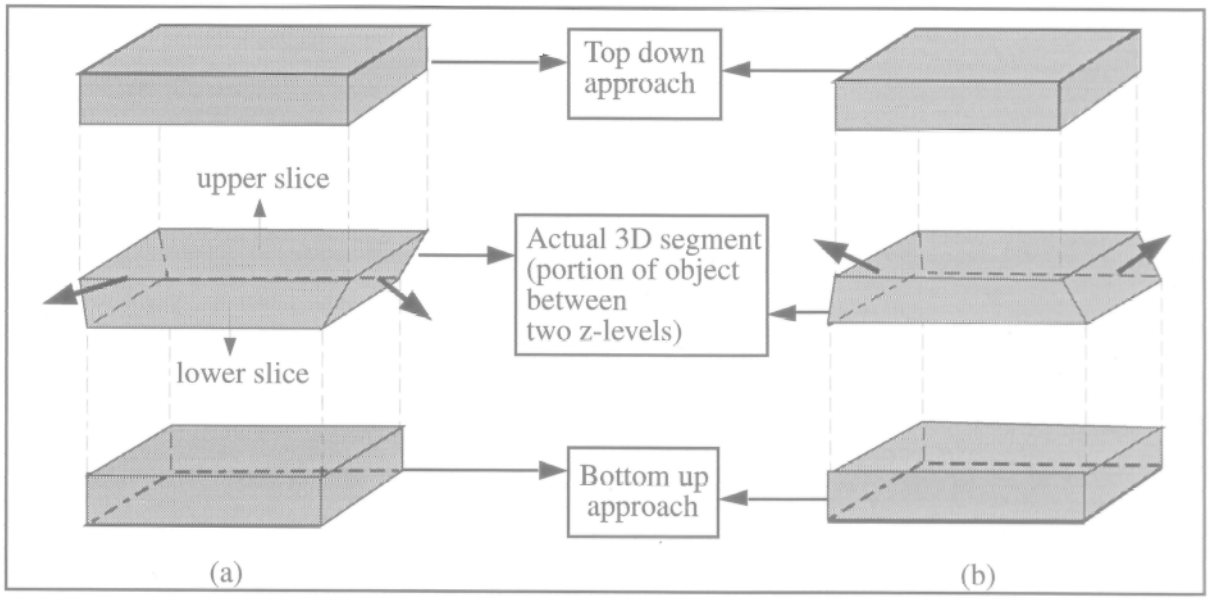


segment of an object (CAD model) has downward pointing normals all around. That is, the upper slice of the 3D segment when projected onto the plane of the lower slice, will properly contain the lower slice. To satisfy deficient (excess) deposition criteria, the bottom-up (top-down) approach is adopted and the lower (upper) contour is extruded up (down). The upper (lower) slice in Figure 5(a) is used to generate manufacturing information, such as nozzle paths etc., for excess (deficient) deposition. A complementary situation with upward pointing surface normals is illustrated in Figure 5(b).

## 3.2 Extension of Adaptive Slicing to Heterogeneous Solid Models

Whereas the CAD model of a homogeneous object usually contains exterior surfaces (representing the object boundary), the CAD model of a heterogeneous object also contains "interior" surfaces. Such surfaces typically delineate distinct material regions in a multi-material object as well as correspond to sharp changes in material/density/other gradation.

To generate a heterogeneous slice at height z*, each material domain in the heterogeneous object is intersected with the plane z = z*. Using the notations from (EQ-3) and denoting the slice by L(z) and the slicing plane by SP(z), we have:

$$L(z^*) = S \cap SP(z^*) = \{(P_j \cap SP(z^*), B_j \cap SP(z^*)), \forall j = 1 \ldots k\} \quad (6)$$

All surfaces, interior and exterior, of the material domains of the heterogeneous model are considered. Each slice is now comprised of several material regions corresponding to the different material domains. Within each region, the material composition can be constant or continuously varying. The material distribution for each region of the slice is evaluated from the material distribution function corresponding to that domain of the heterogeneous object.

The circular approximation of the vertical normal section is still used to calculate the layer thickness. However, both the external and internal surfaces need to be considered. Several different strategies for dimensional and position control can be derived based on the application. In addition to *Exterior Dimensional Control*, where only the external surfaces are considered for computing the layer thickness, the user can require *Complete Dimensional Control*. Here, all surfaces (both external and internal) are assumed to be critical for the application and are included in the layer thickness computation. If the user specifies *Exterior Positional Control*, the internal edges/contours between material regions in the slices are ignored and only the external contour of the slice is considered while generating the layer. Refer to [5] for details on all positional/dimensional control and methods to achieve them.

## 3.3 Other Process Planning Tasks

As mentioned earlier, our research focus has been on the development of computational tools for process planning tasks in layered manufacturing. A suite of tools for ho-

**Figure 6**
*Model of cementite precipitates and austenite grain boundaries in a high carbon steel.*

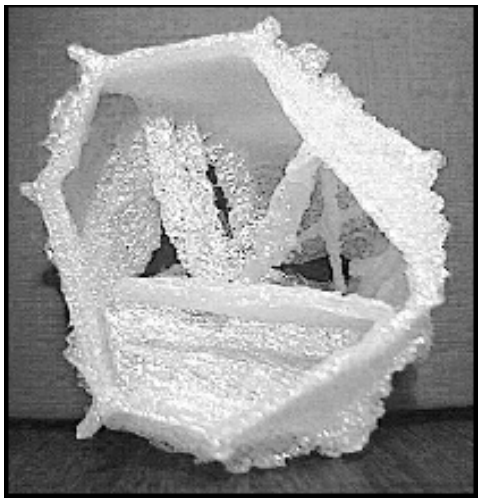

mogeneous models have been developed. Their extension to heterogeneous models is in progress.

A Solid Builder Module (SBM) has been developed that generates a solid model of an object from information contained in a 3D image [6]. There are numerous sources of 3D images that represent objects, such as CT and MRI scans, and FEM output. In addition to a description of the boundaries of the object, the solid model is being extended to contain material information. This solid model can then be used as an input for process planning.

Figure 6 displays a three dimensional model of a real microstructure, manufactured for the Naval Research Laboratory using the Stratasys 3D Modeler. It depicts a model of the cementite precipitates (the white solid) within an austenite grain (the austenite corresponds to the empty areas, but there is a cementite "shell" coating the boundaries of the austenite grain) in an Fe-1.3%C-13%Mn model steel alloy isothermally heat treated at 650 $^{o}$C for 50 seconds [7]. A series of 128 images taken by optical microscopy from serial sections at 0.2 micron depth increments were read into SBM. Each image was used to generate one slice for the layer manufacture of the model.

The capability to link layered manufacturing directly to image data can be useful. For example, our SBM can enable the rapid creation of physical models of strategic terrains obtained from satellite images.

Our orientation module, ORM, determines possible build orientations for parts to be fabricated by LM [8]. It determines the orientation based on one of the following criteria: minimum build height, maximum support contact area, maximum area of base, minimum volume of supports and minimum average surface roughness. The user can select an orientation that minimizes (or maximizes) any of the preceding objectives. The effect of choosing different deposition paths on a specific LM process (FDM) has also been investigated [9]. The stiffness of parts manufactured using the different strategies was experimentally determined. It was then compared with an analytical model developed by using laminate analysis. A good conformance of the models enables the laminate model to be used as a design aid in tailoring the deposition strategy to the stiffness requirements. Finally, we are also developing methods to enable interoperability of (layer manufacturing) data between various commercial machines. Once accomplished, it will allow for a seamless integration of various LM machines which can be operated using heterogeneous solid models and the process planning tools.

# 4.0 Acknowledgments

Financial support for this work was received from Office of Naval Research grants N00014-95-1-0767 and N00014-97-1-0245 and is gratefully acknowledged. We also acknowledge other members of our layered manufacturing research group, namely, Paul Alexander, Seth Allen, Anne Marsan and Xiaoping Qian, whose research was mentioned in Section 3.3.

# Biographies

Debasish Dutta received his PhD from Purdue University and is currently on the faculty of Mechanical Engineering & Applied Mechanics at the University of Michigan, Ann Arbor. His current research interests are in heterogeneous solid modeling and layered manufacturing. He is an Associate Editor of ASME J of Mechanical Design, SME J of Manufacturing Systems, and J of Mechanics of Structures & Machines. Dutta is the General Chair of the upcoming 5th ACM Solid Modeling Symposium, in June 1999.

Prashant Kulkarni recently completed his Ph.D. from the Mechanical Engineering and Applied Mechanics Department at the University of Michigan. His research interests are in Layered Manufacturing, Computer Aided Design & Manufacturing and Solid/Geometric Modeling.

Vinod Kumar is currently a Ph.D. candidate at the University of Michigan, Ann Arbor. His primary interests are in Solid/Geometric Modeling, Computer Aided Geometric Design and Layered Manufacturing.

# REFERENCES

1. C. M. Hoffmann, Geometric & Solid Modeling, Morgan Kaufmann Publishers, 1989.
2. A. Requicha, *Representations for Rigid Solids: Theory, Methods and Systems*, Computing Surveys, Vol. 12, No. 4, 1980.
3. V. Kumar and D. Dutta, *An Approach to Modeling & Representation of Heterogeneous Objects*, ASME

Journal of Mechanical Design, in review, available as Technical Report UM-MEAM-97-05, Department of Mechanical Engineering, University of Michigan, Ann Arbor, 1997.

4. P. Kulkarni and D. Dutta, *An Accurate Slicing Procedure for Layered Manufacturing*, Computer Aided Design, Vol. 28, No. 9, pp. 683-697, 1996.
5. V. Kumar, P. Kulkarni and D. Dutta, *Adaptive Slicing of Heterogeneous Solid Models for Layered Manufacturing*, Technical Report UM-MEAM-98-02, Department of Mechanical Engineering, The University of Michigan, Ann Arbor, MI 48109.
6. A. Marsan and D. Dutta, *Construction of a Surface Model and Layered Manufacturing Data From 3D Homogenization Output*, Journal of Mechanical Design, Vol. 118, No. 3, 1996, pp. 412-418.
7. M. V. Kral and G. Spanos, *personal communication*, Naval Research Laboratory, January 1998.
8. S. W. Allen and D. Dutta, *Determination and evaluation of support structures in layered manufacturing*, Journal of Design and Manufacturing, Vol. 5, 1995, pp. 153-162.
9. P. Kulkarni and D. Dutta, *Deposition Strategies and Part Stiffnesses in Layered Manufacturing*, Proceedings of the 1997 ASME Design Automation Conference, Sacramento, CA, Sept. 1997.